RESPIRATORY MUSCLE PHYSIOLOGY DURING ASSISTED MECHANICAL VENTILATION

FROM A TECHNOLOGICAL PERSPECTIVE

Minke Holleboom

Master Thesis Technical Medicine

Respiratory muscle physiology during assisted mechanical ventilation from a technological perspective

Intensive Care, Amsterdam UMC, location VUmc

Minke Holleboom
November 2021

Supervisors
prof. dr. Leo Heunks
dr. ir. Frans de Jongh
dr. Annemijn Jonkman
dr. Marleen Groenier

External member
dr. Eline Mos-Oppersma

Chair of Committee
prof. dr. ir. Michel van Putten

UNIVERSITY OF TWENTE.

Amsterdam UMC
Universitair Medische Centra

Preface

Deze thesis is het eindresultaat van een jaar stage lopen op de IC van het Amsterdam UMC, locatie VUmc, waar ik het ontzettend naar mijn zin heb gehad. Vanaf dag één voelde ik me er welkom om veel te gaan leren over intensieve zorg, beademing en de ademhalingsspieren. Het was een druk jaar, waarin ik topsport combineerde met de ambitie om zo veel mogelijk uit mijn stage te halen. Gelukkig gaf mijn stage mij energie voor het roeien en gaf het roeien mij weer inspiratie voor mijn stage. Ik ben trots op de stage en deze thesis als resultaat, maar dat was niet mogelijk geweest zonder de hulp en steun van de volgende personen, die ik bij deze graag zou willen bedanken.

Allereerst wil ik graag prof. dr. Leo Heunks bedanken voor de kans die ik heb gekregen om zonder M2-ervaring op de intensive care te gaan afstuderen. Ik heb ontzettend veel van je geleerd en ik ben er dankbaar voor dat ik mijn stage mocht combineren met mijn andere passie, het roeien. Daarnaast wil ik graag dr. Annemijn Jonkman bedanken. Je bent een groot voorbeeld voor me. Desondanks heb jij me het afgelopen jaar het zelfvertrouwen gegeven dat ik een goede TG'er ben geworden, door jouw tips en enthousiasme, maar vooral door het vertrouwen wat je altijd in me had. Ook wil ik graag alle artsen en verpleegkundigen op de afdeling bedanken voor alles wat ik van hen geleerd heb en de hulp bij het doen van studiemetingen. Vanuit de UT ben ik begeleid door dr. ir. Frans de Jongh, u wil ik graag bedanken voor uw intensieve begeleiding, de gezellige kletsuurtjes en de kritische en 'out of the box' vragen die u altijd had! Ook wil ik graag prof. dr. ir. Michel van Putten bedanken voor zijn voorzitterschap van de commissie en dr. Eline Mos-Oppersma als buitenlid. De afgelopen twee jaar ben ik op procesgebied begeleid door dr. Marleen Groenier, waarbij je af en toe mijn stelligheid over hoe het 'hoort' of 'moet' in twijfel trok, wat altijd leerzame situaties opleverde. Dank daarvoor!

Daarnaast wil ik alle andere (student)onderzoekers bedanken voor de fijne werksfeer en gezelligheid op de afdeling. In het bijzonder wil ik Heder bedanken voor alle uurtjes dat je mij uitleg hebt gegeven en de hulp en samenwerking bij het analyseren van jouw prachtige data. Daarnaast, Myrte, dankjewel dat je je op dag één al meteen over mij ontfermde, dat ik altijd bij je terecht kon en bedankt voor de gezellige en productieve samenwerking.

Ook mijn leven buiten de universiteit en het ziekenhuis, heeft aan de afronding van mijn studie bijgedragen. Lieve studievriendinnen, huisgenoten, ploeggenoten, commissiegenoten en mijn leuke dispuut, bedankt voor de geweldige studietijd samen. Tot slot wil ik graag mijn familie en Stephen bedanken. Mam, dankjewel voor je geweldige opvoeding en de stimulans om overal uit te halen wat er in zit. Maar ook bedankt voor de herinnering 'goed is goed genoeg', die ik de afgelopen twee jaar af en toe echt nodig had. Lieve Rens en Nans, bedankt voor jullie steun en afleiding. Bedankt voor het perfectioneren van mijn literatuurverwijzingen (Renske) en het me eraan herinneren dat ik nog steeds geen salaris krijg (Nantske). En als allerlaatst misschien wel de allerbelangrijkste, Stephen. Je was er altijd voor me en het was altijd zo fijn om terug bij jou thuis te komen en even in de watten te worden gelegd. Ik heb er veel bewondering voor dat jij mijn wilde plannen altijd accepteert en meestal zelfs toejuicht.

Table of contents

Abstract

Introduction: Mechanical ventilation is often needed in critically ill patients, to improve gas exchange and reduce the work of breathing. While mechanical ventilation is life-saving, it can also be harmful for the lung tissue as well as the diaphragm. The optimal strategy for maintaining breathing effort in mechanical ventilation is a double-edged sword, aiming to prevent the development of atrophy due to over-assistance as well as muscle injury due to under-assistance. Research mainly has focused on the diaphragm as main inspiratory muscle, but the expiratory muscles and the expiratory phase of breathing are often neglected. The coordination between inspiratory and expiratory muscles is complex, and the prevalence of respiratory muscle activity during pressure support ventilation is largely unknown.

Methods: In a observational clinical study, patients are measured during a spontaneous breathing trial, with the aim to assess functional and timing coordination of the respiratory muscles, focused on the expiratory phase of breathing. Functional coordination parameters included pressure swings, work of breathing and pressure-time-product parameters. Timing coordination parameters included phase angle analysis of starting and end points of pressure (Pes, Pga, Pdi) and EMG signals. Using data of 15 subjects from a clinical trial, the prevalence and level of commonly known and newly defined pressure-derived (expiration) parameters are analysed. In the reliability study, the intra class correlation of echogenicity measurements of the diaphragm is assessed.

Results: The observational clinical study shows preliminary results of two subjects, of whom one subject failed the SBT and the second subject succeeded. The failing subject did not show significant expiration effort, while the successful subject did. Analysis of functional as well as timing coordination analysis, per interval of the SBT, showed to be feasible. The additional data analysis showed significant expiration effort ($\Delta Pga,exp > 2$ cmH_2O and $PTPga,exp > 40$ cmH_2O) in one third of the analysed patients. The reliability of echogenicity measurements was found to have good agreements (ICC values from 0.75 for interrater to 0.88 for intrarater).

Discussion: Further inclusion of subjects should provide clarification in whether the notable results in the observational clinical study are exceptions. The newly defined expiration parameters give additional insight in the respiratory mechanics, but their purpose should be investigated in future research. Future studies should focus on technical improvements such as filtering of pressure signals and automated ROI selection. Several clinical questions remain. What causes expiration effort in which patient population? Is expiratory muscle recruitment beneficial for these patients?

List of abbreviations

Abbreviation	Definition
ARDS	Acute Respiratory Distress Syndrome
AUC	Area Under the Curve
BMI	Body Mass Index
CMV	Controlled Mechanical Ventilation
COPD	Chronic Obstructive Pulmonary Disease
EAdi	Electrical Activity of the Diaphragm
ED85	85^{th} percentile of echogenicity histogram
EMG	Electromyography
ICC	Intra Class Correlation
ICU	Intensive Care Unit
NAVA	Neurally Adjusted Ventilatory Assist
NME	Neuromechanical Efficiency
Pdi	Transdiaphragmatic Pressure
PEEP	Positive end expiratory pressure
PEEPi	Intrinsic positive end expiratory pressure
Pes	Oesophageal Pressure
Pga	Gastric pressure
Pmus	Respiratory muscle pressure
PSV	Pressure support ventilation
PTP	Pressure-time-product
RIP	Respiratory Inductance plethysmography
RMS	Root-mean-square
ROI	Region of Interest
SBT	Spontaneous breathing trial
sEMG	Surface electromyography
VIDD	Ventilator Induced Diaphragm Dysfunction
VILI	Ventilator Induced Lung Injury
WOB	Work of Breathing
ZOA	Zone of Apposition

1 General introduction

The critically ill patient population at the intensive care unit is in need of intensive monitoring of vital functions and often treatment to support their vital functions is required. Consequently, many patients receive mechanical ventilation during their intensive care (ICU) sray, to support or take over their respiratory function [1].

Research over the last decennia has mainly focused 'lung-protective mechanical ventilation', to protect the lung tissue from global and regional stress and strain. [2-4]. Besides the effects of mechanical ventilation on lung tissue, it also has been shown that both mechanical ventilation as well as critical illness can have adverse effects on the respiratory muscles [5, 6]. Diaphragm atrophy and weakness rapidly occurs in critically ill patients due to mechanical ventilation, but also critical illness, like in sepsis, can play a role[2, 7]. Studies have shown that respiratory muscle weakness is associated with adverse outcome, including longer duration of mechanical ventilation and mortality [5, 7-9]. As atrophy develops rapidly [7], ventilator support should be lowered as soon as possible to protect the diaphragm, but excessive effort due to under-assistance should also be avoided [10]. Thus, there is a balance between lowering the work of breathing of a patient to assure adequate unloading and allowing the patient to generate spontaneous effort to avoid respiratory muscle atrophy [2, 5, 11-13]. Although the debate is still going on, it is thought that an inspiratory effort level similar to quiet breathing in healthy subjects could accelerate liberation from the ventilator [8, 14]. These concepts come together in the novel approach of lung and diaphragm-protective mechanical ventilation, with the aim to limit the side effects of mechanical ventilation in critically ill patients on both the diaphragm and the lung tissue [4].

While research in mechanical ventilation and the respiratory muscles has mainly focused on the diaphragm, the effects of critical illness and mechanical ventilation on the expiratory muscles are poorly understood. A proper expiratory muscle function is needed to enhance minute ventilation when the inspiratory load increases, and to generate enough pressure to be able to cough and clear the lungs [15]. Different studies have shown that during a weaning trial, the patients who fail the trial more often show expiratory muscle recruitment [15-17], likely as a result of increased respiratory load and/or reduced inspiratory muscle capacity [15]. While it is thought that expiratory muscle activity supports the diaphragm in the inspiration phase [18], it is questionable whether expiratory muscle recruitment aids patients when weaning from the ventilator [16, 17].

Another aspect to clarify is the role of the diaphragm during expiration. Pelligrini *et al.* (2017) showed diaphragmatic activity during the expiratory phase in pigs, in which they found that the diaphragm showed eccentric contraction, acting like a brake during expiration [19]. The expiratory diaphragm activity in humans is seldom investigated and the functional effects of increasing respiratory loading on the expiratory diaphragm function still need to be determined. Doorduin *et al.* (2018) only found a negligible low tonic expiratory diaphragmatic activity during a spontaneous breathing trial. It is debatable whether electrical activity of the diaphragm during expiration is persistent activity or should be interpreted as termination of the inspiratory activity. This phenomenon clearly asks for more research, to determine whether the measured activity of the diaphragm is present in ICU patients during expiration and whether this is influenced by changing respiratory load [16]. The coordination of the respiratory muscles and the neuromechanical coupling consists of complex mechanisms. Research in healthy subjects suggests that the diaphragm is inhibited by a reflex of central neural output during acute respiratory loading [18].

All in all, the coordination between the inspiratory and expiratory muscles is highly complex, especially during the expiratory phase of breathing, and the functional effects of expiratory muscle recruitment are poorly understood [15]. In order to better adjust ventilator settings to the patient's physiology, with the ultimate goal of quick liberation from mechanical ventilation without lung nor respiratory muscle injury, it is important to get more insight in the respiratory muscle physiology and

the coordination between the inspiratory and expiratory muscles within the expiratory phase of respiration. The timing and functional coordination between the inspiratory muscles, expiratory muscles and the ventilator should be investigated further to understand the (pathophysiology of) the respiratory muscle pump during mechanical ventilation. When and why do patients recruit their expiratory muscles and how do they interact with the inspiration muscles and the ventilator?

Additionally, muscle tissue quality could impact the function of the diaphragm. If this can be assessed using a non-invasive tool, such as ultrasound, it could help in daily practice to diagnose diaphragmatic dysfunction and predict weaning outcome.

1.1 Thesis outline

This thesis unites three distinct projects, with different research aims. The background (chapter 2) provides in the clinical and physiological principles underlying the performed measurements, consisting of a clinical and a technical part. An in-depth rationale for the outcome measures used in chapter 3 and 4 is presented. The background is followed by the three main chapters of this thesis, starting with the clinical study of physiological measurements during a spontaneous breathing trial (SBT) with the aim to assess the functional and timing coordination of the respiratory muscles in chapter 3. In chapter 4, physiological data (pressure and flow signals) of a clinical trial are used for an additional analysis to get insight in the prevalence and level of respiratory muscle activity and effort during the expiratory phase of breathing. Chapter 5 focusses on echogenicity measurements of the diaphragm, with the aim to develop a standardized echogenicity measurement method and assess its reliability. The overall conclusion, clinical relevance and implications for future research are stated in the general discussion, chapter 6.

2 Background

2.1 Clinical background

2.1.1 Mechanical ventilation

Mechanical ventilation is a life-saving technique which is often applied in the intensive care unit (ICU) in critically ill patients with acute respiratory failure, circulatory failure, sepsis or in a post-operative or deeply sedated setting. Acute respiratory failure can be seen as a mismatch between respiratory load, capacity and drive and can be divided into hypoxemic and hypercapnic failure. In hypoxemic failure (type I), the primary cause of respiratory failure is shunting, causing a defect in oxygenation. In case of hypercapnic failure (type II), the primary cause is increased dead space ventilation. [20]. Mechanical ventilation can partially or fully take over the work of breathing of the patient, with main goal to reduce the patients' work of breathing, improve gas exchange and maintain a patent airway [5, 12].

Mechanical ventilation can be divided into two main modes, namely fully controlled mechanical ventilation (CMV) and assisted mechanical ventilation. In CMV, a breath is initiated at fixed intervals and with a fixed pressure or volume set by the clinician, and the work of breathing is fully taken over by the ventilator. In assisted mechanical ventilation the patient has to trigger the ventilator by means of flow or a pressure decrease which is detected by the ventilator. In this way, the work of breathing is shared by the patient and the ventilator [12]. Pressure support ventilation (PSV) is the assisted mode most commonly used at the ICU. During PSV, inspiratory assist is triggered by a decrease in airway pressure caused by inspiratory effort and supported with a fixed positive pressure applied to the airways [21]. A challenge in assisted ventilation is patient-ventilator synchrony, as asynchrony is associated with worse outcome [5, 12]. When aiming to improve patient-ventilator interaction, proportional modes can be a solution, since they are more physiological and therefore improve the match between patient and ventilator [11, 22]. For example, in neurally adjusted ventilator assist (NAVA) the electrical activity of the diaphragm (EAdi) is used to trigger the ventilator and deliver an airway pressure proportional to the EAdi signal [21]. The end of inspiratory flow is determined by the decrease of the inspiratory flow, depending on respiratory system mechanics, which could result in a late cycling off of the machine in patients with airway obstruction. Thus, even if cycling-off criteria are adapted to the needs of the patient [23], the switch to the expiration phase is still dependent of the flow curve in case of PSV. Hence, the end of inspiratory flow in PSV is independent from the patient's neural inspiratory drive [24].

Even though mechanical ventilation is life-saving is in critically ill patients, it also can entail complications and challenges. An important challenge is the development of secondary injury of the lung tissue, caused by mechanical stress and strain of the tissue. Especially in the heterogeneous lungs of respiratory failure patients, the applied pressure can cause deleteriously high local pressures, causing ventilator induced lung injury (VILI) [4, 12]. To prevent VILI, the pressures applied by the ventilator should be within a so-called 'lung-protective' range. This concept of 'open lung ventilation' in patients suffering from Acute Respiratory Distress Syndrome (ARDS) has shown to result in better patient outcome and downregulation of pro-inflammatory pathways [3, 25].

2.1.2 Respiratory muscles

Besides causing lung tissue injury, mechanical ventilation can also impact the respiratory muscle pump. In a healthy subject, the work of breathing is performed by the respiratory muscles. The main inspiratory muscle is the diaphragm. Contraction of the diaphragm shortens its muscle fibres, resulting in a caudal movement of the diaphragm. As a result, the pleural pressure decreases and the

abdominal pressure increase. In case of an open airway, this pressure decrease causes inspiratory flow and hence tidal volumes [26, 27]. When inspiratory load increases, the accessory inspiratory muscles can also be recruited to maintain or enhance minute ventilation. The accessory inspiratory muscles include the external intercostal muscles in the dorsal portion of the rostral interspaces, the parasternal intercostal muscles and the scalene muscles [27].

In quiet breathing, expiration is traditionally considered a passive process. When the diaphragm relaxes, the elastic recoil energy stored during inspiration drives deflation of the lungs. When the inspiratory load further increases (due to exercise, increased resistance or diaphragm weakness), expiratory muscles are often recruited. When the abdominal wall muscles contract, the abdominal pressure increases, causing the relaxed diaphragm to ascend which will increase the pleural pressure to enforce expiratory flow [13, 26, 27]. The abdominal wall muscles are the main expiratory muscles, consisting of the transverse abdominal (TA) muscles, the internal and external oblique (IO and EO), and the rectus abdominal (RA) [13, 26, 27], shown in **Figure 1**. These muscles are recruited hierarchically, in the mentioned order [15]. The rectus abdominal muscle is less involved in expiration, its main function is to provide stability to the trunk .

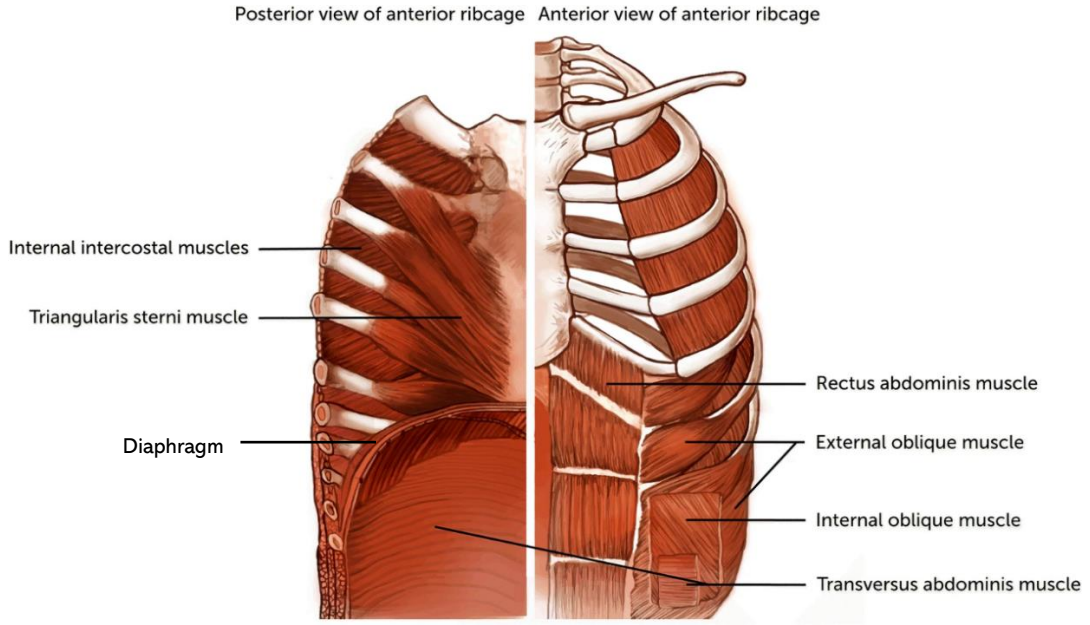

Figure 1: Schematic of the expiratory muscles, showing abdominal wall muscle anatomy at the right side. Diaphragm can also be seen in the posterior view at the left. Diaphragm is the main inspiratory muscles, while the abdominal muscles have a function in expiration. Adapted from Shi et al. (2019) [15].

The abdominal wall muscles can be assisted by the accessory expiratory muscles, namely the internal intercostal and the triangularis sterni muscles, providing contraction of the rib cage which assists the deflation of the lung [27]. It is thought that recruitment of the expiratory muscles also facilitates inspiration by two mechanisms. First, the lung volume is reduced below functional residual capacity inducing inspiratory elastic pressure and second, the diaphragm is shifted to a more optimal position for tension generation [13].

2.1.3 Respiratory muscles and mechanical ventilation

The effects of mechanical ventilation on the respiratory muscles are studied extensively over the past decades. Disuse of the diaphragm during mechanical ventilation is found to result in muscle atrophy [6, 7, 28], and also critical illness can have a negative impact on the muscle tissue [6]. Diaphragm dysfunction impairs clinical outcome of critically ill patients [5] and can be caused by mechanical ventilation, which is called ventilator induced diaphragm dysfunction (VIDD) [29]. Previous research has shown that diaphragm dysfunction is associated with increased mortality, longer ICU stay and difficulties in weaning from the ventilator [8]. Taking into account the negative effects of mechanical

ventilation on lung tissue and respiratory muscles, it is important to disconnect patients from the ventilator as soon as feasible and safe. Longer duration of mechanical ventilation is associated with worse outcome [12]. Weaning from the ventilator often starts with transitioning from CMV to PSV and lowering the level of support. When the ventilator assist is reduced, patients are subjected to a weaning trial or spontaneous breathing trial (SBT) with the goal of assessing liberation readiness [5, 30, 31].

Despite less research on the expiratory muscles is performed compared to the diaphragm, they do play an important role in mechanically ventilated patients and during weaning [15]. It is known that strength of the expiratory muscles and thus the ability to produce high cough peak flow is a predictor of extubation outcome, morbidity and mortality [32]. On the other hand, activity of expiratory muscles in tidal breathing during an SBT seems to be associated with SBT failure, shown in a recent study of Doorduin *et al.* (2018). They suggest that the impaired pressure generating capacity of the diaphragm plays a role in failure to wean and activation of the expiratory muscles [16]. Shi *et al.* (2021) showed that expiratory muscle thickness can increase as well as decrease in mechanically ventilated patients, independent of diaphragm thickness [33]. In sum, the expiratory muscles are frequently recruited in critically ill ventilated patients, but additional research is needed for a fundamental understanding of their function [15].

2.1.4 Eccentric contraction of the diaphragm

For all skeletal muscles there are three forms of contraction; concentric (muscle shortening), isometric (unchanged muscle length) and eccentric (during muscle lengthening). It is found that eccentric loading is more injurious compared to concentric loading. Recently, experimental work has emerged that offer contradictory findings about the activity of the diaphragm during expiration, which implies that the diaphragm is lengthening [19]. Animal studies show that the diaphragm can be active during the expiratory phase of breathing. The electrical activity of the diaphragm as well as the generated pressure difference over the diaphragm was found to increase with lowering the PEEP in a ARDS-like animal model. Pellegrini *et al*. (2017) concluded that these measurements confirm that the diaphragm acts as a brake during the expiratory phase of breathing [19]. This challenges the concept that expiration is simply a result of complete relaxation of the diaphragm, but implies that there may be an aspect of eccentric contraction.

Whether this also occurs in the human diaphragm is yet uncertain. Doorduin *et al.* (2018) investigated the activity of the diaphragm in the expiratory phase during an SBT. A negligibly low tonic diaphragmatic activity in the last quartile of the expiratory phase was found, but in the first expiratory quartile, diaphragm activity was approximately 40% of its peak value. However, they argue that this electrical activity could as well be defined as termination of the inspiratory activity instead of persistent expiratory activity. No difference between activity of the diaphragm during expiration between weaning failure and weaning success patients was found [16]. Goligher *et al.* (2019) reasons that muscle injury as a result of eccentric contraction of the diaphragm can originate from different causes [34]. It could be a result of the diaphragm acting as a brake during the expiratory phase [19], but can also be the consequence of asynchrony between the patient and the ventilator, which is the case during ineffective triggering, as well as reverse triggering. During ineffective triggering, the patients effort to start the inspiration phase is not strong enough to trigger the ventilator, resulting in inspiratory effort of the diaphragm during ongoing expiratory flow. This can also occur in reverse triggering, in which the patient shows effort shortly after the ventilator-delivered breath, potentially resulting in “breath stacking” with high inspiratory volumes [35]. At last, contraction of chest wall inspiratory muscles could force a weakened diaphragm to move upwards during inspiration, in spite of the diaphragm attempting to move caudally by its contraction. This leads to abdominal paradox, in which the abdominal wall will move inwards during inspiration [36].

2.2 Technical background

2.2.1 Lung mechanics

The respiratory system can be divided into different structures and compartments, of which the mechanics can be understood by the defined pressure definitions as described in this section. The pleural space is surrounded by the chest wall and the diaphragm and separated from the lung by the visceral pleura. The abdominal space is surrounded by the abdominal wall and separated from the thorax by the diaphragm [26, 37]. A schematic representation of the respiratory system is presented in **Figure 2**.

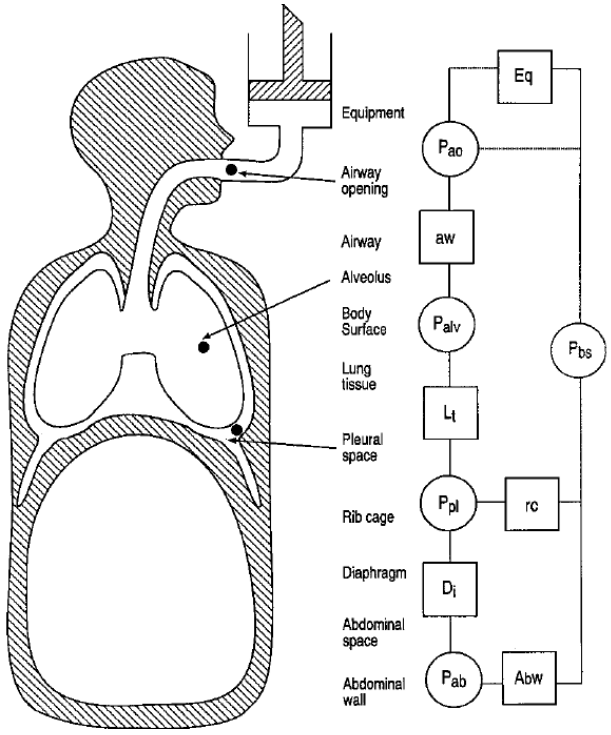

Figure 2: Schematic of the respiratory system with different compartments (airway, alveoli, pleural space, abdominal space) represented as circles and their local pressures and trans-structural pressures, as pressure differences between these compartments, represented as boxes. Copied from [37].

The mechanics of the respiratory system can be quantified using measured volumes, displacements, pressures and rates of change of these variables over time [37]. It is important to distinguish between pressures at a certain location, expressed relative to atmospheric pressure, or trans-structural pressures, defined as the pressure difference between the two compartments opposing the structure(s) [37]. The elastic recoil of the lung results in a tendency of the lungs to collapse. The resulting pressure is called *elastic recoil pressure of the lung* ($Pel_{(L)}$) and is expressed in equation 1 [37]. In the meanwhile, the elastic recoil of the chest wall tends to pull the thoracic cage outward. The resulting pressure is called the *elastic recoil pressure of the chest wall* (Pcw) or the pressure across the chest wall, as shown in equation 2 [26, 37, 38].

$$Pel_{(L)} = Palv - Ppl \quad (1)$$

$$Pcw = Ppl - Pbs \quad (2)$$

In this equation, Palv represents the alveolar pressure and Ppl the pressure within the pleural space. Pbs is the pressure at the body surface, normally equal to atmospheric pressure [26, 38]. The opposing directions of $Pel_{(L)}$ and Pcw cause the pleural pressure to be negative compared to atmospheric pressure, on average -5 cmH_2O. The transpulmonary pressure (P_L) is the pressure gradient over de

lungs, driving airflow, which is defined as the difference between the pleural pressure and the airway opening pressure [13, 37, 38], as shown in equation 3.

$$P_L = Pao - Ppl \qquad 3$$

At any time, Ppl depends on the pressure generated by all the respiratory muscles (Pmus) and the pressure gradient over the chest wall (Pcw) [13]. Contraction of the respiratory muscles causes a decrease in Ppl, enlarging the pressure difference between the airway opening and the pleural pressure, resulting in airflow [26].

Mechanical ventilation adds some additional elements to the respiratory mechanics. As mentioned, P_L (= Pao – Ppl) is the driving pressure for airflow. During spontaneous breathing, this pressure difference is enlarged by the lowering of Ppl by the respiratory muscles. However, in mechanical ventilation, an external pressure is applied. So, Pao is increased by the pressure applied by ventilator. During MV in assisted mode, the total pressure (Eq.4) applied to the respiratory system (Ptot) is the sum of the ventilator pressure (Pvent) and muscle pressure (Pmus) [38] (Eq.4). This Ptot can also be written as the equestion of motion of the respiratory system, summing the resistive pressure (*flow × resistance)* and elastic retraction pressure (*volume × elastance*) needed to insufflate the lung [39].

$$Ptot = Pvent + Pmus = flow \times resistance + volume \times elastance \qquad 4$$

2.2.2 Measurement techniques

The majority of pressures as defined in section 2.2.1 cannot be measured directly, but are derived from pressure measurements in the oesophagus and the stomach. These pressure measurements are performed using a Nutrivent™ catheter, shown in **Figure 3**. With an air-filled balloon the pressure in the oesophagus (Pes) is measured as a reflection of Ppl and the gastric pressure (Pga) is measured as a reflection of the Pab in the stomach [37].

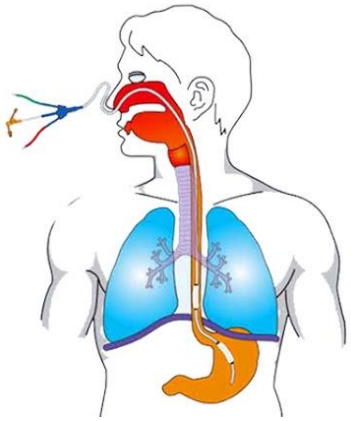

Figure 3: *Schematic of a Nutrivent catheter with balloons in the oesophagus and stomach, used for measurement of Pes and Pga. Image from Nutrivent™ (nutrivent.eu/en/indications.php).*

The difference between Paw and Pes during an occlusion is a valid estimate of transpulmonary pressure (P_L) [38]. Pes can be viewed as the static recoil pressure of the relaxed chest wall (Pcw,rel) minus the inspiratory pressure developed by inspiratory muscles (Pmus) [38].

$$Pmus = Pcw,rel - Pes \qquad 5$$

In which

$$Pcw,rel = \frac{V}{Ccw} = Ecw \times V \qquad 6$$

From here on, Pcw,rel is be referred to as Pcw. Pcw can be calculated by used of the volume signal (V) and the compliance (Ccw) or elastance (Ecw) of the chest wall. Pes measurements are mostly used for research purposes, but can also be used in a clinical setting to gain additional insight in the stress on the lung tissue, detect asynchrony, and determine respiratory breathing effort [40]. The additional

measurement of the gastric pressure as a reflection of the abdominal pressure, allows us to calculate the pressure difference over the diaphragm, called transdiaphragmatic pressure (Pdi).

$$Pdi = Ppl - Pab \approx Pes - Pga \quad (7)$$

2.2.2.1 Analysis method

From the measured pressure signals, breathing effort can be calculated, for which different quantification approaches are available. Work of breathing (WOB) is the classic method for assessing breathing effort [13]. Work of breathing is the area enclosed by the pressure-volume curve, in which lung volume is plotted against trans pulmonary pressure, and can be described by the following formula [13, 38].

$$WOB = P[cmH_2O] \times V[L] = \int P\,dV \quad (8)$$

WOB is normally expressed in J/min or J/L. Limitations of this method are the insensitivity to isometric contractions and the fact that duration and frequency of contractions are not considered [13]. This can be resolved by using the pressure-time-product (PTP) to quantify breathing effort, which is commonly reported over a one-minute interval (cmH_2O*s/min) and correlates well with energy expenditure of the respiratory muscles (Eq. 9) [13].

$$PTP = P\,[cmH_2O] \times t\,[s] = \int P\,dt \quad (9)$$

Since PTP parameters are a time-integral of a pressure signal of interest, they can be calculated for Pes, Pdi, Pmus or Pga. There is a great importance in using precise and well-reasoned definitions of the timing (start and end time) and baseline, as these choices can have a large impact on the results of PTP analysis. Past research has used several different definitions of PTP parameters. In this section, the exact definitions and their rationale are discussed per parameter used in further analysis (Chapter 3 and 4). Before looking into the definitions per parameter precisely, it is useful to discuss the starting point of the expiration. Considering the available signals, it is a practical approach to take the flow signal as an indicator for the start and end of inspiration and expiration phase. Using the flow signal enables us to investigate eccentric contraction, as the diaphragm almost certainly is moving upwards during expiratory flow. However, we have to keep in mind that in ventilated patients, the timing of the end of inspiratory flow is influenced by the flow cycling-off setting of the ventilator applied by the clinician and not exactly the neural expiration of a patient. Hence, it could be argued and may be more precise to use the neural drive as an indicator for the start of inspiration and expiration, but the exact time point of start of neural expiration is also a topic of debate.

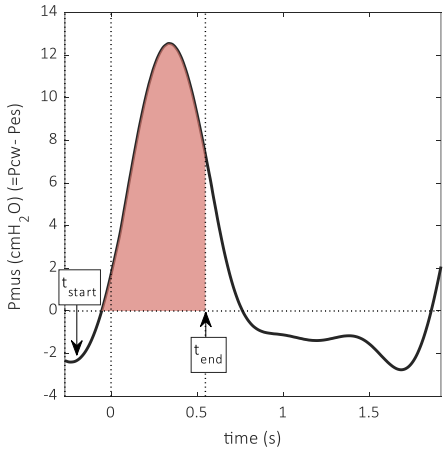

PTPmus,insp is enclosed by:

- t_{start} = *start of inspiratory Pes activity (decrease)*
- t_{end} = *end of inspiratory flow*
- ***Upper boundary*** = *Pmus signal*
- ***Lower boundary*** = *Pmus zero line (corrected for ΔPga,exp in previous breath)*

Figure 4*: Definition of the inspiratory Pmus, PTPmus,insp. PTPmus,insp is enclosed by the upper and lower boundaries as defined in the box, from t_{start} to t_{end}. Vertical dotted lines represent start and end of inspiratory flow.*

From the Pmus signal, three PTP measures are derived. PTPmus,insp reflects the effort of all inspiratory muscles together during inspiratory flow. It is important to be aware that in literature, the terms PTPes and PTPmus are often used interchangeably. However, most of the time, PTPes parameters do also include the Pcw curve as upper boundary [16, 41, 42]. Thus, they take into account not only the absolute lowering of Pes, but also the expansion of the chestwall, which is the total pressure carried out by all respiratory muscles together (=Pmus) either. Some studies report a flow-based starting point of PTPmus (PTPes) [42]. In our definition, the start of PTPmus area is defined as the start of Pmus rise (≈ Pes decrease) at the start of inspiration (t_{start} in **Figure 4**). This takes place just before triggering and start of inspiratory flow in patients ventilated in assisted modes [16]. However, when expiration effort is detected as a rise in Pga (ΔPga,exp) in the previous breath, the relaxation of the abdominal muscles could also cause a decrease in Pes at the end of expiration, for which is corrected by shifting the Pmus signal downwards [16]. Hence, Pmus at the start of the Pmus rise is a negative value and by using Pmus = 0 as the baseline for PTPmus,insp, the Pmus rise due to relaxation of the expiratory muscles is excluded from PTPmus,insp area. This is shown in **Figure 4** (Pmus is ± -2 at t_{start}) , along with the exact definition of the boundaries and the resulting area of PTPmus,insp.

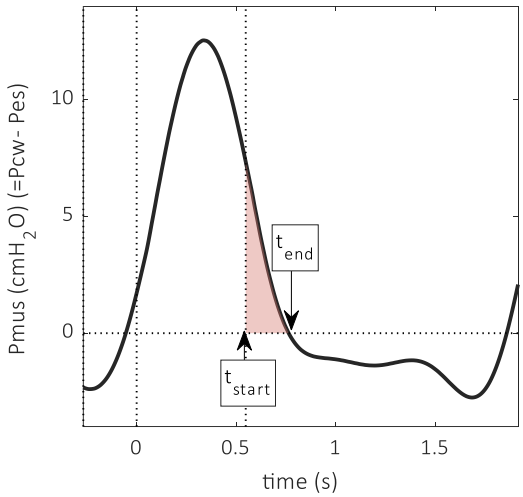

PTPmus,exp(+) is enclosed by:

t_{start} *= end of inspiratory flow*

t_{end} *= first event of: a) return to 0 Pmus or b) first local minimum of Pmus*

Upper boundary *= Pmus signal*

Lower boundary *= Pmus zero line (corrected for Pga rise in previous breath)*

Figure 5: *Definition of positive expiratory PTPmus, PTPmus,exp(+). PTPmus,exp(+) is enclosed by the upper ans lower boundaries as defined in the box, from t_{start} to t_{end}. Vertical dotted lines represent start and end of inspiratory flow.*

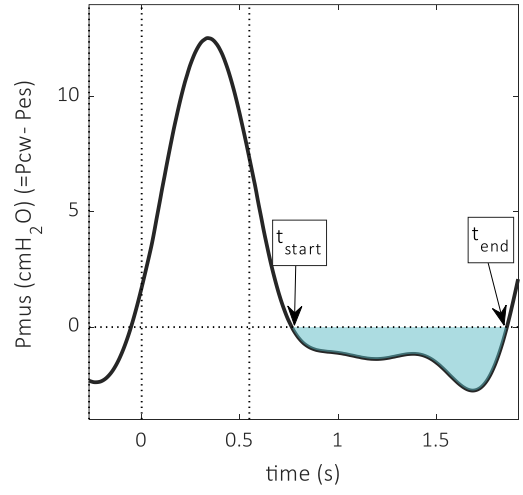

PTPmus,exp(-) is enclosed by:

t_{start} *= start of negative Pmus after start of expiratory flow*

t_{end} *= end of negative Pmus during expiratory flow start of next inspiration*

Upper boundary *= Pmus zero line (corrected for Pga rise in previous breath)*

Lower boundary *= Pmus signal*

Figure 6: *Definition of negative expiratory PTPmus, PTPmus,exp(-). PTPmus,exp(-) is enclosed by the upper and lower boundaries as defined in the box, from t_{start} to t_{end}. Vertical dotted lines represent start and end of inspiratory flow.*

The PTPmus during expiration consists of two parameters, namely the positive (**Figure 5**) and the negative (**Figure 6**) expiratory PTPmus. The positive expiratory PTPmus (PTPmus,exp(+)) reflects the amount of inspiratory effort that occurs during expiratory flow, and therefore is substantially dependent of the ventilator settings. PTPmus,exp(+) is the part of the inspiratory Pmus curve after inspiratory flow ended (t_{start} in **Figure 5**). The return to Pmus = 0 or the first local minimum of Pmus is the end time (t_{end} in **Figure 5**) of PTPmus,exp(+), depending on what happens first. This parameter is not described in literature before. The negative expiratory PTPmus (PTPmus,exp(-)) in **Figure 6** is thought to reflect the effort of a patient enhancing expiration compared to a passive expiration process. Since Pes should coincides with Pcw in a fully relaxed expiration, exceeding of Pcw by Pes (resulting in a negative Pmus) reflects expiration effort. This is previously described as the expiratory PTP [41] and frames the area between the negative Pmus signal during expiration and the zero line of Pmus (**Figure 6**), if a negative Pmus signal is present, i.e. Pes signal exceeds Pcw.

From the Pdi signal, two PTP parameters are derived, applying the same method as for PTPmus,insp and PTPmus,exp(+). As the starting point of the inspiratory PTPdi (**Figure 7**), start of inspiratory flow often is used before [42-44]. However, when using a similar approach as for PTPmus [16], the start of inspiratory diaphragm activity, quantified as the start of Pdi rise, should be used as starting point, to include all inspiratory diaphragm activity. The lower boundary or baseline for PTPdi parameters is defined as the level of Pdi at t_{start} of PTPdi,insp[43, 44]. The expiratory PTPdi (PTPdi,exp) was defined as the part of the inspiratory Pdi curve after inspiratory flow ended (t_{start} in **Figure 8**), reflecting the amount of diaphragm effort during expiratory flow. The end point (t_{end} in **Figure 8**) is chosen as the first event of a local minimum or returning to Pdi baseline. The definition of this novel parameter PTPdi,exp is shown in **Figure 8**.

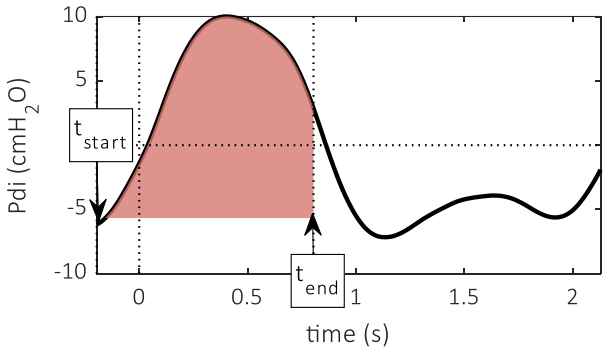

PTPdi,insp is enclosed by:

t_{start} *= start of inspiratory Pdi activity (increase)*

t_{end} *= end of inspiratory flow*

Upper boundary *= Pdi signal*

Lower boundary *= Pdi at t_{start} (= Pdi baseline)*

Figure 7: *Definition of the inspiratory PTPdi, PTPdi,insp. PTPdi,insp is enclosed by the upper and lower boundaries as defined in the box, from t_{start} to t_{end}. Vertical dotted lines represent start and end of inspiratory flow.*

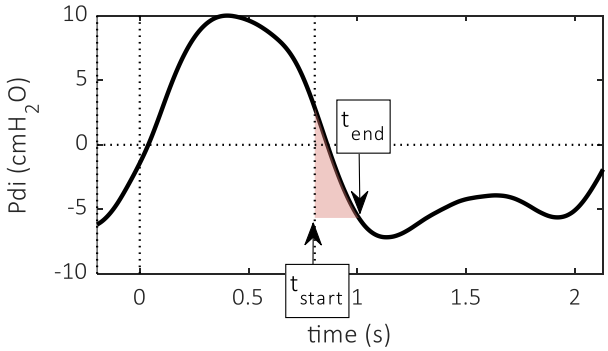

PTPdi,exp is enclosed by:

t_{start} *= end of inspiratory flow*

t_{end} *= first event of: a) return to Pdi baseline or b) first local minimum of Pdi*

Upper boundary *= Pdi signal*

Lower boundary *= Pdi baseline*

Figure 8: *Definition of the expiratory PTPdi, PTPdi,exp.PTPdi,exp is enclosed by the upper and lower boundaries as defined in the box, from t_{start} to t_{end}. Vertical dotted lines represent start and end of inspiratory flow.*

The gold standard for quantification of expiration effort is measurement of the Pga, including PTPga during expiration (PTPga,exp) [16, 43, 44]. For this PTPga,exp, the area is bounded by the 'baseline of Pga' [44] or 'the resting end-expiratory Pga from the preceding breath' [15], lacking a precise

definition. In our definition for PTPga,exp (**Figure 9**), expiratory Pga baseline was defined as the minimum Pga value during the first half of the expiration phase. The timing of this baseline value was also used as t_{start}, shown in **Figure 9**. Another factor affecting the PTPga,exp is the recoil pressure of the abdominal wall. While there is a standardized method to calculate a reasonably good estimate for the chest wall recoil pressure [13], this complex and not commonly known for the abdomen [45]. The measurements needed to determine abdominal compliance are outside of the scope of this study. Although abdominal pathology such as ascites can have a significant impact on respiratory mechanics [46], abdominal compliance is considered to have a negligible influence on the PTPga,exp. Therefore, a horizontal line of Pga baseline (Pga at t_{start}) is be used for calculating PTPga,exp, as described previously [16, 43, 44].

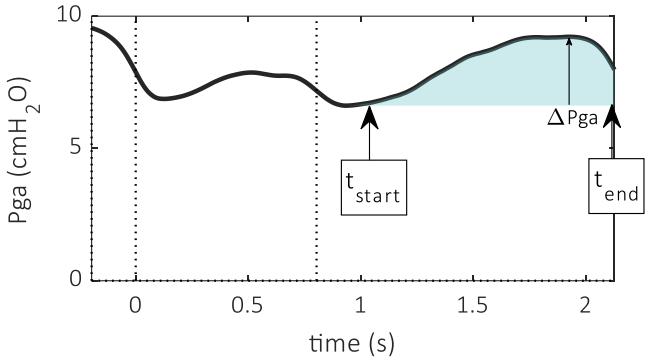

PTPga,exp is enclosed by:

t start *= Pga minimum in first half of expiration*

t end *= end of expiration*

Upper boundary *= Pga signal*

Lower boundary *= Pga at t_{start} (= baseline)*

Figure 9: *Definition of expiratory PTPga, PTPga,exp. PTPga,exp is enclosed by the upper and lower boundaries as defined in the box, from t_{start} to t_{end}. Vertical dotted lines represent start and end of inspiratory flow.*

In addition, several relative PTP parameters, based on the six PTP parameters defined above, can be derived from the six abovementioned PTP parameters. The sum of PTPdi,insp and PTPga,exp results in the total respiratory muscle effort (PTPtot, Eq. 10). This can also be used to calculate the relative contribution of the abdominal expiratory muscles to the PTPtot, defined in Eq. 11 [16].

$$\mathrm{PTPtot} = \mathrm{PTPdi,insp} + \mathrm{PTPga,exp} \qquad 10$$

$$\mathrm{PTPga,exp(rel,\%)} = \frac{\mathrm{PTPga,exp}}{\mathrm{PTPtot}} \qquad 11$$

For the other PTP parameters during expiration, PTPmus,exp(+) (Eq. 12) and PTPdi,exp (Eq. 13) their proportion relative to the total positive PTP is also defined, reflecting the percentage of the total PTP taking place during expiratory flow. Once more, the amount of effort during expiratory flow depends not only on the patient, but a large causative component is the cycle-off setting of the ventilator.

$$\mathrm{PTPmus,exp(+)(rel,\%)} = \frac{\mathrm{PTPmus,exp(+)}}{\mathrm{PTPmus,insp+\ PTPmus,exp(+)}} \qquad 12$$

$$\mathrm{PTPdi,exp(+)(rel,\%)} = \frac{\mathrm{PTPdi,exp}}{\mathrm{PTPdi,insp+\ PTPdi,exp}} \qquad 13$$

2.2.2.2 Respiratory inductance plethysmography

The excursion and synchrony of the thorax and abdomen during breathing will be measured using respiratory inductance plethysmography (RIP) straps. One strap placed around the thorax, under the armpits, and the other one around the abdomen, at the level of the umbilicus, enables us to measure the expansion of the compartments. Expansion stretches the RIP straps and influences the self-induction of the sinusoid wire coils within the straps. The phase angle differences (Θ) between the thorax and abdomen expansion can be evaluated and after adequate calibration also evaluation of lung

volume is possible [37, 47]. The method for determining the phase angle difference is shown in **Figure 10** and can also be defined as described in equation 14.

$$\phi = \frac{\text{time(A)} - \text{time(B)}}{\text{Ttot}} \cdot 360° \qquad 14$$

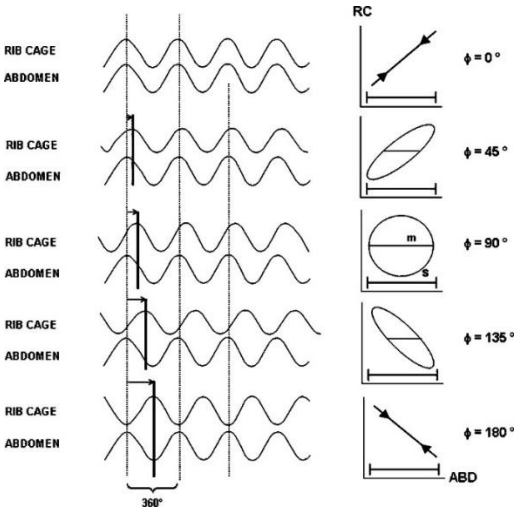

Figure 10: Phase angle analysis of rib cage and abdomen expansion. Phase angle phi can be expressed as sin ϕ= m/s where m is the length of the midpoint of the rib cage excursion and s is the length depicting the abdominal excursion, copied from [47].

2.2.2.3 Electromyography

Electromyography can be used to measure the electrical activity of the respiratory muscles. The depolarization of a muscle fibre membrane, caused by a flow of ions, generates an electric field outside the muscle fibre, which can be detected as voltage changes over time by recording electrodes [37]. All individual motor fibres of a motor unit are activated almost simultaneously, causing a motor unit action potential (MUAP). The observed interference pattern measured by EMG is a result of the number of active motor units, their firing rates and synchronization, the shapes of individual MUAPs and cancellation of opposite phase potentials. EMG measurements can be used for determination of the timing and level of muscle activation and in combination with pressure measurements, the electromechanical "efficiency" of the respiratory muscles can be determined.

Surface electrodes are used for measuring the abdominal wall muscles, the parasternalis intercostalis and optionally for the diaphragm in the measurements of Chapter 3. Their placement location is based on previous research [48-50]. The transverse abdominal muscle cannot be evaluated using sEMG as it is situated too deep to measure electrical activity [48, 49]. It is found that the best placement location for rectus abdominis and external oblique is respectively 3 and 15 cm para-midline of the umbilicus [48-50]. Different descriptions for the best location for internal oblique are reported, but placement below the external oblique electrodes and just superior to the inguinal ligament showed good prediction of transverse abdominis muscle activity [48-50]. The electrode placement as performed by Ito *et al.* (2016) is shown in **Figure 11** [48]. Unfortunately, the fact that sEMG always reflects the sum of different muscles in the area of the electrodes complicates completely separate recording of different abdominal muscles [48]. Therefore, in our experience, measurement of the RA and a sum of the EO, IO (and TRA) is often the most precise sEMG measurement that can be achieved. The electrical activity of the diaphragm (EAdi), can be recorded using sEMG, but a more sophisticated method is to use a nasogastric catheter [51]. Using the 'double subtraction method' for the signals from seven electrode pairs on the catheter, a relatively noise-free EAdi signal of the crural part of the diaphragm can be derived [52].

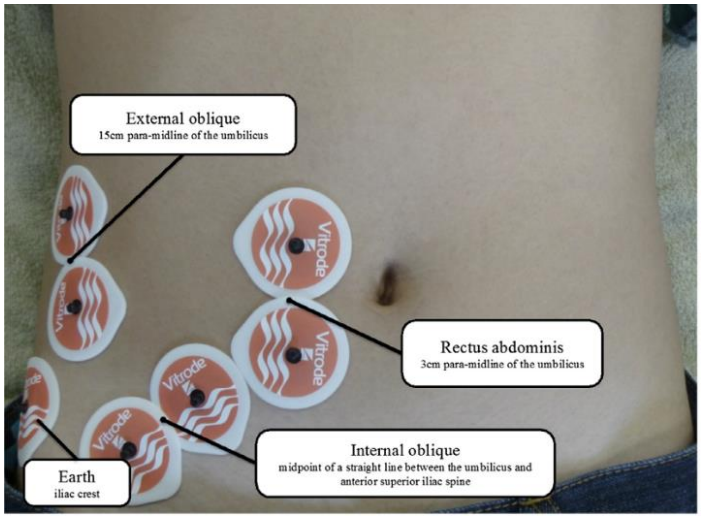

Figure 11: Placement locations of surface EMG electrodes of abdominal wall muscles as performed by Ito et al. (2016) [48].

2.2.2.3.1 Time domain analysis

EMG signals can be analysed in the time domain as well as the frequency domain. A common method to analyse in the time domain by use of the root mean square (RMS) of the signal, which reflects the power output of the muscle. This is used to quantify the existence and timing of activation of the expiratory muscles [53]. The onset and offset times resulting from this analysis can be used to calculated phase angles between activation of different muscles or muscle groups (e.g. expiratory muscles). Phase angle parameters represent the phase difference between two events relative to the total respiratory cycle.

2.2.2.3.2 Frequency domain analysis

Besides analysis in the time domain, EMG analysis in the frequency domain can provide greater insight in the muscle coordination and neural connectivity [54]. For frequency domain analysis, available analysis methods are power spectral density (PSD) and computing the centre frequency of the signal [54]. These frequency measures can give information on muscle fatigue [37]. A particular form of frequency analysis is coherence analysis, which we will get into more specific.

Coherence analysis is based on the cross-correlation of electrical physiological signals, such as electromyogram (EMG) and electroencephalogram (EEG). For our studies, only containing EMG signals, intermuscular or EMG-EMG coherence is most relevant. Intermuscular coherence can give insight in whether signals from different motor units share a common neural drive, because their activities are simultaneously influenced by and therefore synchronized by that common drive [54-56]. It is found that the same drive that leads to coherence between cortex and muscle also leads to coherence between the EMG signals of agonist muscles co-activated in the same task [57, 58]. Coherence yields the degree of linear dependence between respective signals in the frequency domain by use the formula in Eq. 15 [59-61].

$$MSC=\left|C_{xy}(w)\right|^2=\frac{\overline{\left|G_{xy}(w)\right|}^2}{\overline{G_{xx}(w)}\cdot\overline{G_{yy}(w)}} \qquad 15$$

In this formula, MSC is the magnitude squared coherence, G_{xx} and G_{yy} are the averaged power spectra of signals x and y throughout the segments in the frequency (w) domain, and G_{xy} is the averaged cross-power spectrum of signals x and y at frequency *w*. Coherence analysis results in a coherence value, ranging from 0 to 1, and indicates the strength of correlation, also seen as oscillatory coupling, between muscular activity of two muscles across the frequency spectrum [61]. Commonly used outcome measures of coherence analysis are frequency at which maximum coherence occurs, within

a frequency range specified beforehand. This can be the whole spectrum of interest for EMG signals, which starts at 15 Hz and up to 230 Hz [62] or even 500 Hz [54]. Also a more narrow frequency range can be chosen, for example Bèta band (15-30 Hz) [60] or Gamma (30-60 Hz) [59]. Besides frequency at which maximum coherence occurs, the coherence value itself at a specified frequency can also be used as an outcome measure. Another possibility is to calculate the area under the coherence curve (and above 95% confidence limit) as the outcome measure, within a specified frequency range (e.g. Bèta band) [61].

In the coherence analysis some specific problems of recording and interpretation should be considered. As coherence is a measure of linear dependence between two signals in the frequency domain, one should be careful that common artefacts in analysed channels lead to high coherence values over the relevant frequency band. These artefacts, such as mains interference, occur with zero phase delay, while biological signals would be expected to demonstrate phase differences. Regarding the equipment, surface EMG is the most practical way of recording and besides that, sEMG records multiple motor units. However, it may be limited by volume conduction between muscles, which can be ruled out if there is a constant phase lag between the two EMG signals in the range of significant coherence. Therefore, ideally, separated muscle pairs are studied to assure a phase lag [60]. For coherence analysis often rectification of the EMG signal is proposed as a pre-processing step. However, it is also argued that due to the nonlinear operation of rectification (negative phases of the raw signal are transformed into positive values) new frequency ranges arise, which were not present in the raw signal. Farina *et al.* (2013) have shown that in some cases it may be a necessary pre-processing step to identify oscillatory common inputs, but this depends on the degree of cancellations [63].

Currently, there is only limited research on coherence of respiratory muscles. The mechanisms causing intermuscular coherence are also not yet fully understood [55]. Results are limited to three studies, from one research group in Alberta [59, 61] and one older study from Smith and Denny [62]. These studies found that chest wall EMG signals changed with task-dependent muscular demand, with relatively higher expiratory muscular demands showing significantly greater coherence compared with tasks requiring relatively lower muscular demands. They found that coherence occurred at higher frequency with increasing muscular demands as well [59]. Earlier, the same researchers demonstrated that motor cortex control of the chest wall during voluntary expiration, varies as a function of different breathing tasks. Based on these findings, they concluded that intermuscular coherence is, in part lung volume excursion dependent [61]. The study from 1990 showed that in deep breathing, significant coherence was present in ranges 20-60 Hz and in 60-110 Hz range during voluntary controlled breathing. Across different tasks, the same levels of coherence persisted in the 20-60 Hz range, while in the 60-110 Hz range the coherence was significantly reduced in speech and speech-like breathing compared to deep breathing [62].

2.2.2.4 Ultrasound

The ultrasound machine has obtained a prominent position in the ICU, as it is a safe, easy and bedside tool for diagnosing numerous diseases. Ultrasound is often used for monitoring respiratory muscles [64]. Thickness of the respiratory muscles as measured by ultrasound gives insight in the amount of atrophy [8]. To quantify contractile activity thickening fraction can be used [64, 65]. Recent studies also show that ultrasound can give insight in the role of the expiratory muscles [33]. Besides these straight-forward measurements of thickness and thickening fraction, also several new and sophisticated ultrasound techniques are available, such as tissue Doppler, speckle tracking and echogenicity analysis [65]. Echogenicity analysis is discussed and investigated in Section 5.

3 Assessing coordination of the respiratory muscles during a spontaneous breathing trial

observational clinical study

3.1 Introduction

Research on the respiratory muscle pump in mechanically ventilated patients has mainly focused on the diaphragm as the main inspiratory muscles. As described in section 2, VIDD is related with worse outcome [5, 6, 8, 29]. However, over the past decades, the interest in the role of the expiratory muscles in mechanically ventilated and critically ill patients has increased [15, 33]. Expiratory muscles are recruited when respiratory load increases, and their strength determines coughing ability and so the readiness for ventilator liberation [27, 32].

Doorduin *et al.* (2018) found that weaning failure is associated with increased effort of the respiratory muscles in tidal breathing during a spontaneous breathing trial (SBT). They concluded that monitoring of the expiratory pressure-time-product of the gastric pressure signal (PTPga,exp) is an important aspect of the energy expenditure during an SBT. As this study only measured pressure signals and diaphragm electromyography (EAdi), the results do not give insight in the timing coordination between inspiratory and expiratory muscles [16]. Other research, investigating the recruitment pattern of extradiaphragmatic inspiratory muscles, showed increasing electrical activity of extradiaphragmatic muscles when decreasing pressure support [53].

In the study of Laghi *et al.* (2014), the role of extradiaphragmatic muscles during respiratory loading was explored in healthy subjects, as it is hypothesized that recruitment of extradiaphragmatic muscles protect the diaphragm against contractile fatigue and improve diaphragmatic neuromechanical coupling by limiting diaphragmatic shortening. Among other results, it was found that increased loading caused a growing contribution of extradiaphragmatic muscles (ΔPga/ΔPes ratio) and expiratory muscle recruitment, suggesting that loading triggered a coordinated action of extradiaphragmatic muscles. During loading a progressive increase in EAdi and diaphragmatic neuromechanical coupling was found, accompanied by an increase in phasic activity of the abdominal wall muscles during inhalation. This finding suggests the presence of post-expiratory expiratory muscle recruitment, which should still be investigated in patients, in whom abnormal pulmonary mechanics and pathophysiological processes could alter these mechanisms [18]. To investigate these phenomena in patients and get additional insight in the timing coordination of both inspiratory and expiratory muscles, similar measurements should be performed, but should be expanded with EMG of the muscles of interest and RIP measurements.

At last, the activity of the diaphragm during the expiratory phase of breathing, as stated by Pellegrini *et al.* (2017), in critically ill is of interest [19]. However, Doorduin *et al.* (2018) did not find a change in tonic or electrical diaphragm activity in patients during an SBT [16]. To properly investigate the activity of the diaphragm during expiration, the raw EAdi signal is needed. This was used by Doorduin *et al.* (2018) but not by Pellegrini *et al.* (2017).

Therefore, the aim of this physiological study is to expand the physiological knowledge of the coordination of the respiratory muscles, with a specific focus on the expiratory muscles and the expiratory phase of breathing. To do so, detailed measurements of pressure, muscle electrical activity and torso movement are carried out to investigate the functional and timing coordination between respiratory muscles during the increased respiratory load of an SBT [16, 18, 27]. Electromyography also allows us to study the coordination of respiratory muscles more extensively by investigating the

coherence between muscle groups [59]. The resulting parameters can help in understanding the coordination of respiratory muscles in the expiratory phase of breathing and thereby play a role in determining the direction of future research.

3.2 Methods

3.2.1 Subjects

Patients were eligible for this study if they were mechanically ventilated in PS or NAVA-mode and had a dedicated catheter for measuring oesophageal and gastric pressures (Nutrivent, Sidam, Italy) in situ for clinical reasons. An extra catheter for measuring electrical activity of the diaphragm (EAdi) was desired, but not required. However, patients with an EAdi-catheter, were also enrolled when they had solely an oesophagus balloon catheter (Cooper surgical, Inc., Trumbull, USA). Further inclusion criteria were a minimum age of 18 years, informed consent and the readiness for an SBT as per the decision of the clinical team. Exclusion criteria were a past medical history of neuromuscular disorders, a BMI > 30 kg/m^2 as this impedes surface electromyography (sEMG) measurements and/or inability for placing sEMG electrodes due to drains or wounds. This explorative physiological study aims to include 20 patients.

3.2.2 Measurement setup

The following signals were measured and recorded simultaneously via a dedicated measurement setup (BIOPAC MP160, BIOPAC Inc., USA): airflow, airway pressure (Pao), oesophagus pressure (Pes), gastric pressure (Pga), respiratory inductance plethysmography from the thorax (RIP_{thorax}) and abdomen ($RIP_{abdomen}$), raw EAdi (8 separate electrode pairs), surface electromyography (sEMG) of the parasternalis intercostalis (PS), rectus abdominis (RA), sum of the external and internal oblique (OBL) at the left and the right side of the abdomen and of the diaphragm (DI) when EAdi catheter was absent. Airway pressure, flow, and filtered EAdi signal were recorded from the Servo-U ventilator (Getinge, Solna, Sweden) as well using Servo-tracker software (release 4.2, Getinge, Solna, Sweden). Patients in isolated rooms (due to Covid-19 or other infection risk) were included, however, due to hygiene regulations, RIP measurements were left out.

The position of the oesophagus balloon was confirmed using Baydur manoeuvre [66] and with the presence of cardiac pressure artifacts in the Pes signal. The position of the gastric balloon was confirmed by applying external pressure on the abdomen and making sure gastric pressure increases at the moment of patient inspiratory effort as it would do when the balloon is positioned in the stomach. Additionally, cardiac artefact should be less prominent in gastric compared to oesophagus pressure. EAdi catheter positioning was done using the tool provided on the Servo-U ventilator.

3.2.3 Experimental protocol

Before the start of the SBT, the measurement started with recording all signals at clinical ventilator settings at that point. After 30 minutes of measuring the 'status quo', the SBT started by turning the support level to 0 cmH2O and keeping the PEEP setting equal. Measurements were executed for 30 minutes during the SBT, or until SBT failure. SBT failure was defined as respiratory rate >35 breaths/min, oxygen saturation <90%, heartrate >140 beats/min or an increase >20% from baseline, systolic blood pressure >180 or <80 mmHg or a change of >20% from baseline, and the subjective signs of increased work of breathing or distress, according to international criteria [31].

3.2.4 Data acquisition

The signals measured with BIOPAC measurement setup were sampled at a sampling frequency of 2000 Hz. Servo-tracker saved ventilator waveforms with a sampling frequency of 100 Hz. All signals were loaded into MATLAB R2020b (Mathworks®, Natick, Massachusetts) and saved in an organized data file structure. Ventilator waveforms were resampled at 2000 Hz and synchronized with BIOPAC

signals using the time delay between airway pressure peaks during an occlusion manoeuvre. The minor time delay between the signal from the two BIOPAC MP160 hardware units was rectified by used of the ECG in both the raw EAdi and the sEMG of the PS signals.

In addition to the physiological measurements, other parameters are demographics (age, sex, BMI), daily dosage of drugs with known adverse effect on muscles (sedatives, corticosteroids and neuromuscular blockers), fluid balance, protein intake, primary reason for mechanical ventilation, ventilator settings, reason for PEEP removal at time of measurements during PEEP removal, weaning outcome (success, days taken to wean, attempts of spontaneous breathing trials, hours tolerated without ventilator support) and ICU readmission.

3.2.5 Signal pre-processing

From the eight electrode pair signals measured from the EAdi catheter, a single EAdi signal is constructed using the double subtraction method [52]. To reduce ECG interference in the EAdi and sEMG signal, an adapted version of the template subtraction method is used. This method involves detection of ECG interference and subtracting an average QRS segment, of which the peak heights are individually scaled [67]. When detection of ECG on raw EAdi signal was not effective, the parasternalis sEMG signal is used for detecting the ECG location. The window length around R peak was adjusted when prominent P and/or T waves are present. For the sEMG signals in which ECG detection was not effective, solely the wavelet-based adaptive filtering was used. After band pass filtering (4^{th} order Butterworth between 2 and 150 Hz), the envelope signal of sEMG and EAdi was calculated as the moving average (window size 400 samples = 200 milliseconds) of the RMS of the filtered signal.

Pressure signals (Pes, Pga, Pao) were band pass filtered using a 2^{nd} order Butterworth filter (cut-off 0.3 to 10 Hz) and a moving average filter of 33 milliseconds. The baseline of the signals was restored by adding the median of the signal after filtering. Transdiaphragmatic (Pdi) and dynamic transpulmonary ($P_{L,dyn}$) pressure was calculated after filtering as Pga – Pes and Pao – Pes respectively [13, 37]. Flow signal was also filtered using a moving average filter of 33 milliseconds, and offset was calculated and removed by use of the volume (= cumulative sum of the flow signal). The volume signal was filtered further using a 4^{th} order high-pass Butterworth filter with a cut-off of 0.05 Hz. For Pmus calculation, the chest wall recoil pressure (Pcw) is calculated as the filtered volume divided by the chest wall compliance. Chestwall compliance is estimated as 4% of the estimated vital capacity [13, 37].

3.2.6 Data analysis

Inspiration and expiration phases were based on flow zero-crossings. Inspiratory and expiratory occlusions, “double inspirations”, coughing and oesophagus spasms where excluded. Since the subjects are connected to the mechanical ventilator, the timing of the start of inspiratory flow depends on the ventilator, triggered by inspiratory effort of the patients. Therefore, the start of inspiratory effort in Pes, Pdi, envelope of EAdi and sEMG signals is detected by a mathematical algorithm. Thereafter, the earliest starting point of flow, EAdi, Pes or Pdi is be used as the starting point of the breath. Breaths are excluded from analysis if EAdi envelope decreases (slope < -2 μV/s) in the period from 40 to 200 ms after detected starting point, indicating residual interference of ECG despite extensive filtering.

3.2.7 Outcome measures

The outcome measures discussed in the next sections are calculated for pre-defined intervals. Considering the failure of some of the subjects before the SBT duration of 30 minutes, the signal of the SBT is divided into five parts of equal length. At the start and the end of the 30-minute period before SBT, and (if present) the period after the SBT an analysis interval of equal length is chosen.

3.2.7.1 Functional coordination parameters

After filtering, optimizing start and end time of breaths, and checking validity of breaths, for every breath within the analysis intervals separately, numerous parameters are calculated. Inspiratory time

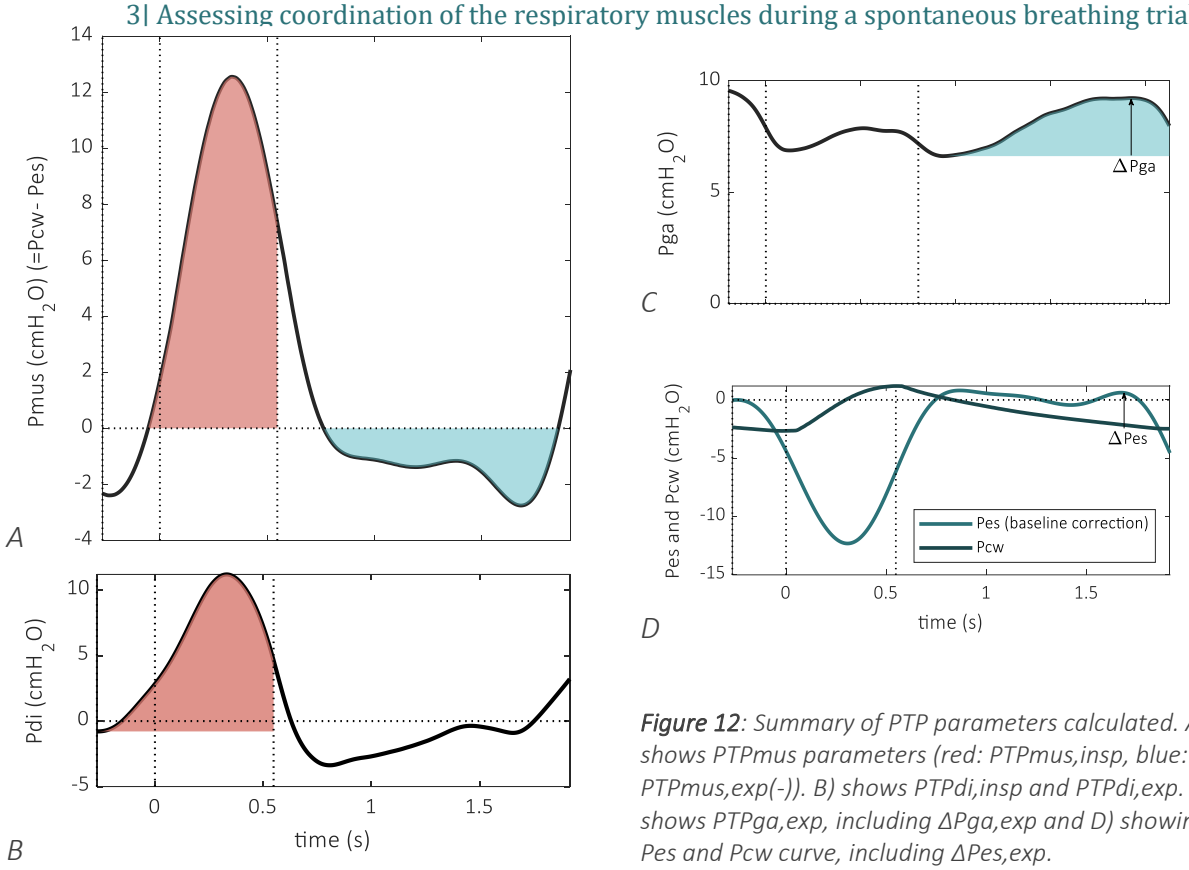

***Figure 12**: Summary of PTP parameters calculated. A) shows PTPmus parameters (red: PTPmus,insp, blue: PTPmus,exp(-)). B) shows PTPdi,insp and PTPdi,exp. C) shows PTPga,exp, including ΔPga,exp and D) showing Pes and Pcw curve, including ΔPes,exp.*

(Ti) and expiratory time (Te) are flow based, and the combination of these two gives the total respiratory time (Ttot) and respiratory rate (RR = 1/Ttot). Combined with the inspiratory tidal volume – calculated as the cumulative sum of the flow – the minute ventilation can be calculated. The difference between Pmus at the start of Pes decrease and peak Pmus results in the inspiratory Pmus delta (ΔPmus), which is corrected for the Pga rise in the previous breath [17, 68]. Similarly, inspiratory ΔPes and ΔPdi are calculated as the difference between the pressure at start and the minimum and maximum respectively [13]. The expiratory rise in Pga (ΔPga,exp) is calculated as the rise of Pga during expiration after its expiratory baseline value, which is define as the minimum during the first half of expiration [16]. For the same purpose (measuring expiration muscle effort), the rise of Pes above Pcw during expiration (ΔPes,exp) is calculated as the maximum exceeding of Pes above Pcw, shown in **Figure 12**D. The tonic activity of the diaphragm at the start of expiratory flow (Pdi,end-insp) is calculated as the Pdi value at the end of inspiratory flow, minus the Pdi value at the start of Pdi activity (Pdi baseline). This is also calculated as a percentage of peak Pdi. As described in background section 2.2.2.1, total work of breathing is calculated per breath. Also expiratory work of breathing is calculated, defined as the part of the P-V loop exceeding the Ccw line [13, 69].

The pressure-time-product (PTP) parameters (PTPmus,insp, PTPmus,exp(-), PTPdi,insp, PTPdi,exp, PTPga,exp, and PTPga,exp,rel) are calculated as described in background section 2.2.2.1. A summary of these parameters is shown in **Figure 12**A-D. The PTP parameters are calculated per breath but are reported over a one minute interval (cmH_2O*s/min), by use of the respiratory rate of that specific breath. Diaphragm activity (EAdi) is determined at peak EAdi, the start of expiratory flow and the start of Pes increase at the end of inspiration. This is also done for EAdi filtered by Servo ventilator, if present. The area under the EAdi curve (AUC) is calculated for flow-based inspiratory time and for the total EAdi wave. The end point of the EAdi curve is chosen as the point at which it returns to baseline or the first local minimum after peak EAdi. The neuromechanical efficiency (NME) is calculated as Pdi/peak EAdi. When Pdi was not available, it was substituted by Pmus.

3.2.7.2 Timing coordination parameters

To quantify timing coordination, phase angle (PA) parameters are calculated. PA shows the delay between two events (A and B) within the respiratory cycle, relative to the total time of the respiratory

cycle (Ttot). Phase angle is expressed in degrees and can be calculated using equation 14 in section 2.2.2.2. Phase angle between inspiratory muscle activity and functional inspiration (flow/pressure), expiratory muscle activity and functional expiration and between inspiratory and expiratory muscle activity are calculated. The phase angle parameters reported in the preliminary results are shown in **Table 1**. The timing of these events in the different signals is also illustrated in Figure 13. Different end points of diaphragm activity are used; peak value, decrease to 70% of the peak [21] and decrease to zero or baseline.

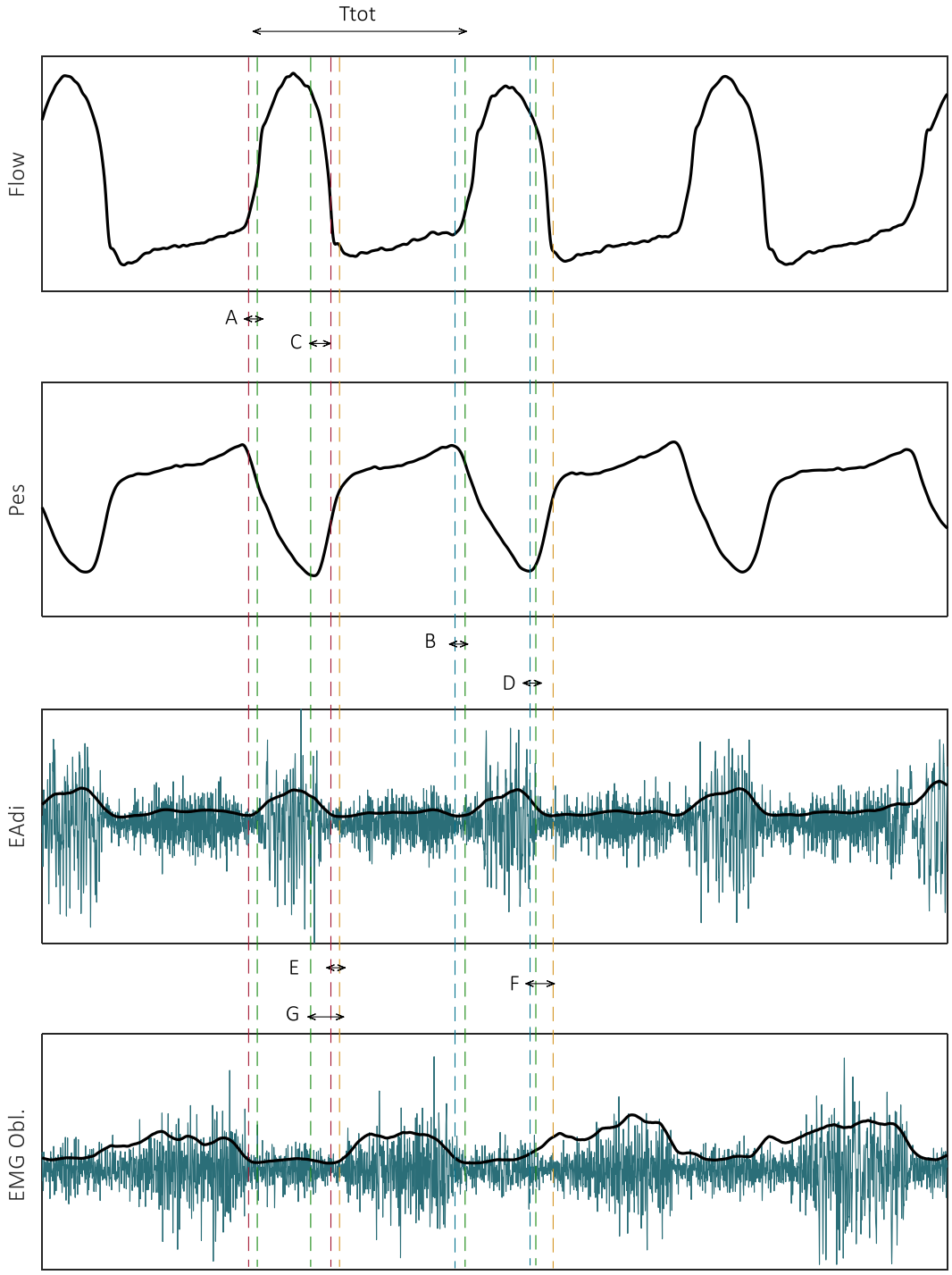

***Figure 13**: Flow, Pes, inspiratory EMG (diaphragm) and expiratory muscle EMG (oblique) are plotted. For the EMG signals, raw (blue) as well as RMS (black) is plotted. Dashed lines represent start and end of inspiratory flow (red), start of Pes decrease and start of Pes increase (blue), start of EAdi and decay to 70% (green) and start of oblique activity (yellow). Letters correspond to the most right column of Table 1.*

Table 1: Phase angle parameters. Letters in right column correspond to letters in Figure 13.

Event A		Event B	Prerequisite	Fig.
Onset EAdi	-	Onset flow		A
Inspiratory Pes decrease	-	Onset EAdi		B
Expiratory flow start	-	EAdi 70%		C
Pes increase (end inspiration)	-	EAdi 70%		D
Expiratory flow	-	Obliques activation start	*Expiratory effort present*	E
Pes increase (end inspiration)	-	Obliques activation start	*Expiratory effort present*	F
EAdi 70%	-	Obliques activation start	*Expiratory effort present*	G

3.2.7.3 EMG coherence

For the coherence analysis, all EMG signals (diaphragm as well as sEMG) are wavelet filtered and high pass filtered with a 4th order Butterworth filter with a cut-off frequency of 2 Hz. The intervals at which an ECG artefact was present (determined by the template subtraction algorithm) were not included in the coherence analysis (by replacing these periods with 0) to prevent overestimating coherence caused by frequencies from the ECG. For the coherence analysis the segment length was 2^{11} samples, which is 1.024 seconds. The area under the coherence curve in the Alpha (8-12 Hz), Bèta (15-35 Hz) and Gamma (35-60 Hz) frequency band are calculated per analysis interval, as well as the frequency at which peak coherence occurred.

3.2.8 Statistical analysis

The preliminary results are presented as boxplots, which a separate box for each analysis interval (duration 20% of SBT). The central mark of a box (ranging from 25th to 75th percentile) indicates the median, the whiskers extend to the most extreme data points not considered outliers. Outliers are plotted with a plus (+) symbol. For the preliminary results, intervals were compared by computing the distribution (95% confidence interval) for the difference of the means (at the 0.05 significance level) between analysis intervals per subject. In the final results, mean values per interval per subject will be analysed by a two way ANOVA with factors group (SBT failure or success) and time (interval of SBT).

3.3 Preliminary results

At the current moment, two patients have been included in this study. Therefore, only preliminary results of these patients are presented. Because of the sample size of two, the nature of the results is mainly descriptive. Besides that, due to the differences in missing signals (Pga in subject 1 and oesophageal EAdi in subject 2), the results of these subjects are discussed separately. In Appendix 8.1.2 and 8.1.4 a summary table can be found, with the means of all parameters per analysis interval.

3.3.1 Subject 1

The first subject included in this study was a male subject of +- 75 years old (BMI 20.5). He was diagnosed with a COVID-19 pneumonia and mechanically ventilated for 38 days at the moment of the study. For this subject, the study SBT was the first SBT attempt. At the moment of the study, ventilation in NAVA mode was used, with a PEEP of 8 cmH_2O. Regardless of a first attempt of study measurements on pressure support mode (according to the protocol), discomfort and systolic hypertension forced us to return to NAVA mode. Therefore, measurements were performed with 30 minutes on present NAVA settings, and thereafter an SBT with NAVA level on 0. SBT Failure occurred after 16:40 minutes, reflected in an increase in end-tidal CO2 (around 7 kPa to 10 kPa), increasing heart rate from 100 bpm to 120 bpm and visibly increased breathing effort. Subdividing the SBT interval resulted in analysis window sizes of 3:20 minutes (**Figure 14**). Thus, every box in the following boxplots represents all the breaths within a 3:20 min analysis window. RIP measurements were omitted and

this patient had no gastric balloon in situ. Thus, measurement included Pao, flow, Pes, EAdi and sEMG of abdominal and parasternalis intercostalis muscles.

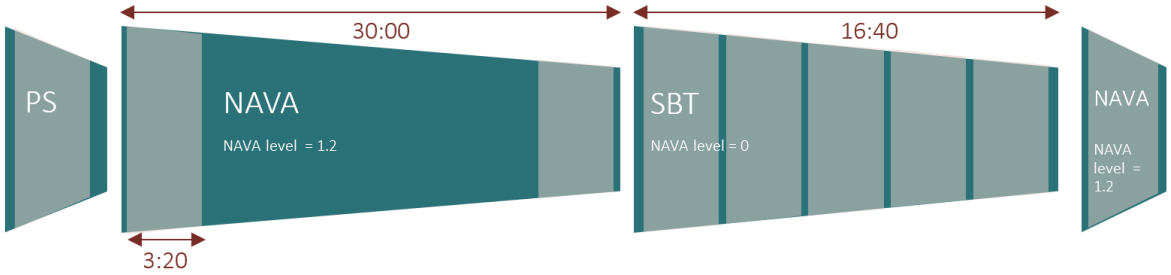

Figure 14: Timeline of measurements in subject 1. A short period of pressure support ventilation was followed by 30 minutes of NAVA. The SBT failed after 16:40 minutes. Analysis intervals are 3:20 minutes and are depicted as highlighted periods.

3.3.1.1 Functional coordination

The results of the minute ventilation show that the minute ventilation decreases during the SBT, and remains within the same range during the SBT (**Figure 15**). The decrease in minute ventilation during the SBT is mainly caused by a decrease in tidal volume, which decreases from approximately 900 to 750 mL after starting the SBT (Appendix 8.1.1.1). The respiratory rate remains the same (Appendix 8.1.1.1). Inspiratory time during NAVA mode slightly increased compared to PS (Appendix 8.1.1.1).

The Pmus pressure swings are shown in **Figure 15**B. A rise of the pressure swings during the SBT (ca. 33 cmH_2O) compared to the NAVA period before (ca. 31 cmH_2O) can be seen. A small decrease of Pmus swings can be seen when changing from PS to NAVA before the SBT. During the PS phase, the ventilator assist was lower (airway pressure swings were smaller during PS). Pes swings (Appendix 8.1.1.1) show a similar pattern, with Pes swings consistently around 5 cmH_2O lower than Pmus, explained by the Pcw component in Pmus. While there are clear changes between the periods, it is questionable whether a change of 2 to 3 cmH_2O on a total pressure swing of around 30 cmH_2O is clinically relevant. Furthermore, the absolute Pes (and Pmus) swings surpass values that are thought to be a physiological and safe range [4, 14]. The respiratory effort parameters (PTP and WOB) are shown in **Figure 16**. The inspiratory PTPmus (16A) slightly increases during the SBT compared to the period before, but does not continue to increase over the duration of the SBT. Total WOB (16C) does not remarkably change

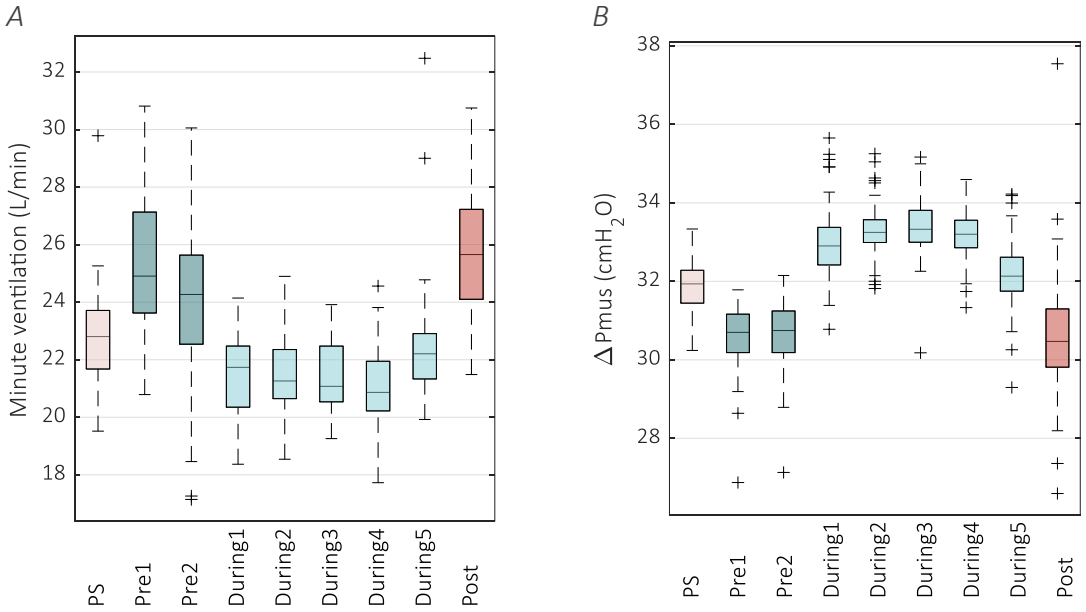

Figure 15: Basic respiratory parameters for the whole experiment, calculated for every breath separately. Figure A) shows minute ventilation for every analysis window. Figure B) shows inspiratory Pmus swings.

during the SBT, but in the pressure support phase before the NAVA period, a lower WOB is found compared to NAVA. Although expiratory WOB (16D) is a small component of total WOB, it increases during the SBT, showing a similar pattern as for PTPmus,exp(-) (16B) and also expiratory Pes rise (Appendix 8.1.1.1). Namely, a rise in Pes above Pcw is detected in this patient, although no expiration muscle activity was detected by EMG.

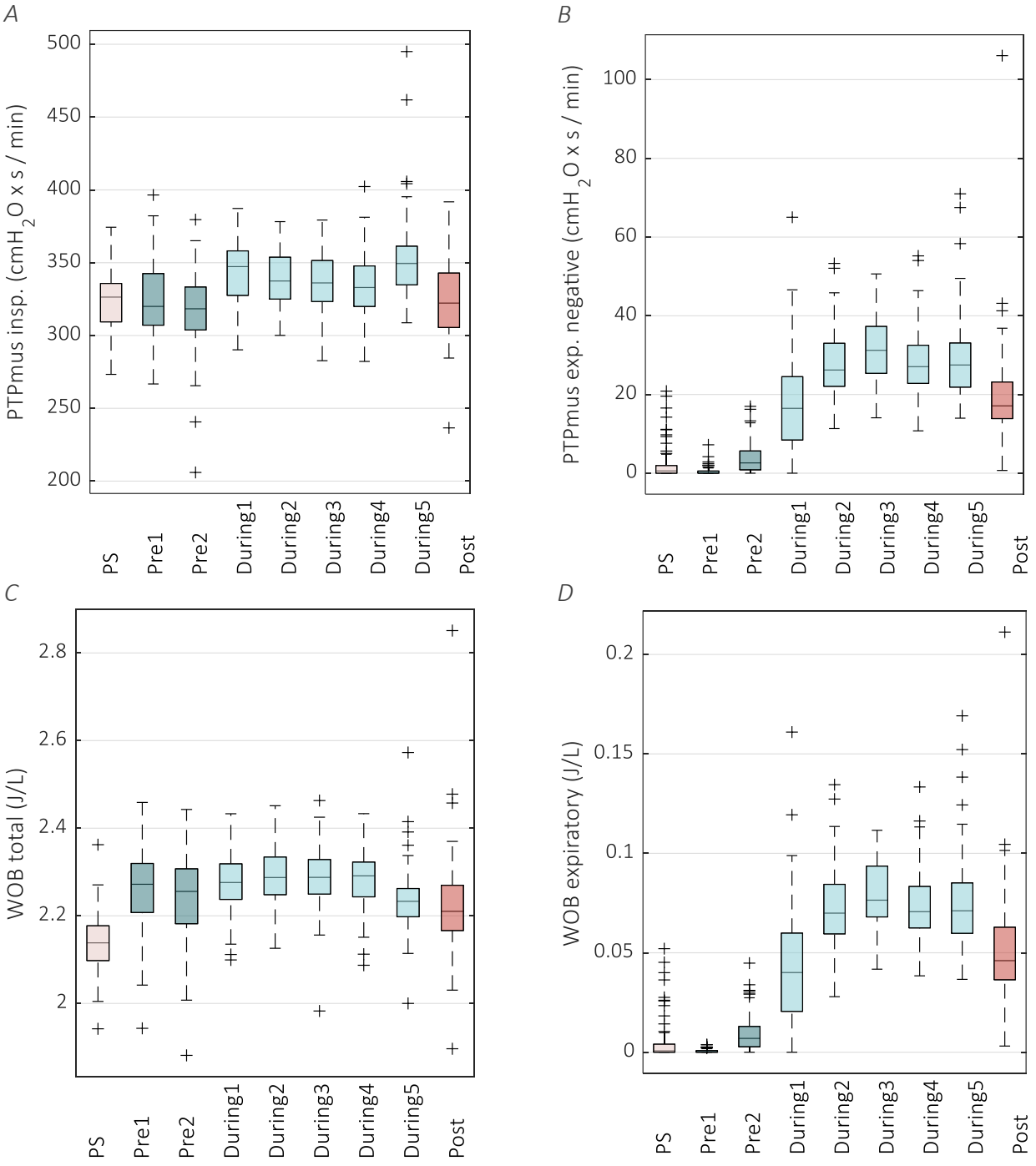

***Figure 16**: Parameters on respiratory effort, **A)** delta Pmus in cmH₂O, **B)** total PTP in cmH₂O*s/min, **C)** total WOB in J/L and **D)** expiratory WOB in J/L during the analysed time windows.*

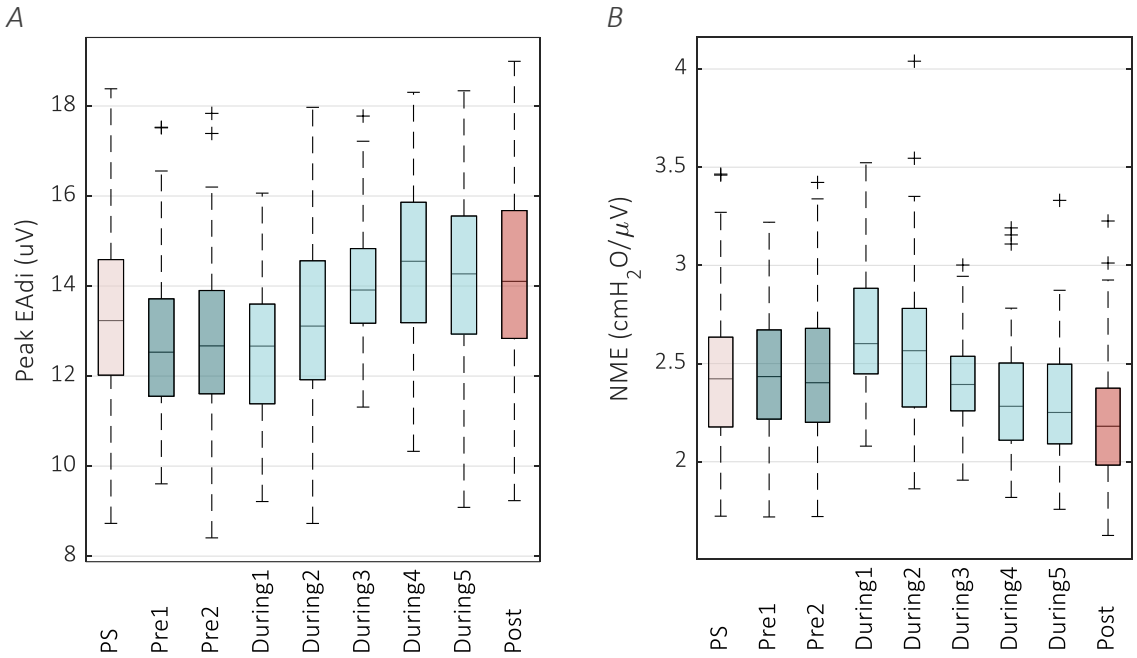

*Figure 17: Boxplots for diaphragm activity. Figure **A)** shows peak of the raw EAdi. Figure **B)** shows the neuromechanical efficiency, defined as ΔPmus/peak EAdi*

Figure 17A shows the peak of the EAdi, which is increasing over the duration of the SBT. While the EAdi increases, Pmus remains relatively stable and slightly decreases at the end of the SBT. As a consequence, the NME, shown in **Figure 17**B, decreases over the duration of the SBT. EAdi at other time points during the respiratory cycle (start of Pes increase and start of expiratory flow also show small increases over the duration of the SBT, and can be found in Appendix 8.1.1.2. Some notable differences between EAdi derived from raw signal and EAdi of servo tracker are described in Appendix 8.1.1.2.

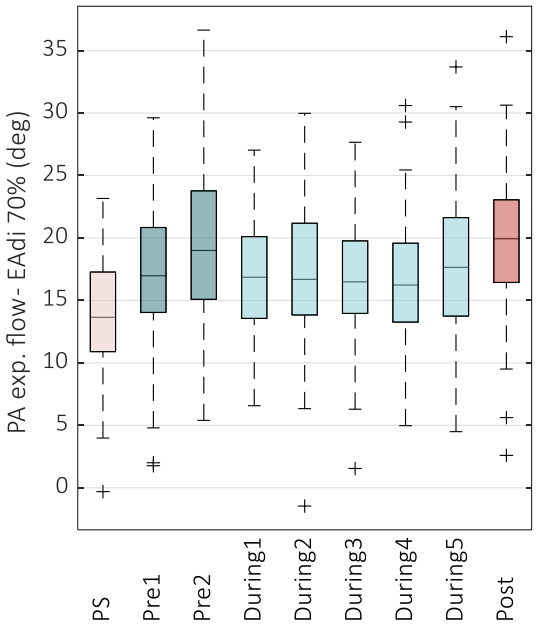

Figure 18: Boxplots for one of the phase angle results, showing phase angle between the start of inspiratory flow and the start of EAdi,

3.3.1.2 Timing coordination

The primary interest of the timing coordination analysis was the timing between inspiratory and expiratory muscles. Since no expiratory muscle activity was present in tidal breathing in the measured patients, only timing coordination results of the diaphragm are analysed. The phase angle between EAdi end (70% of peak EAdi) and the start of expiratory flow is around 17 degrees and does not change over the duration of the SBT (**Figure 18**). The PA between Pes increase and EAdi end (defined as decrease to 70%) also remains stable during the SBT at around -4 degrees (Appendix 8.1.1.3). The PA results between EAdi and inspiratory flow (Appendix 8.1.1.3) and inspiratory Pes onset (Appendix 8.1.1.3) show larger variability and are circa 50 degrees, but with outliers up till ca. 150 degrees. Hence, diaphragm activity always starts before the start of inspiratory flow and the start of Pes decrease.

3.3.1.3 EMG coherence

Since the first subject did not show abdominal muscle activity, the coherence results are shown in Appendix 8.1.1.5. The majority of coherence areas increase over the duration of the SBT. The alpha coherence area was highest between the parasternalis intercostalis and the oblique abdominal muscles, showing a similar pattern for the oblique muscles left and right. In the beta range, the coherence between the inspiratory muscles (parasternalis and diaphragm) appeared to have the largest area and increases over the duration of the SBT (and thereafter). Meanwhile, the other expiratory-expiratory and inspiratory-expiratory coherence areas do not increase or slightly decrease. The coherence in the gamma band shows high values (also compared to alpha and beta area) for the diaphragm and the left oblique, but not for the right oblique. Therefore, the validity of this result is questionable. Peak coherence values and detailed coherence results per interval for one specific muscle combination (diaphragm and obliques) can be found in Appendix 8.1.1.4.

3.3.2 Subject 2

The second subject was a +- 65 years old female (BMI 25.2), diagnosed with a COVID-19 pneumonia with subsegmental pulmonary embolism. The measurements were performed after 18 days of mechanical ventilation. The day before the study measurements the subject already went through a CPAP trial and prior to the measurements the ventilator settings were PS 5 over PEEP 10. During the first 30 minutes measurement, the support was increased to 7 cmH_2O after 15 minutes. The SBT was successful, resulting in 5 analysis windows of 6 minutes (with a total recorded duration of 30 minutes SBT), summarized in **Figure 19**. Thus, every box in the following boxplots represents all the breaths within a 6 minute analysis window (20% of SBT duration). RIP measurements were omitted and this patient had no EAdi catheter in situ. Thus, measurements included Pao, flow, Pes, Pga and sEMG of diaphragm, abdominal muscles and parasternalis intercostalis muscle.

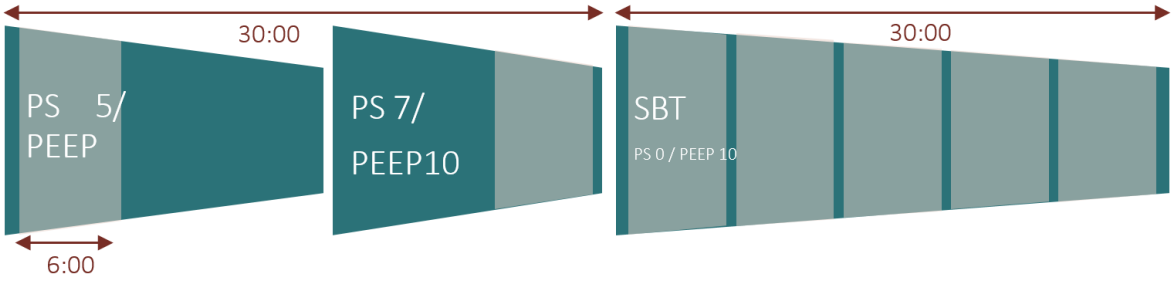

Figure 19: Timeline of measurements in subject 2. During pressure support period, the support was increased from 5 to 7 cmH_2O half-way through the 30 minute recording before the SBT. SBT was successful, resulting in 30 minutes SBT measurements. Every box represents an analysis intervals of 6 minutes.

3.3.2.1 Functional coordination

The results of the minute ventilation in **Figure 20**A show fluctuations during the measurement. This can also be seen in the respiratory rate (Appendix 8.1.3.1), fluctuating between 23 to 26 breaths per minute, while the tidal volume sustains at around 1000 mL. Nevertheless there is no continuous increase or decrease over the duration of the SBT. The pressure support increase from 5 to 7 cmH2O in the second half of the period before the SBT does cause an increase in tidal volume from around 1000 mL to 1100 mL. The inspiratory pressure swings (**Figure 20**B and C) during the experiment show an effect comparable to the minute ventilation and respiratory rate. Inspiratory pressure swings of Pmus and Pdi both increase in the second analysis interval of the SBT, but they also all decrease again in the interval thereafter. This is also found for the Pes pressure swings, shown in Appendix 8.1.3.1. From the fact that inspiratory Pdi swings are lower than Pes swings, it can be deduced that the Pga also decreases during the inspiration, perhaps due to relaxation of the abdominal muscles.

Concerning the pressure swings that quantify expiration effort, a decrease of the Pga rise during expiration (ΔPga,exp, **Figure 21**A) is found at the start of the SBT. However, the ΔPga,exp increases again to the level during pressure support and a slightly higher level during the fourth part of the SBT. This is also the case for the expiratory rise of Pes above Pcw (Appendix 8.1.3.1). The absolute Pdi at the start of expiratory flow shows a different, decreasing trend which can be seen in **Figure 21**B. At the end of the SBT, Pdi(end-insp) decreased significantly from 12.7 to 7.4. Whilst the total Pdi swings are also smaller during the 5th interval of the SBT, the decrease in Pdi cannot be explained by this, as the relative Pdi at sthe start of expiration compared to the total Pdi swing during inspiration decreases from a median of nearly 60% before the SBT to 36% during the 5th interval (Figure is shown in Appendix 8.1.3.1).

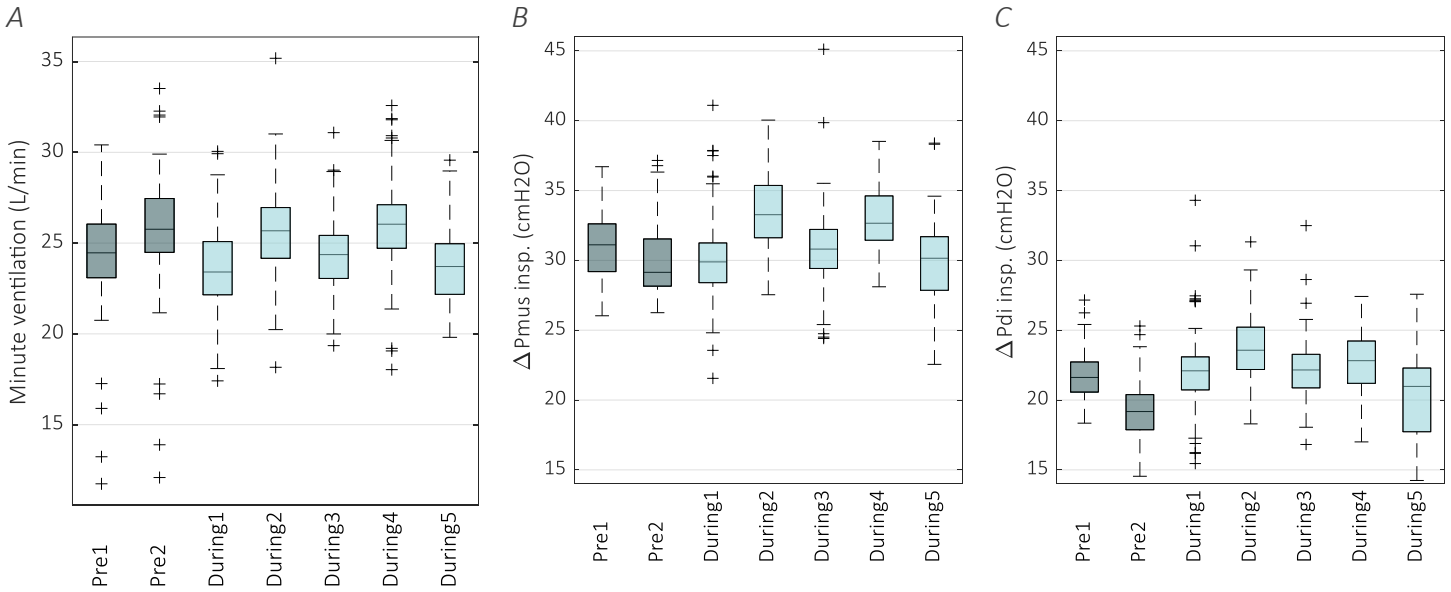

*Figure 20: Boxplots for the inspiratory pressure swings. **A)** shows minute ventilation for every analysis window, **B)** inspiratory Pmus swings and **C)** inspiratory Pdi swings.*

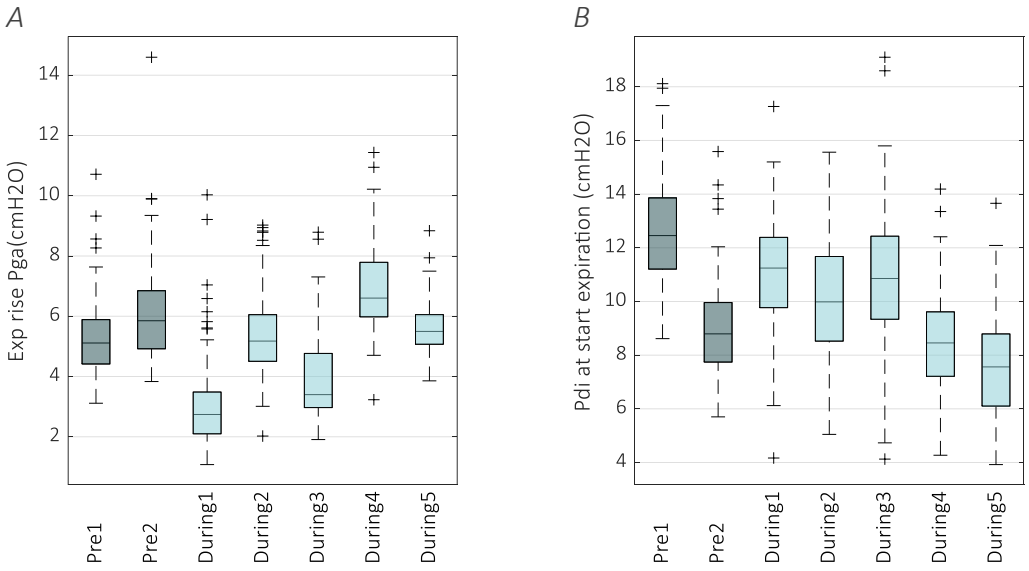

*Figure 21: Boxplots for the expiratory pressure (swings). **A)** shows the expiratory rise of Pga, **B)** expiratory rise of Pes above Pcw (which is equal to the negative of Pmus during expiration), **C)** Pdi (end-insp) compared to Pdi at start of inspiration effort (of the diaphragm) at end of inspiration (start of expiration).*

Figure 22A and B shows that the inspiratory PTP measures (PTPdi,insp and PTPmus,insp) increase at the start of the SBT compared to PS7 (*Pre 2*). The PTPga,exp (**Figure 22**C) shows a similar pattern as the ΔPga,exp, it decreases at the SBT start, thereafter varies and returns to the level of the pressure support before the SBT at the end of the 30 minutes of the SBT. The results of the relative PTPga,exp (to PTPtot) are comparable to the absolute PTPga,exp, these results are shown in Appendix 8.1.3.1. PTPdi,exp (**Figure 22**D) does not change in the first half of the SBT, but in interval 4 and 5, it decreases compared to the pressure support ventilation before the SBT. The WOB (**Figure 22**E) results show a pattern similar to inspiratory PTP parameters, as it increases during the SBT, but in the last interval in decreases back to the starting level. There is a small variation in expiratory work of breathing (**Figure 22**F), but the increase during the second interval of the SBT does not continue up till the end of the SBT. No expiratory WOB is present during PS, while there is relevant PTPga,exp during the PS period.

The functional coordination results are concluded with the EMG parameters. The sEMG signals of the second subject, showed an alternating pattern of inspiration muscle effort and expiration muscle effort, showed in **Figure 23**. The envelope waveform of the diaphragm and parasternalis sEMG start often simultaneously (e.g. at red vertical line) when assessed visually. When these signals diminish, the activation of the expiratory muscles (e.g. blue vertical line) starts. The sEMG of the rectus abdominis showed no relevant information of respiratory muscles and can be considered as noise. It can be seen in **Figure 24**A that peak EMGdi (derived from the diaphragm sEMG) does not vary over the duration of the duration of the SBT. This is also the case for EMGdi at other time points within the respiratory cycle, namely the start of Pes increase and start of expiratory flow (Appendix 8.1.3.2). Additionally, the NME (calculated with sEMG of diaphragm) remains stable during the SBT (**Figure 24**B).

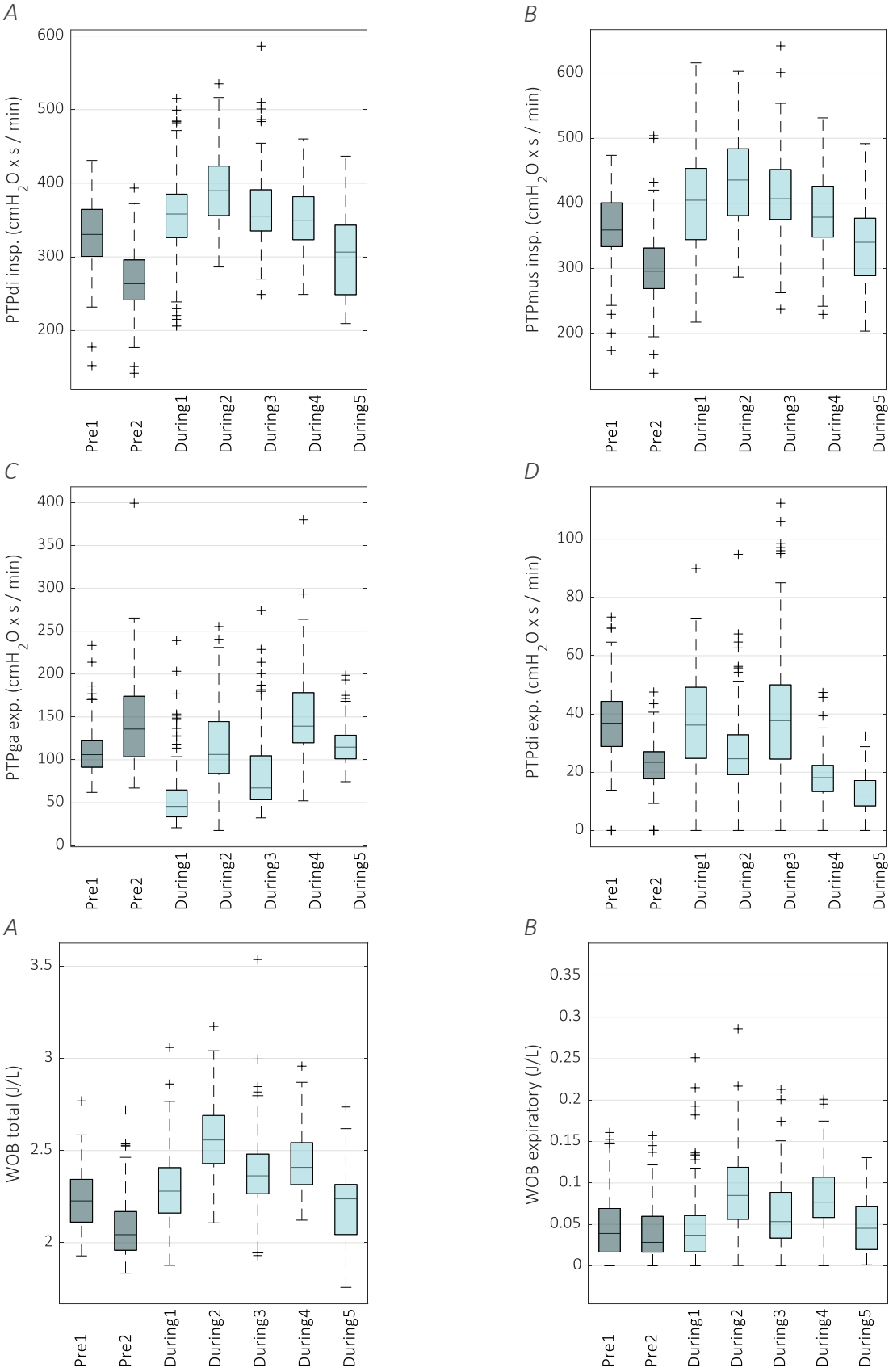

Figure 22: *Parameters on respiratory effort,* ***A)*** *PTPmus,insp,* ***B)*** *PTPdi,insp* ***C)*** *PTPga,exp* ***D)*** *relative PTPga,exp compared to PTPtot (PTPga,exp + PTPdi,insp). WOB parameters, left: total work of breathing, right: expiratory work of breathing.*

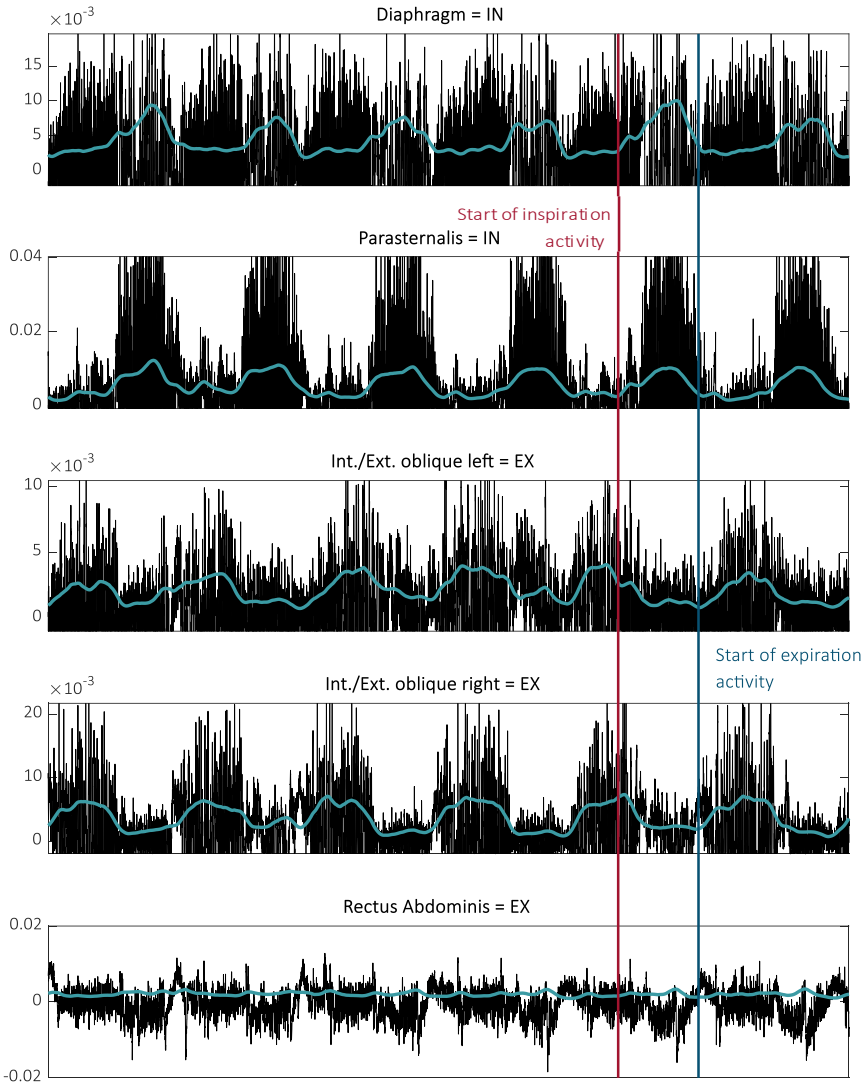

***Figure 23**: sEMG of the diaphragm, parasternalis intercostalis, oblique muscles left, oblique muscles right and rectus abdominis. Black signal shows raw EMG, blue signal shows envelope of raw EMG (moving average of RMS). Red vertical line is placed at one of the neuronal inspiration starting points, while the dark blue vertical line is placed at the start of expiration effort of the oblique muscles.*

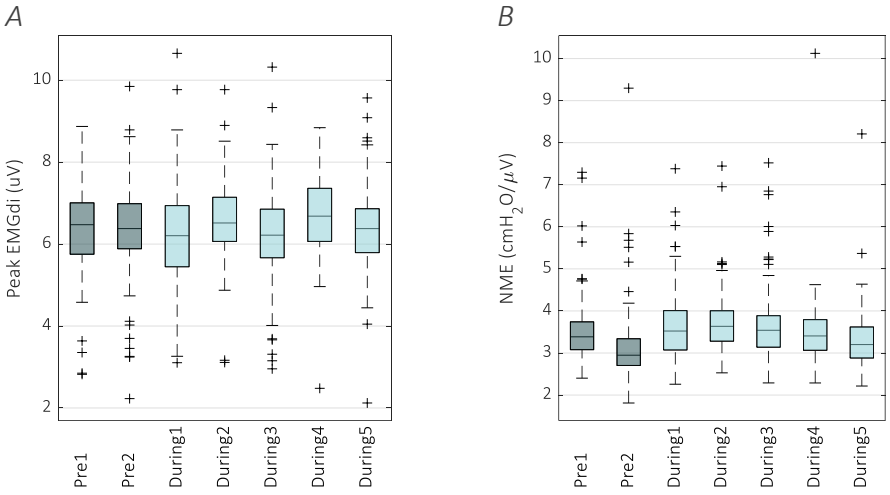

***Figure 24:** Diaphragm activity from envelope of sEMG at different points in time. A) peak level of EAdi, B) EAdi at start of expiratory flow and C) at start of Pes increase.*

3.3.2.2 Timing coordination

In general, the right abdominal muscles (sum of internal and external oblique) was less noisy and showed a more evident respiratory cycle (activity waveform during expiration, no activity during inspiration). Therefore, this signal is used for further analysis timing coordination analysis. **Figure 25**A shows the PA between EMGdi decrease to 70% of peak and the start of obliques activation, showing that on average the obliques activate before EMGdi has decreased to 70%, but it also occurs the other way around. There is large variability with PA results ranging from -70 to 80 degrees. The PA between the start of expiratory flow and EMGdi decrease to 70% is around 20 degrees (**Figure 25**B), indicating return to 70% has occurred before expiratory flow starts. The PA results did not vary during the measurements and the remaining PA results are shown in Appendix 8.1.3.3.

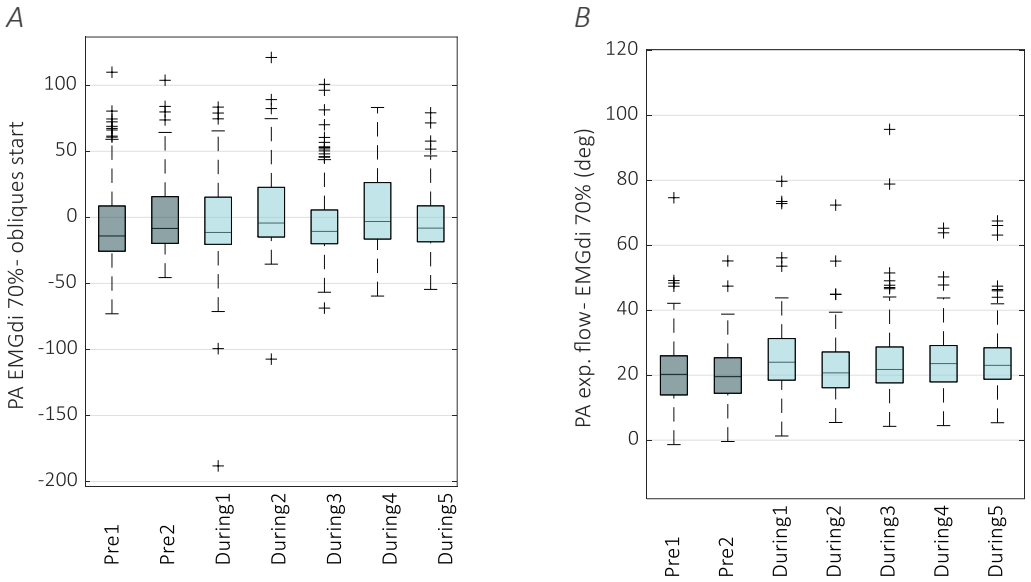

*Figure 25: Boxplots for a selection of the phase angle results. Figure **A)** shows the phase angle between EMGdi decrease to 70% of the peak and the start of the obliques activation. Figure **B)** shows the phase angle of start of expiratory flow and the start of obliques activation.*

3.3.2.3 EMG coherence

The results of intermuscular coherence for subject 2 are shown in **Figure 26**. A relatively high coherence area in the first before interval compared to the SBT period in the alpha and beta band was found. Over the period of the SBT, the coherence in the alpha band between the inspiratory muscles (parasternalis and diaphragm) seems to increase slightly towards the second half of the SBT. The coherence area in de beta band between the diaphragm and the right oblique muscles is greater than the other muscle pairs, also for the coherence between the diaphragm and the left oblique muscles. It is expected that the right and left oblique muscles are activated simultaneously and there is no reason to expect otherwise in this subject. Therefore, the high coherence between the diaphragm and the right oblique muscles is considered as a coherence caused by noise, because their measurement locations were closer to eachother (diaphragm was measured at the right ZOA).

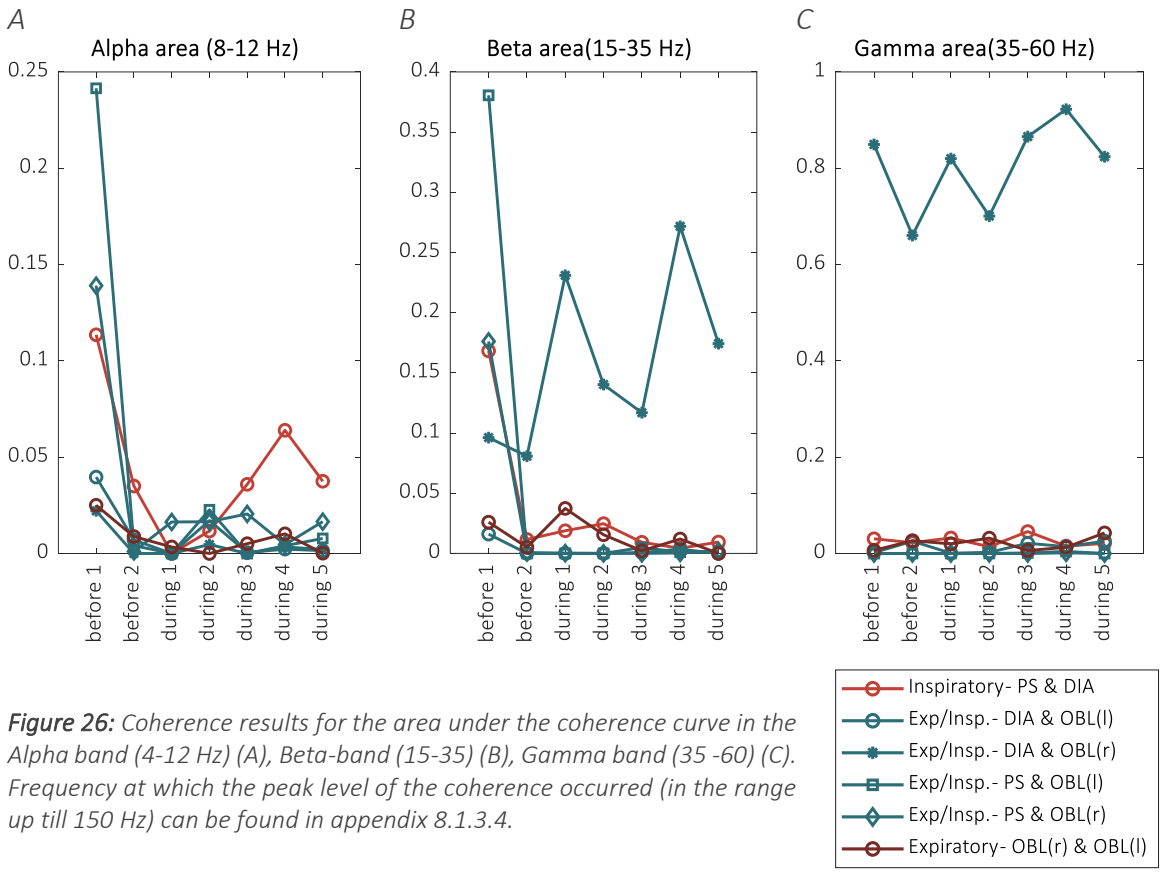

Figure 26: *Coherence results for the area under the coherence curve in the Alpha band (4-12 Hz) (A), Beta-band (15-35) (B), Gamma band (35 -60) (C). Frequency at which the peak level of the coherence occurred (in the range up till 150 Hz) can be found in appendix 8.1.3.4.*

3.4 Discussion

The preliminary findings show that it is feasible to perform the planned measurements during an SBT to investigate respiratory muscle coordination. It is possible to calculate parameters on breathing mechanics and breathing effort, timing coordination parameters and intermuscular coherence parameters from measurements at the same time.

3.4.1 Subject 1

The absence of a gastric balloon in the first subject, resulted in the impossibility for investigating transdiaphragmatic pressure and its derived parameters. Expiration effort could not be assessed, however no expiration effort (contraction of abdominal muscles) was noticed visually as well as on sEMG signals. Although subject 1 did fail the SBT, the subject did not show any significant abdominal muscle effort throughout the whole recording.

During PS period at the start of the recording, the WOB was found to be lower while the ΔPmus was higher compared to the NAVA period thereafter. While patient effort was higher during PS, the ventilator assist (Pao swings) was higher during NAVA ventilation. Thus, the proportion of WOB executed by the ventilator, was higher during NAVA ventilation. This also resulted in higher tidal volumes (volume is also included in WOB calculation).

The calculation of NME in is done by use of the Pmus swings (since Pdi was not available). The decrease of NME values over the duration of the SBT could be caused by a decrease of neuromechanical coupling, however, it could also be explained by the increased recruitment of accessory inspiratory muscles, determining a larger part of ΔPmus. A (relative) increase in Pdi swings cannot be excluded, but the minor decrease in ΔPmus suggest a decrease in neuromechanical coupling.

3.4.2 Subject 2

In the second subject significant expiration activity (as defined by Pga rise during expiration and PTPga) was measured, but seemed not to be depending on the level of support. Notable is the fact that in periods where PTPga,exp is higher, PTPdi,exp is lower. This could indicate that the (faster) relaxation of the diaphragm coordinated a (faster) activation of the abdominal muscles, or vice versa.

The results of subject 2 demonstrate that care should be taken when interpreting respiratory mechanics measurement and functional coordination parameters of an individual subject. While breathing effort parameters change (significantly) this is not necessarily the result of the SBT, but can also be devoted to physiological normal variations, optionally caused by changing metabolic demans, sleep or awakening or physical activity. Values indeed change in both directions and these variations are similar to pressure support ventilation before the SBT.

Subject 2 showed a clear decrease in the tonic activity of the diaphragm at the start of expiratory flow, Pdi(end-insp). Physiologically, this can be caused by a faster decrease of Pdi, a longer inspiratory time or less Pdi effort (ΔPdi,insp). The Pdi(end-insp) relative to the peak Pdi shows the same decrease as the absolute Pdi(end-insp) and the inspiratory time remained equal (Appendix 8.1.3.1). Therefore, a part of the cause of a lower Pdi(end-insp) is considered to be a faster decrease of Pdi after its peak. This could also explain the decrease of PTPdi,exp (**Figure 22**D). Results of additional subjects have to give insight in whether this is a common phenomenon or not.

The diaphragm activity, measured by sEMG, did not change over the duration of the measurement, while physiological parameters clearly did. While clearly inspiratory activity of the diaphragm in (filtered) sEMG signal is visible, it is questionable whether the level of sEMG activity gives reliable information on the quantity of activation. Previous research confirms the uncertainty in identifying the level of activity by sEMG of the diaphragm, as well as extradiaphragmatic muscles [53]. The same applies to the phase angle analysis based on sEMG. The results show feasibility of the calculation of parameters, however, their precision is questionable. The fact that no phase angle parameter did change over the duration of the measurements could be caused by the lack of measuring a precise angle, or simply the true unchanging phase angle.

We hypothesized increasing expiration effort as a result of the increased load in an SBT, especially when the patient fails the SBT. In these preliminary results, not the same effects of an SBT on the expiratory muscles are found like reported before [16], as the successful subject showed expiration activity (during the full measurement) while the failing subject did not. However, these two measurements are far too little to reject the hypothesis, but they do emphasize the complexity and need for additional research on the coordination of the respiratory muscles during an SBT. Besides that, when more subjects are included, analysis of the group results can be performed, instead of individual subject analysis. As physiological variation are expected to be random, this will be averaged out when analysing a larger group of subjects, and the distinction between “normal physiological” changes in breathing mechanics and those caused by the SBT can be made.

3.4.3 Strengths and weaknesses

The preliminary results show the feasibility of these study measurements and the comprehensive possibilities for analysing the data, giving insight in the respiratory muscle coordination during a clinically relevant period (SBT). In the future, several other parameters could be derived from the measured data, ranging from flow or pressure derived parameters (such as flow index [70]) and many more phase angle parameters or additional effort parameters (PTP). While it is not within the scope of this study, the extensive measurements can give additional information about the progress in the weaning process of the measured subject. While measurement of all signals simultaneously enables us to perform complex analysis and investigate respiratory muscle coordination very precise, it also results in difficulties in recruiting subjects for this study with all desired ‘bells on’. Therefore, there is a large risk of delayed study inclusion.

For investigating the activity of the diaphragm during expiration, or even expiration effort of the diaphragm, the cycling-off of the ventilator interferes with the results of interest. However, it is possible to quantify eccentric contraction of the diaphragm and the accompanied electrical activity as eccentric contraction is defined as tonic activity when lengthening (which is the only possibility when expiratory flow is present), but does not give exact information on how neural drive is transferred to mechanical signals. It is important to make well-considered choices on how to handle this precarity and establish exact definitions of the outcome measures, like we did in section 2.2.2.1.

The optimal method to measure EAdi is via a nasogastric catheter, however in subject 2 this is done by use of sEMG. This seems feasible, consistent with previous research [71]. Nevertheless, the signals of sEMG (used for abdominal muscles either way) are more noisy, resulting in difficulties in automatically detecting the starting point of sEMG activity [53]. As can be seen in the third (second yellow line) expiration effort in Figure 13, the location of the start point of sEMG is not always straightforward, as there can be discrepancies between the envelope signal and the raw sEMG signal. Secondly, discrepancies between envelope of raw EAdi signal compared to EAdi filtered by Servo are notable, this is discussed in Appendix 8.1.1.2. These results emphasize the need for raw EAdi measurement. At last, when comparing sEMG of the diaphragm with EAdi from a nasogastric catheter, a different location of the diaphragm is measured (crural vs. zone of apposition respectively), making a fair comparison impossible.

The coherence results show conspicuous findings. While in subject 2 clearly recruitment of the abdominal expiratory muscles can be seen on the (raw) EMG signals, it did not result in a greater coherence area compared to subject 1 (no abdominal muscle activity. Based on these two subjects, no conclusions can be made about the clinical relevance of the results nor the validity of coherence analysis. After measuring all subject, The results can give insight in normal coherence values, but may also help in developing a standardized method to evaluate intermuscular coherence of the respiratory muscles in a valid manner. Currently the physiological foundation is not exactly clear and the frequency spectra (alpha, beta, gamma) are grown historically, but have no physiological base for intermuscular coherence.

3.4.4 Conclusion

The preliminary results show feasibility of performing the intended measurement and analysis, but also bring to light challenges in recruitment of subjects and interpretation of the results. Possibly, parameters giving insight in the extubation readiness can be derived from the final results. However, most important, the final results will help in increased understanding of the coordination of the respiratory muscles.

4 Respiratory muscle activity during expiration in pressure support ventilation

secondary analysis of a randomized clinical trial

4.1 Introduction

The current tools to monitor respiratory muscle weakness in critically ill , such as oesophageal or transdiaphragmatic pressure and diaphragm EMG measurements, are mainly focussed on the diaphragm, and inspiratory muscles in general [5].

Currently, awareness is growing that the coordination of the respiratory muscles during the expiratory phase of breathing is an important aspect in ventilator dependent critically ill patients. The comparison with the left and right ventricles of the heart can be made, and just like the left heart, the diaphragm is not an isolated organ, but always must be considered in the context of the whole respiratory muscle pump [15]. Nevertheless, little quantitative research has been performed on the expiratory phase of breathing and currently the incidence of expiratory muscle activity in the general patient population receiving pressure support ventilation is largely unknown. In patients suspected for expiration activity, Lessard *et al.* (1995) found an average expiratory Pga rise of 3.1 ± 2.7 up till 8.6 ± 5.0 cmH_2O after lowering support (SD). Most of these patients were admitted due to COPD exacerbation [68]. Other studies showed that in patients with stable COPD the active nature of expiration was an important determinant of PEEPi. In 16 of 25 patients abdominal muscle activity was present, resulting in an average Pga rise was 2.4 ± 2.3 cmH_2O [72].

When respiratory load increases, the accessory respiratory muscles will be activated, including expiratory muscles [15]. When the abdominal muscles (transversus abdominus, internal and external oblique) are recruited, they cause an increase in abdominal pressure, which is passed to the thorax under the assumption that the diaphragm is relaxed during expiration [15]. Consequently, expiration is supported by the pressure increase in the thoracic compartment, which could also be caused by thoracic expiratory muscles (internal intercostals) [27]. The gold standard for quantifying expiration muscle effort is the rise of gastric pressure and the pressure-time-product of the gastric pressure during expiration [15, 16, 43, 44]. For these measurements it is required to use a gastric balloon in addition to the oesophageal balloon monitoring, Expertise on these measurements is scarce, so it would be desirable to examine expiration effort with only a less invasive oesophageal balloon.

Possibly, other parameters derived from oesophageal, gastric and/or airway opening pressure can give insight in the muscle activity during the expiratory phase of breathing. These parameters include the tonic activity and effort of respiratory muscles during the expiratory phase of breathing (as of defined by flow). Thus, the aim of this study is to get insight in the prevalence of respiratory muscle activity (including inspiratory and expiratory muscles) during the expiratory phase of breathing in mechanically ventilated patients on a supportive mode. In the first part of this study, the prevalence and level of several commonly used renewed parameters will be evaluated. Secondly, the relation between the evaluated parameters will be investigated, with a specific focus on gastric and oesophageal expiration measures, to identify the need for gastric pressure measurements for quantification of expiration effort. The long duration (24h) of measurements in a representative ICU population gives insight in the (patho)physiological variability of breathing mechanics. The gained extensive knowledge of respiratory muscle effort during expiration will help clinicians in defining their daily focus. Is muscle effort during expiration a common phenomenon in critically ill mechanically ventilated patients?

4.2 Methods

The analysed data was selected from a larger dataset, from a randomized clinical trial, registered at clinicaltrials.gov (study identifier NCT03527797). This trial involved continuous recording of flow, airway opening pressure (Pao), oesophageal pressure (Pes), gastric pressure (Pga) for 24 hours in 39 patients. In the intervention group (19 patients) the support was adjusted based on the mean transdiaphragmatic pressure (Pdi = Pga – Pes) swings in the first two minutes of every hour, aiming for Pdi swings between 3 and 12 cmH_2O, to avoid both over- and under assistance.

4.2.1 Subjects

For the clinical trial, subjects from our adult ICU were included if they were intubated and mechanically ventilated in a partially supported mode, and if the attending physician expected that invasive ventilation would be required for at least 24 to 48 hours at the time of screening. Patients were excluded if they had a past medical history of neuromuscular disorders, a contraindication for placement of a nasogastric catheter, an active air leak in the pleural space or abnormal anatomy of the oesophagus or stomach. For this secondary analysis, data of each subject was inspected in a random order. Subjects were included if at least 20 hours of data with appropriate quality was available and correct positioning and calibration of the balloon catheters was indisputable.

4.2.2 Measurements

To record the flow and pressure signals, a dedicated measurement setup (BIOPAC MP160, BIOPAC Inc., USA) was used, with differential pressure transducers and sampled at 250 Hz. After calibration of the sensors, the transducers were connected to the airway opening and a Nutrivent catheter with its balloons placed in the oesophagus and the stomach. Flow was calibrated using a 1L syringe. Chest wall recoil pressure was calculated by use of the transpulmonary pressure and volume difference between end-inspiratory and end-expiratory holds [37].

4.2.3 Pre-processing

Pre-processing and analysis was performed using MATLAB (Mathworks Inc., version R2020b). The offset drift of all pressure signals was removed by a 4^{th} order Butterworth high pass filter with a cut-off frequency of 0.3 Hz. To remove high frequent noise a moving average filter was used for Pga and Pao. High frequent oscillations (mainly of cardiac origin) of Pes signal were suppressed by a 4^{th} order Butterworth low pass filter with a cut-off frequency of 6 Hz. After filtering, baseline of original signals was restored. Transdiaphragmatic (Pdi) and dynamic transpulmonary ($P_{L,dyn}$) pressure was calculated after filtering as Pga – Pes and Pao – Pes respectively [13, 37]. A difference between inspiratory and expiratory gain factor caused an offset in the flow signal, for which was corrected on a per subject basis. A volume (V) signal was calculated as the time integral of the flow signal and filtered using a 4^{th} order Butterworth filter with a cut-off of 0.05 Hz. Volume and measured Ccw are used to calculate Pmus, which is corrected for the rise in gastric pressure in the previous breath [17, 68].

Inspiration and expiration phases were based on flow zero-crossings. The start of the Pes, $P_{L,dyn}$, Pdi and Pao inspiration or inspiratory determined with a mathematical algorithm depending on the height and the distance from the peak. For every breath, the first detected inspiratory effort (Pdi, Pes, $P_{L,dyn}$ or flow) was used as the start of that particular breath. Single breaths with potential artifacts and outliers based on physiological criteria were removed prior to the analysis (e.g. inspiration time <0.3 seconds, expiration time <0.5 seconds, substantial drift in baseline or peak pressures).

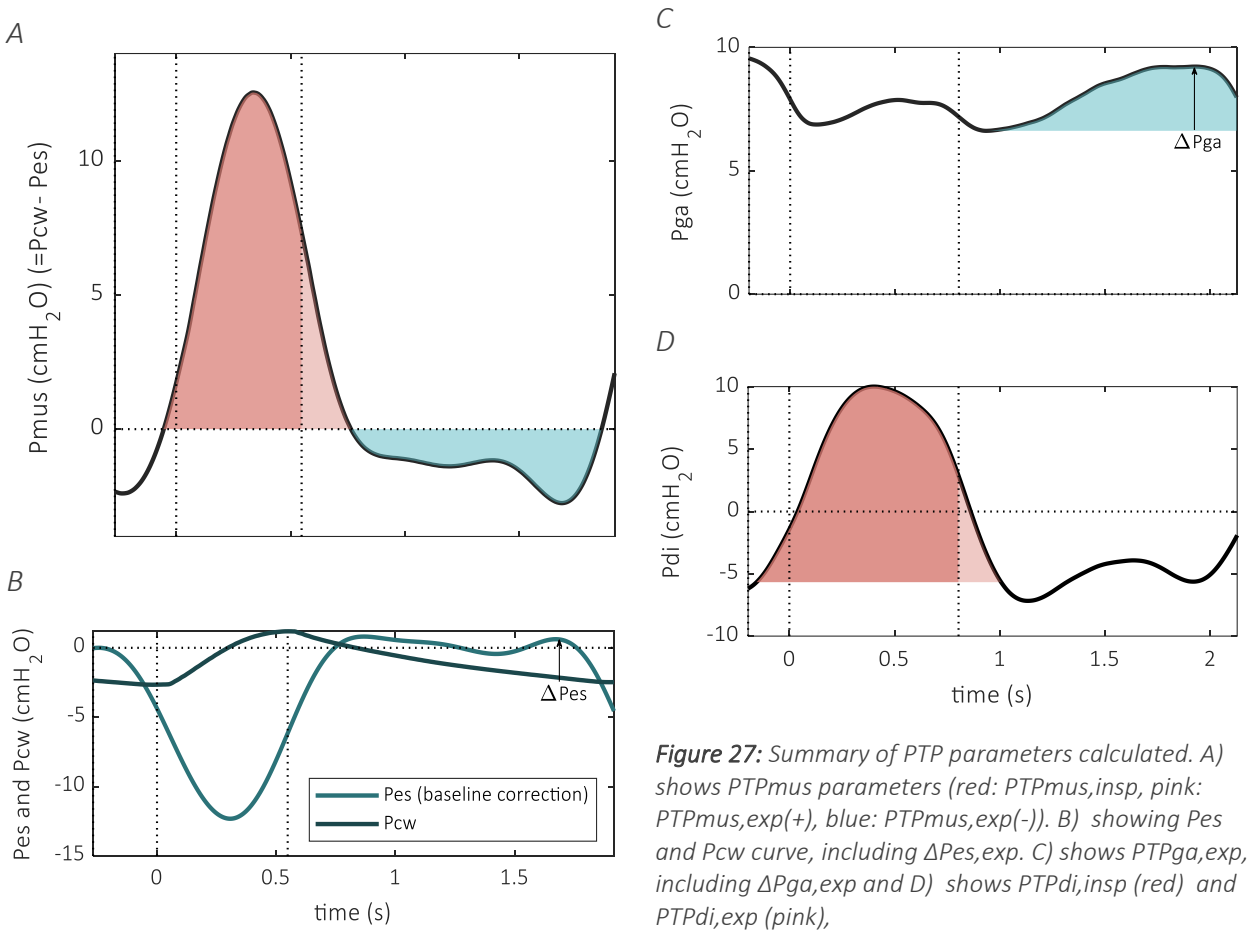

Figure 27: Summary of PTP parameters calculated. A) shows PTPmus parameters (red: PTPmus,insp, pink: PTPmus,exp(+), blue: PTPmus,exp(-)). B) showing Pes and Pcw curve, including ΔPes,exp. C) shows PTPga,exp, including ΔPga,exp and D) shows PTPdi,insp (red) and PTPdi,exp (pink),

4.2.4 Data analysis

After preprocessing and defining the individual breaths, breath-by-breath calculation of the following parameters was performed: ΔPga,exp, ΔPes,exp above Pcw, Pdi(end-exp), PTPdi,insp, PTPdi,exp, %PTPdi,exp of total PTPdi, PTPmus,insp, PTPmus,exp (+), %PTPmus,exp(+) of total PTPmus(+), PTPga,exp, %PTPga,exp of PTPtot (PTPdi,insp + PTPga,exp). A comprehensive rationale for the pressure-time-product (PTP) parameters can be found in the background, section 2.2.2.1 **Figure 27** shows the absolute PTP areas calculated for every breath.

The expiratory rise in Pga (ΔPga,exp) is calculated as the rise of Pga during expiration after its expiratory baseline value, which is define as the minimum during the first half of expiration [16]. For the same purpose (measuring expiration muscle effort), the rise of Pes above Pcw during expiration (ΔPes,exp) is calculated as the maximum exceeding of Pes above Pcw (**Figure 27**D). The tonic activity of the diaphragm at the start of expiratory flow (Pdi,end-exp) is calculated as the Pdi value at the end of inspiratory flow, minus the Pdi value at the start of Pdi activity (Pdi baseline).

Based on previous research, a clinically relevant or significant Pga rise during expiration was considered to be 2 cmH_2O. The PTPga was considered to be meaningful when it exceeds 40 cmH_2O*s/min [16]. For Pes expiratory rise and PTPmus,exp(-) even less reference values are found, but values are expected to be in the same range. However, Pes signal tends to fluctuate more than Pga due to cardiac oscillations. The level of these oscillations is assumed to be around 1 to 2 cmH_2O, based on visual inspection.

4.2.5 Statistical analysis

Visualisation and statistical analysis was performed using MATLAB (Mathworks Inc. version R2020b). To visualize the overall results, density graphs (derived from histograms) were made for the parameters of interest, for all breaths of all subject taken together. Per expiration parameter, a more

detailed figure with the partition of breaths falling in the ranges very low, low, moderate, high and very high. The subdivision within these ranges was based on the histogram of all breaths taken together. To investigate the relation between Pes and Pga measurements during expiration, scatter plots (of 50 samples per hour of the data on average) including linear regression were made of ΔPga,exp and PTPga,exp, ΔPes,exp and neg. PTPmus,exp, ΔPga,exp and ΔPes,exp, PTPga,exp and neg. PTPmus,exp. ROC curves were made for predicting a ΔPga,exp higher than 2 and higher than 3 cmH_2O using the measured ΔPes,exp. For the optimum (defined as maximum of sensitivity + specificity), the threshold value of ΔPes,exp and the corresponding sensitivity and specificity are reported. This is also done for predicting a PTPga,exp larger than 40 and 60 cmH_2O*s/min using the PTPmus,exp(-).

4.3 Results

4.3.1 Sample size

From the total population of 40 patients, data of 29 subjects was screened, of which 15 subjects (with appropriate signal quality) were included. This resulted in 6 subjects from the control group and 9 subjects from the intervention group. Clinical parameters and demographics of the included subjects are shown in **Table 2**. From these signals, 354,047 breaths of a total of (flow-based) 433,297 detected breaths were found to be valid according to stated criteria and included in the analysis.

Table 2: Baseline characteristics of subjects included in the analysis.

	Control group (included) n = 6	Intervention group (included) n = 9
#male	2	6
Mean Age (SD)	67.7 (13.1)	61.2 (16.5)
Mean BMI (SD)	26.7 (3.9)	26.5 (1.6)
Mean SOFA-score (SD)	9.2 (1.5)	10.4 (3.0)
Mean APACHE-II score (SD)	26.7 (4.8)	18.7 (5.8)
Mean days since intubation (SD)	8.8 (5.8)	15.3 (9.8)
Mean days support ventilation (SD)	6.0 (4.2)	5.0 (4.0)
Mechanical ventilation reason		
○ ARDS	6	8
○ COPD/Asthma	0	1

4.3.2 Prevalence and level of respiratory muscle effort during expiration

The distribution of the outcome measures are shown in the density plots in **Figure 28**. It can be seen that inspiratory parameters (PTPmus,insp and PTPdi,insp) show a (non-normal) distribution around the average value of circa 146 cmH_2O*s/min and 134 cmH_2O*s/min respectively. On the contrary, for the expiration parameters, a large proportion of the breaths show no expiration effort, quantified by our definition of ΔPga,exp, PTPga,exp, ΔPes,exp and PTPmus,exp(-). A small – but substantial – part of the breaths shows a relevant amount of muscle effort during expiration (quantified as Pga or Pes rise during expiration > 2 cmH_2O, PTPga,exp > 40 to 60 cmH_2O*s/min). For the expiration parameters the results per subject are shown in Figures 29 to 33. For the relative PTPga,exp during expiration (relative to the sum of PTPga,exp and PTPdi,insp = PTPtot), the results are shown in **Figure 29**. It can be concluded that subject 6 and 15 have a large part of their abdominal muscle effort relative to diaphragm effort and abdominal muscle effort taken together.

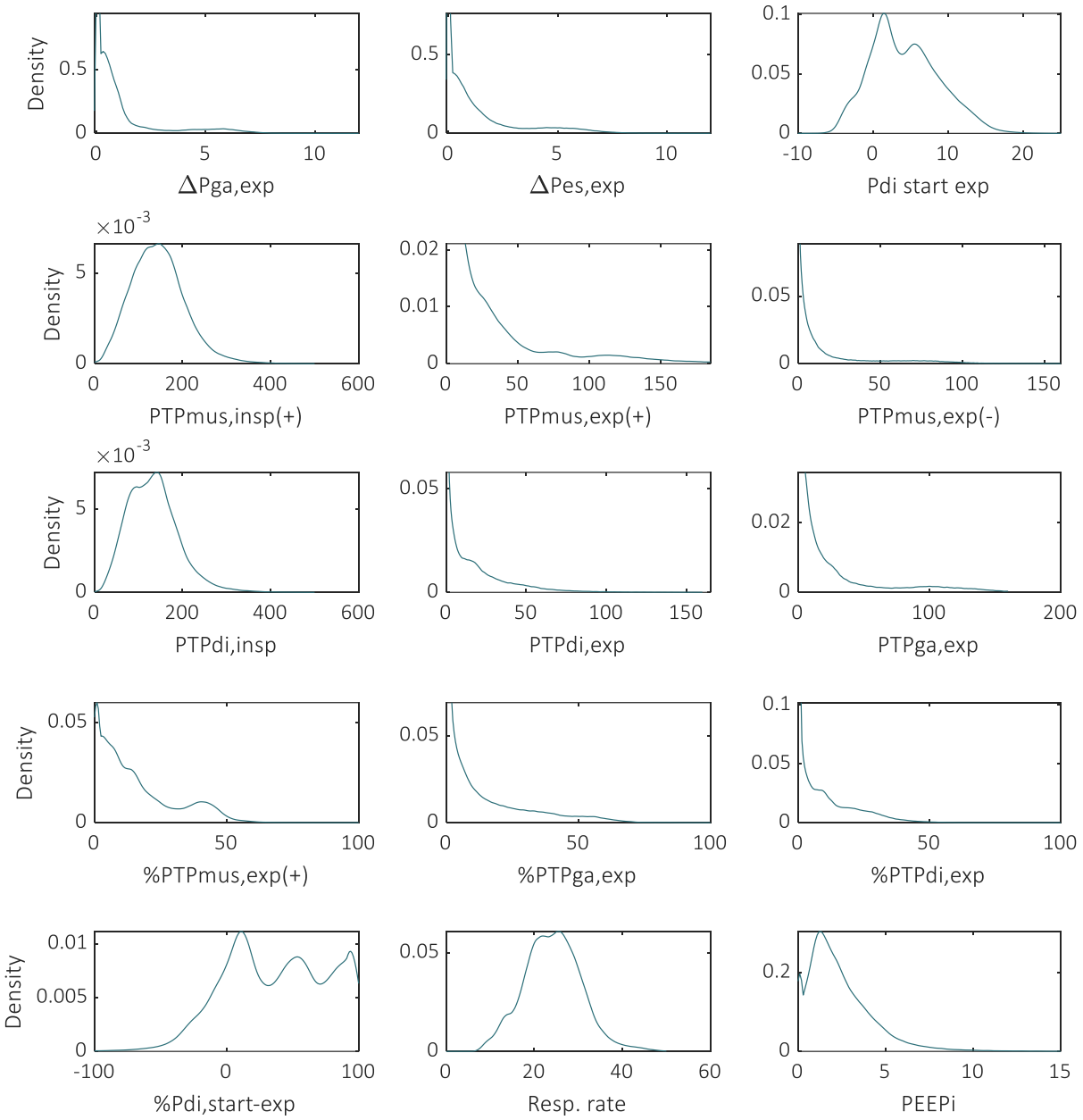

Figure 28: Probability distribution of defined parameters. Epanechnikov kernel function is used to fit a kernel density estimation to the data between the shown limits of the x-axis. Data of all breaths of all patients is taken together.

However, the average PTPga,exp of subject 6 was 109 cmH_2O*s/min, while the average of subject 15 was 24 cmH_2O*s/min. Patients 4, 11 and 12 also have a substantial amount (30 to 40%) of breaths with a relative PTPga,exp higher than 20 percent of their PTPtot, with an average PTPga,exp of 36, 26 and 33 cmH_2O*s/min respectively. The distribution of the absolute PTPga values per subject can be found in Appendix 8.2.2. The expiratory rise of Pga and thus abdominal expiratory muscle effort quantified as PTPga,exp, appears not to be present over the whole duration of the measurements. Figures per subject with the distribution of PTPga,exp per hour is depicted in Appendix 0. The expiratory muscle effort is also quantified using the PTPmus,exp(-), shown in **Figure 30**. Again, subject 6 shows high values of PTPmus,exp(-), on average 69.7 and a PTP over 40 cmH2O*s/min in almost 90% of the breaths. In patient 3, 4, 9 and 12 also a substantial part of all breaths shows a relevant PTPmus,exp(-). The average absolute values are significantly lower in these patients compared to subject 6, ranging from 13.7 to 27.8.

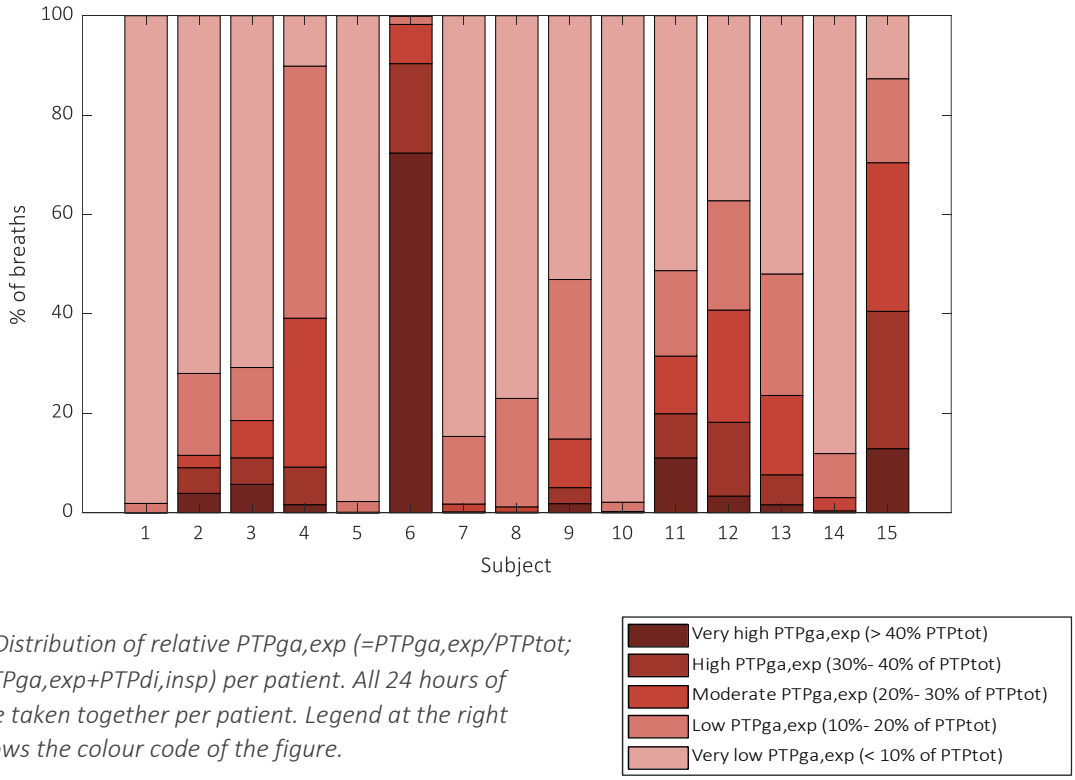

Figure 29: *Distribution of relative PTPga,exp (=PTPga,exp/PTPtot; PTPtot = PTPga,exp+PTPdi,insp) per patient. All 24 hours of analysis are taken together per patient. Legend at the right bottom shows the colour code of the figure.*

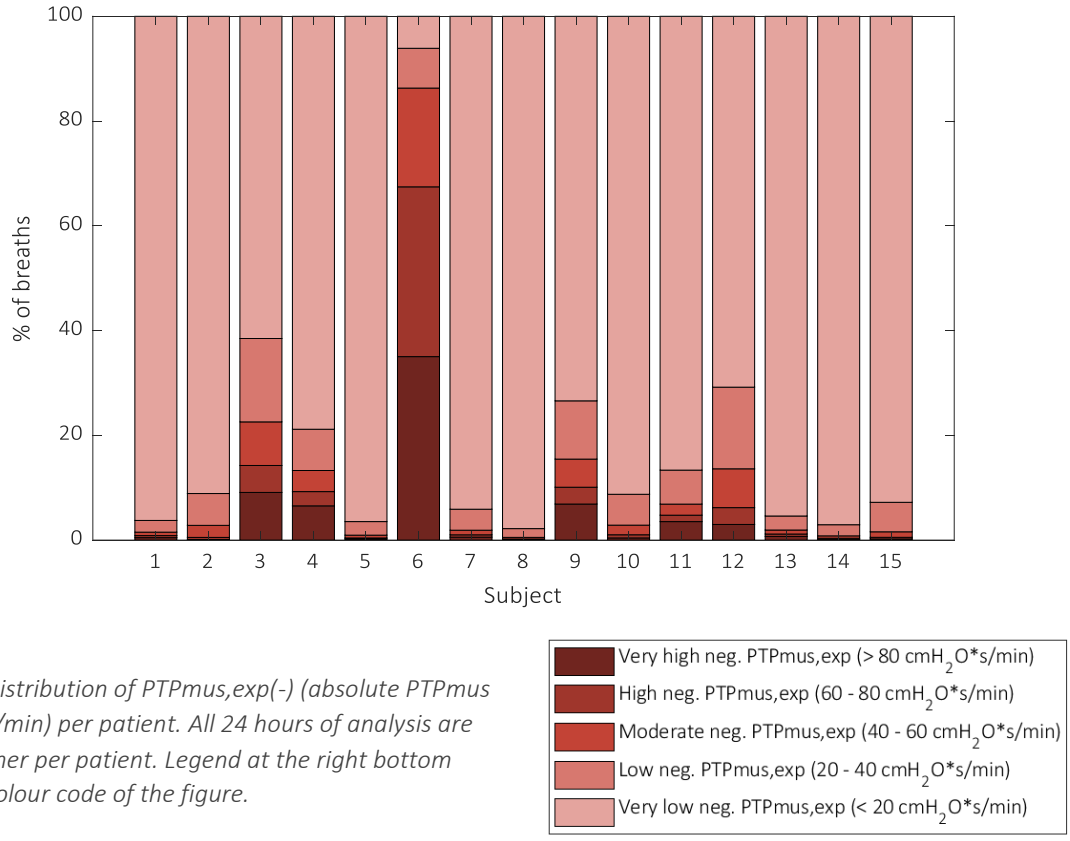

Figure 30: *Distribution of PTPmus,exp(-) (absolute PTPmus in cmH_2O*s/min) per patient. All 24 hours of analysis are taken together per patient. Legend at the right bottom shows the colour code of the figure.*

A relatively simpler way to express expiration effort is just the rise in pressure, including the rise of the Pga and the Pes (above Pcw) during expiration. The ΔPga,exp (shown in Appendix 8.2.1) results are in particular high for subject 6, showing a ΔPga,exp of over 4 cmH_2O in almost 90% of the breaths, resulting in a mean expiratory Pga rise of 5.4 cmH_2O. On the contrary, the average ΔPga,exp varies

from 0.1 to 1.7 in the other subjects. Additionally, subject 4, 9, 11 and 12 show a relevant ΔPga,exp (> 2 cmH_2O) in a considerable amount of their breaths (15-30%). The expiratory muscle activity is also quantified using the expiratory Pes rise above the Pcw curve, ΔPes,exp, of which the distribution per subject is shown in **Figure 31.** The boundaries for small, moderate, large and excessive ΔPes,exp are the same values as for the ΔPga,exp, and the same patients stand out. Again, subject 6 shows high values, with more than ¾ of the breaths having a Pes rise above Pcw larger than 4 cmH_2O. In this patient an average ΔPes,exp of 5.0 cmH_2O was found, while the other patients range from 0.3 to 1.9, which is both comparable to the ΔPga,exp. In the same subjects (4, 9, 11, 12) as for ΔPga,exp a substantial amount of breaths shows a significant ΔPes,exp (>2 cmH_2O). However, subject 3 also shows a substantial number of breaths with a relevant ΔPes,exp, while having almost no relevant ΔPga,exp.

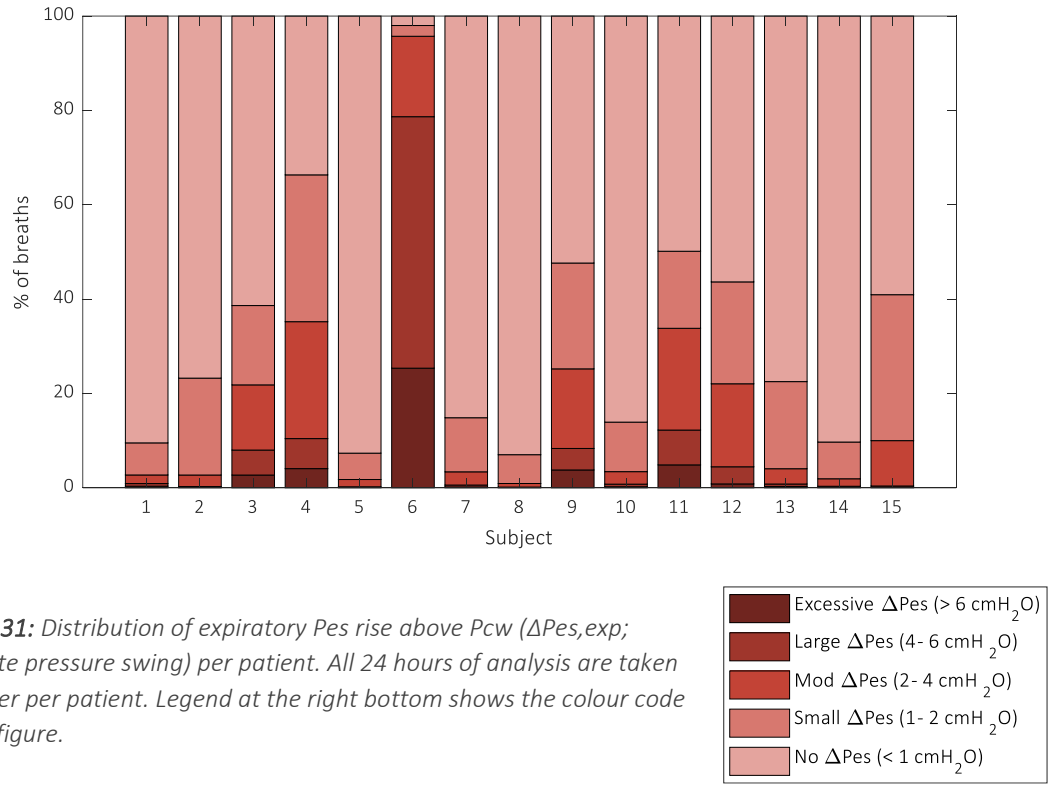

Figure 31: Distribution of expiratory Pes rise above Pcw (ΔPes,exp; absolute pressure swing) per patient. All 24 hours of analysis are taken together per patient. Legend at the right bottom shows the colour code of the figure.

Figure 32 shows the positive PTPmus,exp per patient, in which patient 6 and 15 show in over 90% and 40% respectively that over 30% of the positive PTPmus is during the expiratory flow. Several subjects (1, 2, 8, 9, 11, 12 and 13) show a relative PTPmus,exp of over 20% in a substantial part of the breaths – ranging from 20 to 40% of all breaths per patient, while the other subjects show almost no PTPmus during expiratory flow. In Appendix 8.2.6, examples of the Pmus curve and PTPmus areas of one breath of subject 5, 6, 12 and 15 are shown, to illustrate the origin of the PTPmus,exp(+) values. The graphs for subject 5 show a rapid decrease of Pmus, almost fully lying in the inspiration phase, while Pmus in subject 6 remains high during the first half of expiratory flow. Subject 12 and 15 both have a meaningful part of PTPmus in the expiratory phase. While this is not an high absolute value, for subject 15 it is high relatively tot the total PTPmus. The figure for the distributions of absolute PTPmus,exp(+) values per patient can be found in Appendix 8.2.4. In a similar way, PTPdi,exp is examined. In a large amount of the breaths of subject 6 and 15 the part of PTPdi occurring during expiratory flow exceeds 20% of total PTPdi. The subjects with the highest amount of PTPdi during expiration are the same subjects as for the positive PTPmus during expiration, however, the relative PTPdi during expiration seems to be slightly lower. Full results of relative and absolute PTPdi can be found in Appendix 8.2.5 and 8.2.7.

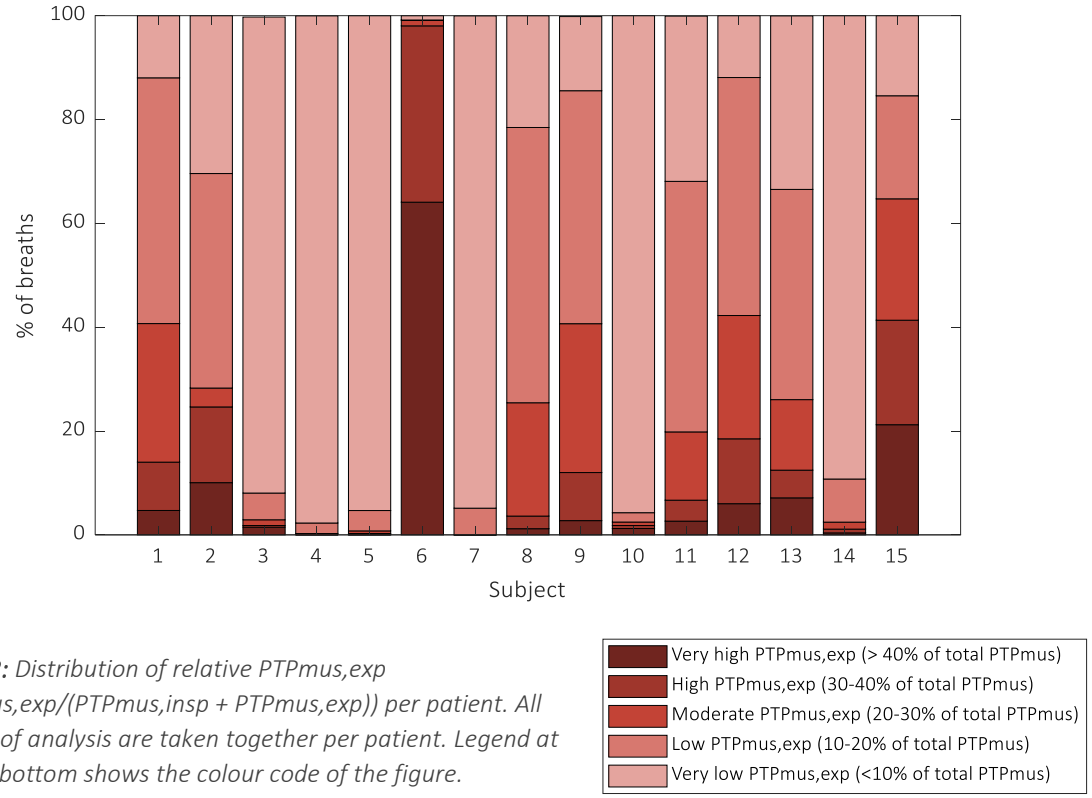

Figure 32: *Distribution of relative PTPmus,exp (= PTPmus,exp/(PTPmus,insp + PTPmus,exp)) per patient. All 24 hours of analysis are taken together per patient. Legend at the right bottom shows the colour code of the figure.*

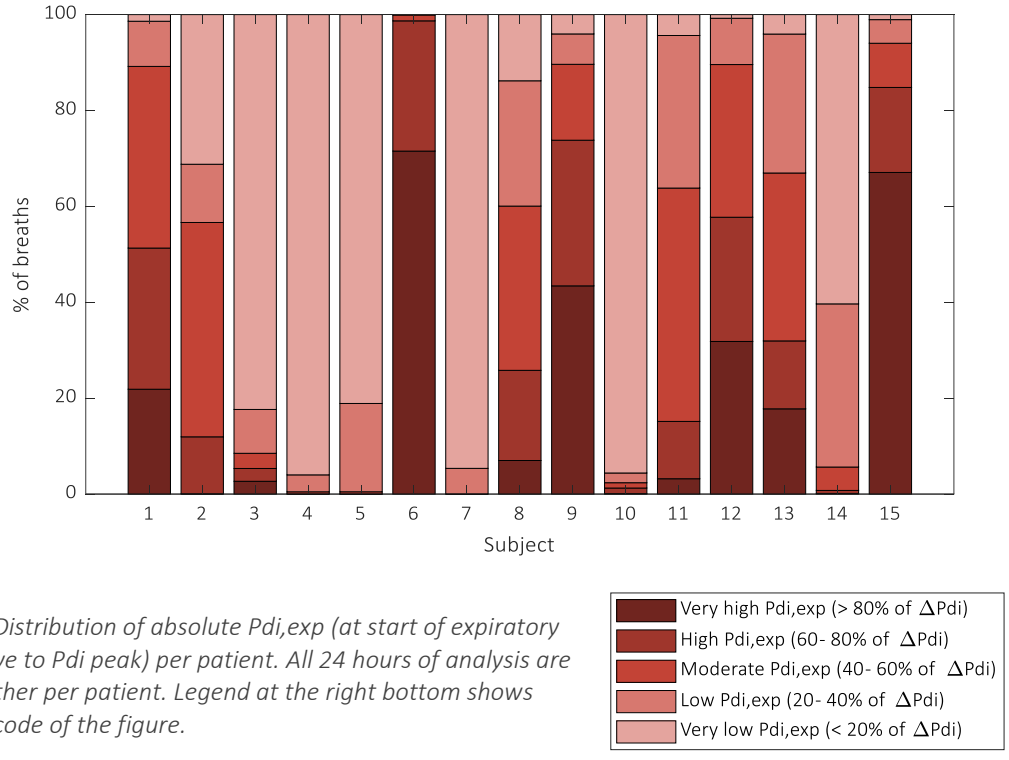

Figure 33: *Distribution of absolute Pdi,exp (at start of expiratory flow, relative to Pdi peak) per patient. All 24 hours of analysis are taken together per patient. Legend at the right bottom shows the colour code of the figure.*

The Pdi relative to peak Pdi value is shown in **Figure 33**, showing a Pdi,end-insp of over 60% in almost all breaths in subjects 6, and also a substantial amount of relatively high Pdi,end-insp (>40% of peak) in the majority of breaths in subject 1, 2, 8, 9, 11, 12, 13 and 15. A few patient show a Pdi,end-insp lower than 20% of peak Pdi in almost all breaths. The absolute Pdi(end-exp) results are shown in Appendix 8.2.8. Distribution of the results of the inspiratory muscle effort per patient (PTPdi,insp, PTPmus,insp) can be found in Appendix 8.2.9 and 8.2.10. The results of the inspiratory muscle effort are more homogeneous for the whole patient groups, thus the amount of inspiratory effort of all analysed patients is similar.

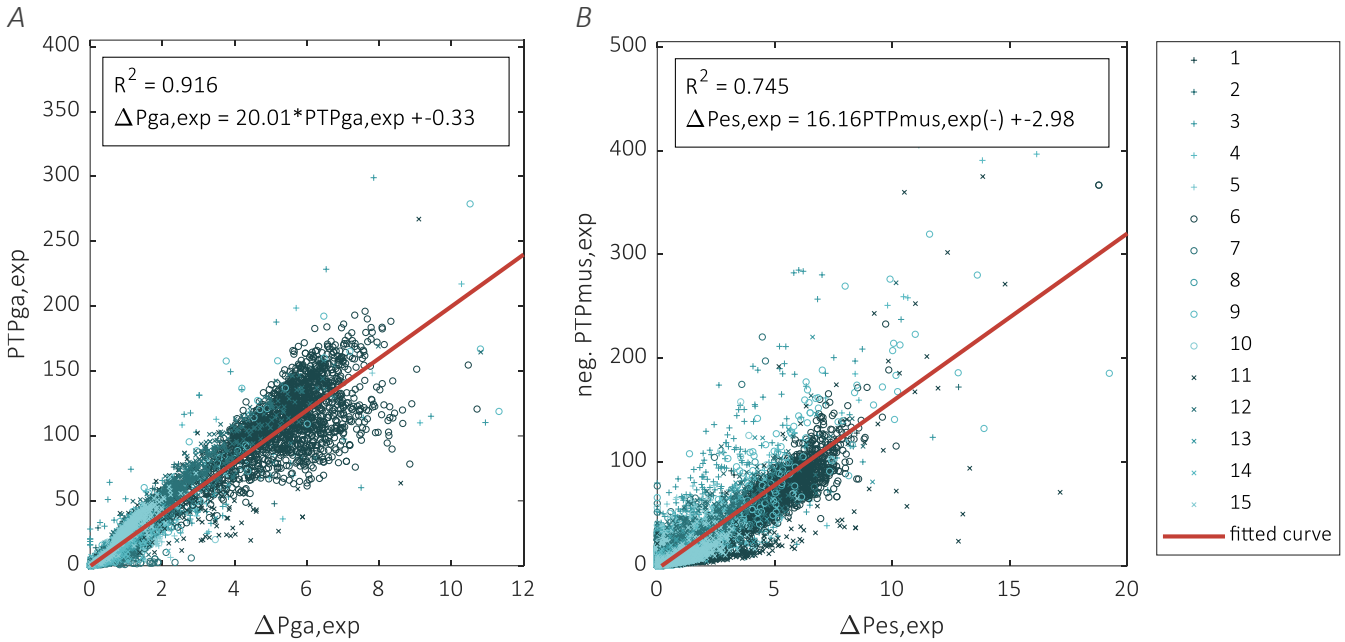

Figure 34: Scatter plots of sample of breaths, showing the correlation of ΔPga,exp and PTPga,exp (A) and ΔPes,exp and PTPmus,exp(-) (B), including the R squared and the fitted curve for linear regression.

4.3.3 Relations between different parameters

Next, the correlation between the investigated parameters is explored. In **Figure 34**A, the relation between ΔPga,exp and PTPga,exp is shown through a scatter plot including the fitted linear regression curve. The R-squared of 0.916 indicates a good relation between the two variables, while for ΔPga,exp and PTPmus,exp(-) the relationship is less evident (**Figure 34**B), with an R^2 of 0.74. When calculating R^2 for the individual subjects, an average R^2 of 0.79 (SD 0.10) is found for the relation between ΔPga,exp and PTPga,exp. For the relation between ΔPes,exp and PTPmus,exp(-) the average R^2 of individual subjects is 0.64 (SD 0.15). All individual R^2 can be found in Appendix 8.2.11.

4.3.3.1 Pes measurements to predict Pga measurements

To identify whether Pga parameters can be predicted by Pes parameters, the rise in Pes during expiration is plotted against the rise in Pga during expiration (**Figure 35**A) and also the PTP parameters (PTPmus,exp(-) and PTPga,exp) defining expiration effort (**Figure 35**B) are examined. The R^2 of this relation is lower, namely 0.62 for the pressure rises and 0.40 for the PTP parameters. When looking at individual subjects, for some subjects a moderate R^2 is found (maximum 0.64 for pressure rises and 0.56 for PTP parameters). However, there are also multiple subjects with a R^2 smaller than 0.1, probably when there is not much variation between measurements. The average individual subject R^2 is 0.19 (SD 0.20) for ΔPga,exp and ΔPes,exp and 0.16 (SD 0.18) for PTP parameters.

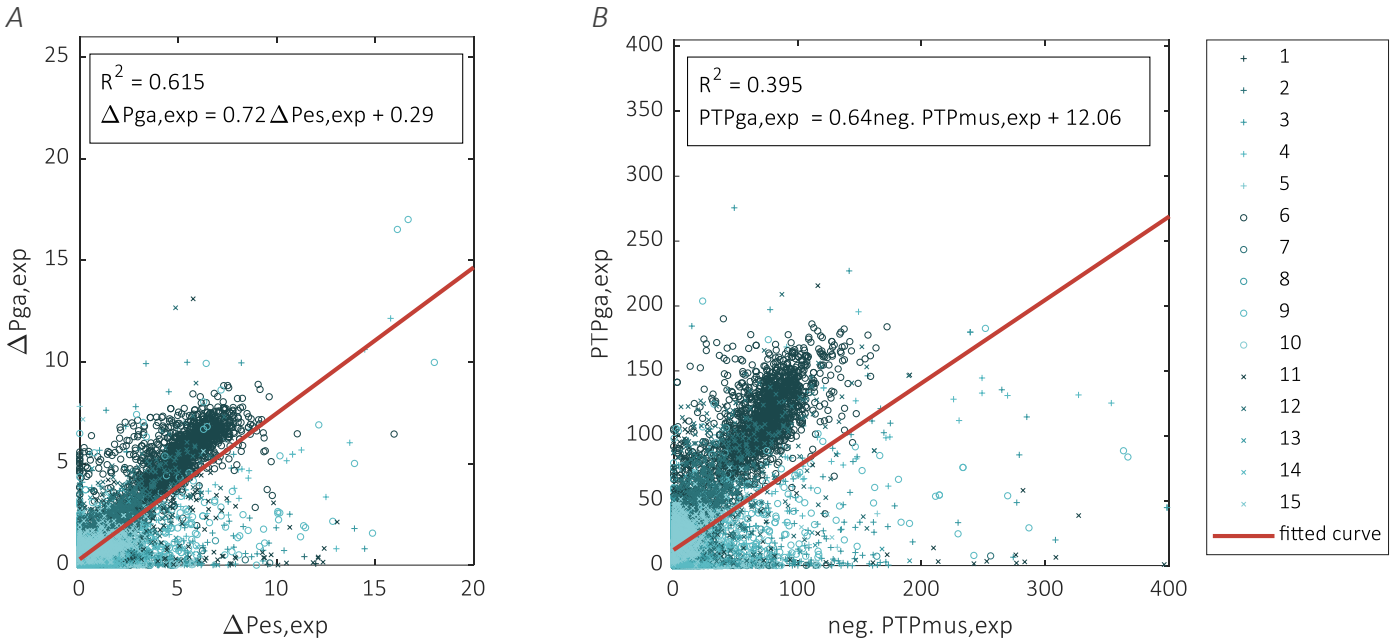

Figure 35: Scatter plots of sample of breaths, showing the correlation of ΔPga,exp and ΔPes,exp (A) and PTPga,exp and PTPmus,exp(-) (B), including the R squared and the fitted curve for linear regression.

For detecting a rise in Pga,exp larger than 2 cmH_2O an optimal threshold of 1,68 in ΔPes,exp was found, resulting in a sensitivity of 88.2% and a specificity of 90.7%. A threshold of 2.27 ΔPes,exp was found to be the optimum for detecting a Pga rise larger than 3 cmH_2O, resulting in a sensitivity of 92,6% and a specificity of 93.0%. Further results and the ROC curve including the AUC can be found in **Figure 36**A. A similar analysis is performed for the PTPmus,exp(-) and the PTPga,exp (**Figure 36**B). For detecting a PTPga larger than 40, the optimal threshold of 14.2 for the PTPmus,exp(-) resulted in a sensitivity of 84.3% and a specificity of 87.4%. Once more, detecting a large PTPga,exp (> 60 cmH_2O*s/min) was optimal for a threshold of PTPmus,exp(-) of 21.8, resulting in 89.5% sensitivity and 90.7% specificity.

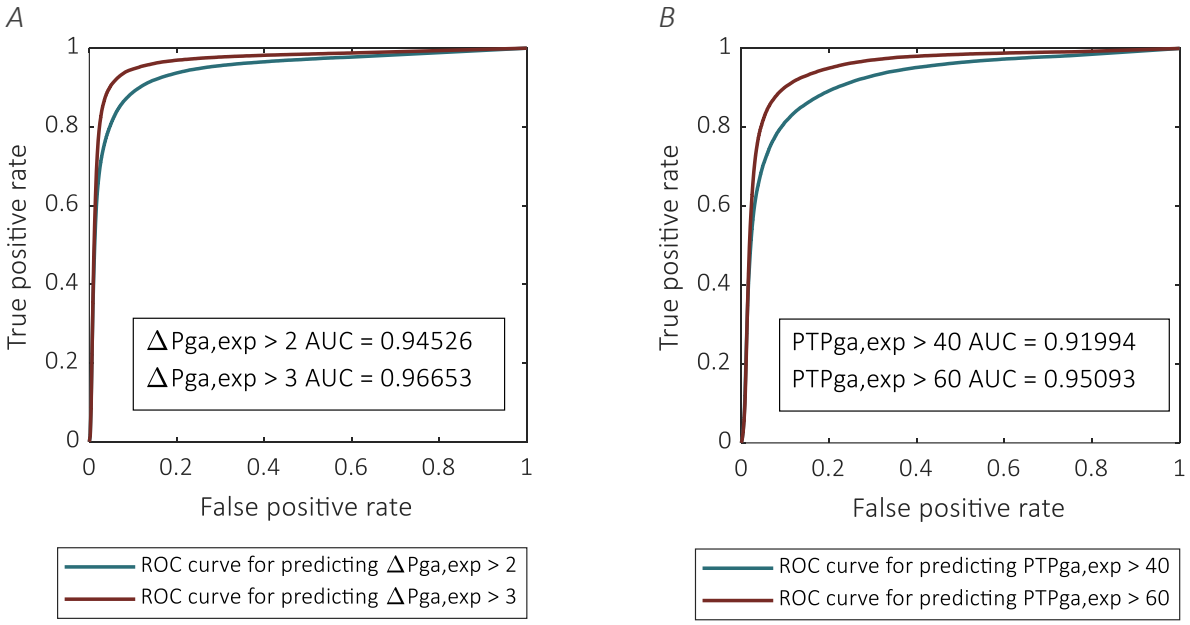

Figure 36: Receiver operating characteristic curve for A) expiratory rise in Pes for detecting an expiratory Pga rise > 2 (blue curve) or >3 (red curve). B) negative PTPmus,exp for detecting a PTPga,exp > 40 (blue curve) or >60 (red curve). AUC values are displayed in the plot.

4.4 Discussion

The results of respiratory mechanics calculated during a 24-hour period, give insight in the prevalence and level of respiratory muscle activity in mechanically ventilated patients in a supportive mode. We found that a substantial part of the included patients shows expiration activity, as defined by Pga parameters ΔPga,exp and PTPga,exp. The level of expiration activity in these five patients with activity is comparable to previous literature [68, 72]. A larger part of the patients shows tonic activity of the diaphragm (Pdi) at the start of expiratory flow. The secondary aim of this study was to investigate whether Pes measures can give information on expiration activity. The results show a moderate relation between ΔPga,exp and ΔPes,exp, while the correlation between PTPga,exp and PTPes,exp is less clear and can be considered weak. When choosing a cut-off value, the results are more promising. Even for predicting PTPga,exp over 40 cmH_2O*s/min using PTPmus,exp(-), the AUC is 0.92, up to 0.97 for predicting a Pga expiratory rise larger than 3 cmH_2O with the expiratory Pes rise above Pcw.

Although the implications and cause of expiration activity cannot be determined, these results show that expiration activity and respiratory muscle activity in general during expiratory flow is quite common. There is uncertainness about the effects of expiration effort and possible eccentric contraction, it could be argued that this expiration effort is a sign of under-assist and that eccentric contraction causes muscle damage. Therefore, clinicians should be aware that muscle effort during expiration (inspiratory as well as expiratory muscles) is common and can probably often be reduced by improving ventilator settings (support level and cycle off criteria).

4.4.1 Strengths and weaknesses

The large dataset and the long duration per patient measurement is a strong point of this study. It helps us give insight in the variations of breathing mechanics over time and delivers a representative dataset for our patient group. Another strength of this study is the analysis of a relatively new parameter, the Pes rise above Pcw, which can also be seen as the minimum Pmus during expiration. This also gives the possibility to investigate relations between the established and newly developed parameters.

Not all included breaths are visually expected, since this is undoable in such a large dataset. This could cause errors, however, in this large dataset, these errors will be averaged out by the huge amount of correct breaths – especially because the majority of erroneous breaths (spasms, coughs) are already filtered out by the named criteria. However, an improvement could be made in filtering the Pes signal, since with the current analysis method, a detected expiratory rise in Pes could originate solely from cardiac interference. In-depth Pes filtering algorithms are proposed in literature [73], however implementation of such a principal component analysis-based filter on our physiological data, did not improve the filtering compared to a simple Butterworth filter. Besides that, enormous processing power is needed to execute such an algorithm on long datasets like in this study. Possibly, he implementation of a template subtraction filter for the Pes signal could be a future solution.

The traditional gold standard for the work a patients delivers, work-of-breathing parameters are not included in this study, however it the agreement with the defined outcome measures could be interesting to investigate. However, the past decades the pressure-time-product measures have taken a more prominent role compared to work-of-breathing in the literature on breathing mechanics. For this study, these measurements were out of scope, and besides that it is hard to calculate work-of-breathing precisely in a breath by breath analysis, because volume variations between inspiration and expiration cause erroneous calculations.

4.4.2 Future implications

Thus, respiratory muscle effort during expiration is common in mechanically ventilated patients on support mode. However, to determine the cause(s) of expiration effort, further research is needed. An option is to study a cohort of patients with expiration effort and determine how expiration effort can

be lowered, or compare this patient group with a patient group without expiration effort, to identify differences between these groups, possibly explaining the origin of expiration effort. To this aim, the demographic data in this study could also be expected. One patients with excessive expiration effort and activity of inspiratory muscles at the start of expiration. This could be a seldom finding, but it could also be the case that several patients show that much expiration activity.

The next step in this research area would be to explore the effects of changes in ventilator setting on the defined expiration activity parameters. Also the effect on the level of Pdi swings or Pdi at end inspiration on expiratory muscle effort can be investigated. However, a clear and concise hypothesis for future research could be formulated, based on the data of all 39 subject and the consequence of changed ventilator support. Another aspect for future research are the effects of respiratory muscle activity during expiration. Is it harmful, and consequently, is awareness of clinicians required?

4.4.3 Clinical relevance

For exact measurement of expiration effort, a gastric balloon seems to be necessary. However, when using a cut-off of 2.3 for Pes rise above Pcw during expiration, a sensitivity of 92.6% is reached for detecting an expiratory Pga rise larger than 3. In clinical practice, a cut-off value of 2 would be more applicable, as bedside measurement of Pes is not as precise as offline analysis. Besides measurement of Pes, there are multiple other tools to screen for expiration effort. Also visual or palpable contraction of the abdominal muscles and an ongoing increase in Paw during an end-inspiratory hold are signs that expiration activity is present.

Compared to previous research, the results of this study mostly give improved insight in the expiration activity in a general population of patients receiving pressure support ventilation on the ICU. Thereby, this study showed the feasibility of several newly defined PTP parameters. The fact that the expiration effort parameters are more heterogeneous compared to the inspiratory effort parameters (PTPmus,insp and PTPdi,insp, shown in Appendix 8.2.9 and 8.2.10) emphasize the relevance of expiratory muscle activity in mechanically ventilated patients in assisted modes. However, questions remain and new questions arise. Why do some patients recruit their expiratory muscles while others don't? What are the effects of expiration muscle effort on critical illness? Is activity of the inspiratory muscles during expiration damaging?

5 Echogenicity to quantify diaphragm muscle characteristics

a reliability study

5.1 Introduction

Ultrasound has earned a prominent position in intensive care medicine, as it is a safe, easy to use and non-invasive technique to support or dispute several diagnoses. Ultrasound assessment can be used as a comprehensive tool to examine multiple organ systems, including the respiratory muscles. The bedside technique can be used to obtain information on global function of the respiratory muscle pump, for example to diagnose diaphragm weakness or paralysis [64]. Ultrasound is used to measure diaphragm thickness and thickening fraction, as an indicator of muscle effort or contractile activity, to predict weaning outcome or help identifying the cause of weaning failure [65, 74]. These measures were found to impact clinical outcome in mechanically ventilated patients [8]. A recent review concluded that ultrasonographic measurement of excursion and thickening fraction has shown to be useful and accurate tool for assessing diaphragmatic dysfunction [65].

While thickness, excursion and thickening fraction have become well-known metrics in intensive care medicine, ultrasound has several other possible features. Echogenicity or echo intensity (EI), for example, is a measure which is commonly used in the field of exercise physiology to measure muscle quality or composition. Lower echogenicity values (darker pixels on average) are assumed to indicate good muscle quality [75]. This technique is based on the fact that every pixel in an ultrasound image represents an 8-bit integer (value ranging from 0 to 255) corresponding to the gray value of that pixel. While the echogenicity of a region-of-interest (ROI) positioned in a muscle is supposed to reflect muscle form and function (strength, adiposity, functional outcomes and fibrous tissue) and acute characteristics (muscle damage and possibly also hydration, intra- and extracellular water and glycogen), it is also influenced by the methodology of the measurements and biological factors [75]. Recently, this novel ultrasound technique has been applied to the diaphragm for the first time, to investigate changes in echo intensity in mechanically ventilated patients [76].

Regarding the methodology of EI-measurements; device settings, subcutaneous fat, subject positioning, rest duration, probe tilt, measuring depth [77] and experience of the researcher are all factors that possibly influence the result of the echogenicity of the tissue [75]. For some factors, such as thickness of the subcutaneous fat layer [78] or different *presets* calibrated in advance [79], correction methods have been proposed. Device settings known to have an impact on the grayscale values and thus the echogenicity are numerous. This was for example shown for the measuring depth, as it changes the image resolution [80]. Also, the gain setting and ultrasound system that is used highly impacts the measured grayscale [81]. Technically, all settings influencing the brightness and contrast of the ultrasound image, probably also influence the echogenicity of the tissue. Thus, as Pillen & van Alfen state, the general consensus is to keep all ultrasound settings constant in investigating echogenicity among and within patients [82].

The study by Coiffard *et al.* (2021) is one of the few studies on diaphragm echogenicity [76]. They found an increased baseline echogenicity value in mechanically ventilated patients compared to younger healthy subjects and a relation between diaphragm echogenicity and prolonged mechanical ventilation duration. Intra- and interrater reliability showed that the analysis method was feasible and repeatable, and a negligible influence of the respiratory cycle on the echogenicity results was found. [76]. However, the influence of muscle contraction on echogenicity is somewhat complex. A study of

the tibialis anterior in healthy subjects showed an echogenicity decrease as a result of contraction [79]. Also, data for the study of Coiffard *et al.* (2021) were not primarily collected to investigate echogenicity, which indicates that the settings used may be suboptimal. Additionally, the variability of performing the ultrasound measurement was not investigated by means of intra- or interrater reliability. A standardized method to perform diaphragm echogenicity measurements could be useful to assess and monitor muscle quality in an easy, non-invasive and bedside manner in patients.

Therefore, the primary aim of this study was to develop a standardized method for measuring and computing diaphragm echogenicity and assess the intra- and interrater of this method in healthy subjects as well as ICU patients. Secondary, the difference between the echogenicity measurement at different locations (zone of apposition vs. frontal) of the diaphragm was determined.

5.2 Methods

5.2.1 Study setup and patients

The study consisted of two steps:

(1) deriving the optimal ultrasound settings, based on measurements in two healthy subjects and thereafter in two critically ill patients, and
(2) performing measurements in critically ill patients and healthy subjects, to determine inter- and intra-rater variability and the factors contributing to the diaphragm echogenicity values.

Measurements were performed in five healthy subjects and ten mechanically ventilated ICU patient. The patient group was divided into a group with breathing effort (n=5) and without breathing effort (n=5). Breathing effort was defined as being invasively ventilated in partially-supported mode, with visible ventilation triggering, indicating patient effort. No breathing effort was defined as being invasively ventilated in controlled mode, without clearly visible patient effort, objectively defined as a maximum RASS-score of -4. We calculated the required sample size for estimating the reproducibility, assuming an intraclass correlation coefficient between two raters of at least 0.85 with 95% CI of width 0.15. With 2 raters per subject, this resulted in a total sample size of 15 subjects, which consists of the heterogeneous group of healthy subjects and ICU patients with and without breathing effort.

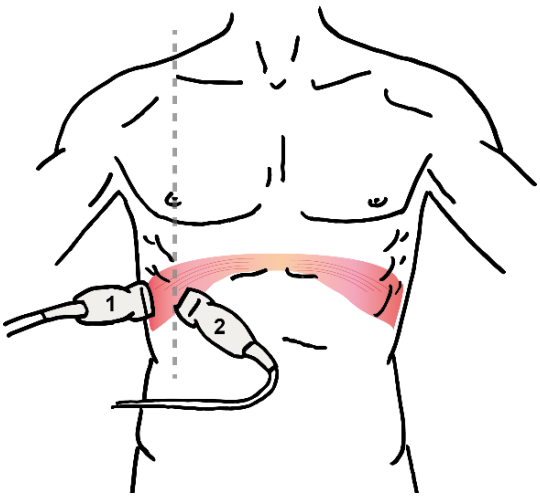

***Figure 37**: Schematic image showing probe positions. For ZOA (1), probe is placed on the mid-axillary line between the 8th and 10th intercostal space, resulting in a sagittal plane. For frontal (2), probe is placed between the nipple-line (dotted gray line) and midclavicular line in the area of the 8th rib, collateral to the rib and then turned cranially to assure a field of view within two ribs. Probe marker is always positioned towards cranially.*

5.2.2 Image acquisition

Measurements were performed using the Philips CX50 (Koninklijke Philips NV, The Netherlands). For every subject, the first observer performed the measurements and marked the probe position on the skin. Thereafter the second observer performed the measurements at the same location, and lastly the first observer repeated the measurement. The probe was placed at two locations, referred to as the frontal and the midaxillary (ZOA) probe position (**Figure 37**).

The settings with a substantial influence on the grayscale were tested in 2 healthy subjects and 2 ICU subjects, to assure optimal settings for all following subjects (step 1). An example of these tests is shown in **Figure 38**, where the effect of the "compress" setting on the image and the histogram is shown. The optimal setting for grayscale analysis results in an histogram with a broad range from low to high gray scale values, but without loss of information due to pixels "falling off" the gray scale (like compress 20 histogram in **Figure 38**). Based on the histograms of the tested settings, the values for the *gain*, *compress*, *persist*, *smooth* and *gray map* were chosen. The combination of settings with the optimal image quality was used for all measurements and is shown in **Table 3**. While almost all image improvement and adaptive filtering settings were turned off, *XRES* was turned on. *XRES* is an adaptive filter, making use of a multiresolution algorithm. It promises to reduce information associated with artefacts directly, while leaving the true tissue information largely unaffected [83]. The risk of using an adaptive filter is that the filtering changes between images, resulting in undesired additional variability between images. However, the images made with *XRES* turned on appeared to have a smaller variability compared to the images made with *XRES* turned off, implicating that the filtering of artefact information resulted in an image mainly representing tissue information. More information can be found in Appendix 8.3.1. Besides that, significantly higher image quality when turning XRES on made segmentation more precise, as the border between muscle and surrounding tissue became easier to distinguish.

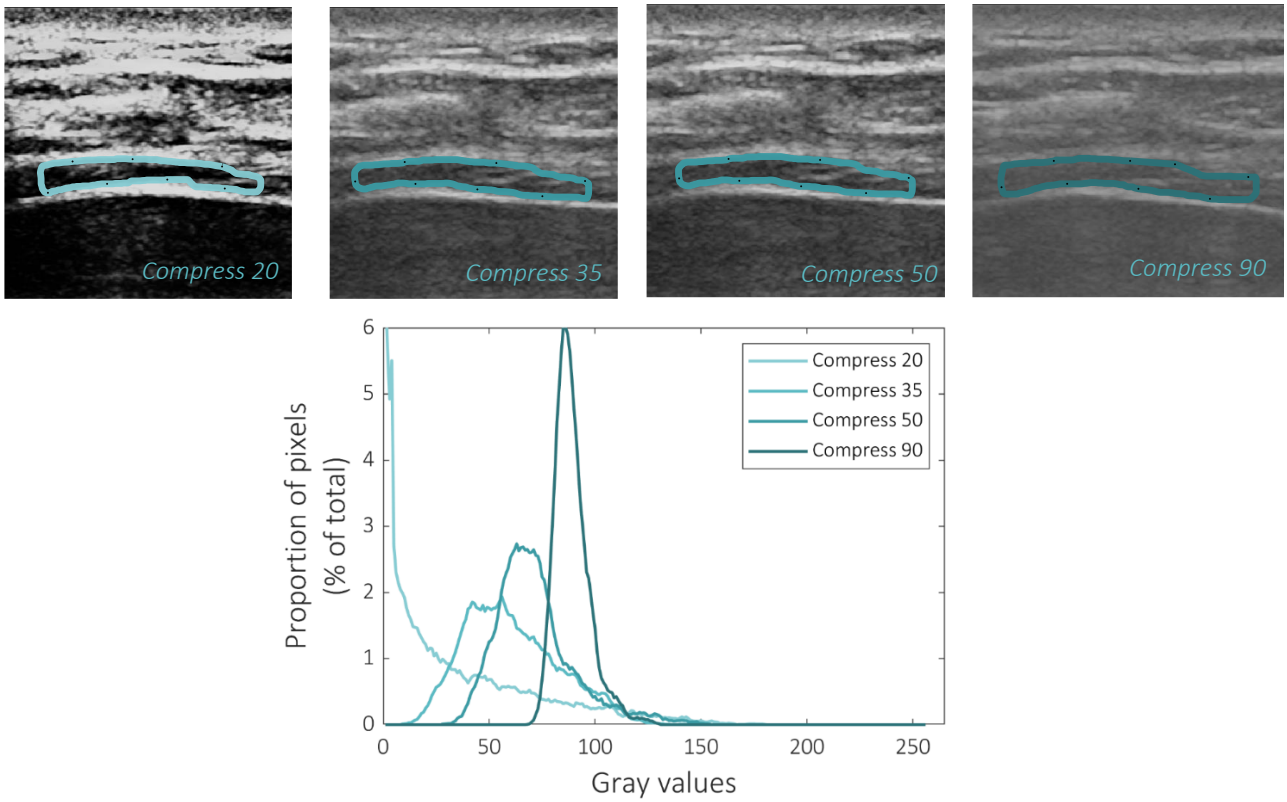

Figure 38: Images and histograms with different compress settings. Histograms show different gray scale distributions caused by different compress settings.

Table 3: Ultrasound measurement settings

Setting	Value
Depth	3.5 and 5 cm
Gain	60
Focus	Always on diaphragm/muscle of interest
Compress	50
Harmonics	Off
Time gain compensation	All on 0 (= straight)
Chroma	Off
Gray map	4
Power	0 dB
Persist	2
Smooth	3
Loop time	12 seconds
XRES	On
iScan gain	0 dB

5.2.3 Image analysis

After ultrasound video acquisition, manual echogenicity analysis was performed offline in MATLAB R2020b (Mathworks®, Natick, Massachusetts). *DICOM* files were loaded into MATLAB and for every video, three end-inspiratory and three end-expiratory frames were chosen by both observers. An average of five frames surrounding the chosen frame number was used for drawing the ROI, like shown in **Figure 39**A. A region as large as possible without crossing the inner edge of the fascia was selected and (reverberation) artefacts were avoided. The histogram of all gray sacle values in the drawn ROI is shown in **Figure 39**B, enabling us to calculate median and 85th percentile (ED85) for the six chosen frame numbers (three inspiration and three expiration) separately. Thereafter, the average median and ED85 were calculated for the three inspiratory frames, the three expiratory frames, and all six frames together.

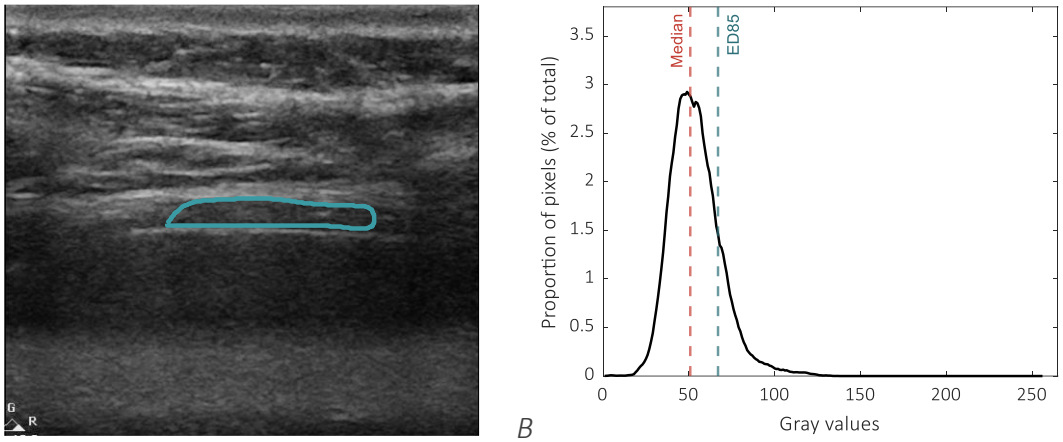

***Figure 39**: **A)** shows an example of manually drawn region of interest in the frontal image of the diaphragm. **B)** Example of the resulting histogram of echogenicity with median and 85th percentile (ED85) as outcome measures.*

5.2.4 Statistical analysis

For the statistical analysis of reliability, R software version 4.0.0 (R Foundation for Statistical Computing, Vienna, Austria) was used. The two-way random, single measures intraclass correlation coefficient (ICC2; absolute agreement) and two-way mixed, single measures intraclass correlation coefficient (ICC3; consistency) were calculated for assessing interrater and intrarater variability respectively. This was done for the average median and ED85 at expiration, inspiration and both expiration and inspiration taken together. To discriminate between the variability of the ultrasound measurement and the analysis of the images, observer 1 also analysed the ultrasound images of observer 2. Also, ICC values for the subgroups (patients and controls) were calculated. Negative ICC

lower bound values were changed to 0 [84]. Echogenicity results were calculated as means with standard deviation (SD) of histogram median and ED85 and Bland-Altman plots were made. To investigate the difference depending on breathing phase (inspiration vs. expiration) and probe position, delta echogenicity values between these conditions were calculated and a paired t-test was performed. Median and ED85 results were tested for normality with Shapiro-Wilk test.

5.3 Results

5.3.1 Reliability

Reproducibility of the measurements quantified as the ICC is shown in **Table 4.** The ICC was calculated separately for expiration (3 frames), inspiration (3 frames) and both inspiration and expiration (6 frames). Interrater ICC ranges from 0.81 to 0.83 and intrarater ICC ranges from 0.85 to 0.87 for median values of the frontal diaphragm. The ICC of the ED85 measurements was slightly lower, ranging from 0.67 – 0.74 for interrater and from 0.82 – 0.84 for intrarater. For the ZOA probe position, ICC ranges from 0.67 to 0.75 for interrater and 0.76 to 0.81 for intrarater. Similarly as for the frontal results, ED85 ICC values are slightly lower (ranging from 0.71 – 0.72 for intrarater and 0.51 – 0.61 for interrater).

Table 4: ICC values with upper and lower bound of median and ED85 of gray scale values. Intrarater refers to 2 observations by the same observer, repeating the whole process of ultrasound image acquisition and analysis. Interrater refers to repeating the whole process by a second observer.

		Frontal		ZOA	
		Median intensity (lower – upper bound)	**ED85** intensity (lower – upper bound)	**Median** intensity (lower – upper bound)	**ED85** intensity (lower – upper bound)
Intrarater	Inspiration	0.88 (0.73 – 0.95)	0.83 (0.63 – 0.93)	0.81 (0.59 – 0.92)	0.71 (0.40 – 0.87)
	Expiration	0.85 (0.66 – 0.93)	0.82 (0.60 – 0.92)	0.76 (0.50 – 0.90)	0.71 (0.41 – 0.87)
	All frames	0.87 (0.71 – 0.95)	0.84 (0.64 – 0.93)	0.79 (0.54 – 0.91)	0.72 (0.43 – 0.88)
Interrater	Inspiration	0.81 (0.45 – 0.93)	0.67 (0.29 – 0.86)	0.75 (0.49 – 0.89)	0.61 (0.25 – 0.82)
	Expiration	0.83 (0.57 – 0.93)	0.74 (0.43 – 0.89)	0.67 (0.36 – 0.85)	0.51 (0.12 – 0.77)
	All frames	0.83 (0.51 – 0.93)	0.71 (0.35 – 0.88)	0.73 (0.44 – 0.88)	0.57 (0.21 – 0.80)

The ICC values for the subgroups – healthy controls and ICU patients – are shown in **Table 5**. The values are only shown for inspiration frames, as we found for the whole group that the ICC of inspiration frames is similar to the all frames (inspiration and expiration) taken together.

Table 5: ICC values of healthy subject and patients measurements separately. Only measurements at inspiration are shown.

		Frontal		ZOA	
		Median intensity (lower – upper bound)	ED85 intensity (lower – upper bound)	Median intensity (lower – upper bound)	ED85 intensity (lower – upper bound)
Healthy	Intrarater	0.50 (0 – 0.90)	0.48 (0 – 0.90)	0.61 (0 – 0.92)	0.86 (0.37 – 0.98)
	Interrater	0.43 (0 – 0.86)	0.10 (0 – 0.75)	0.92 (0.58 – 0.99)	0.38 (0 – 0.83)
Patients	Intrarater	0.96 (0.88 – 0.99)	0.92 (0.77 – 0.97)	0.79 (0.45 – 0.93)	0.73 (0.34 – 0.91)
	Interrater	0.87 (0.63 – 0.96)	0.82 (0.52 – 0.94)	0.75 (0.36 – 0.91)	0.75 (0.40 – 0.91)

The echogenicity values (median of frontal as well as ZOA measurements) of the analysis at end-expiratory frames are shown in Bland Altman plots in **Figure 40.** It can be seen that the difference for interrater reliability is larger than for intrarater. For the ZOA probe position, bias is 1.4 (limits of agreement: -15.9 – 18.8) for the interrater reliability and -0.4 (limits of agreement -22.3 – 21.6) for

the intrarater reliability. For the frontal probe position, a larger bias of 7.2 (limits of agreement: -10.2 – 24.5) for the interrater reliability and 2.9 (limits of agreement -14.9 – 20.7) for the intrarater reliability was found. Limits of agreement and thus the critical difference (1.96 x SD) are wider for the interrater reliability of the ZOA (21.9), compared to intrarater of ZOA (17.4) and both interrater (17.3) and intrarater (17.8) of the frontal measurements. For the ED85 results, Bland Altman plots can be found in Appendix 8.3.2.

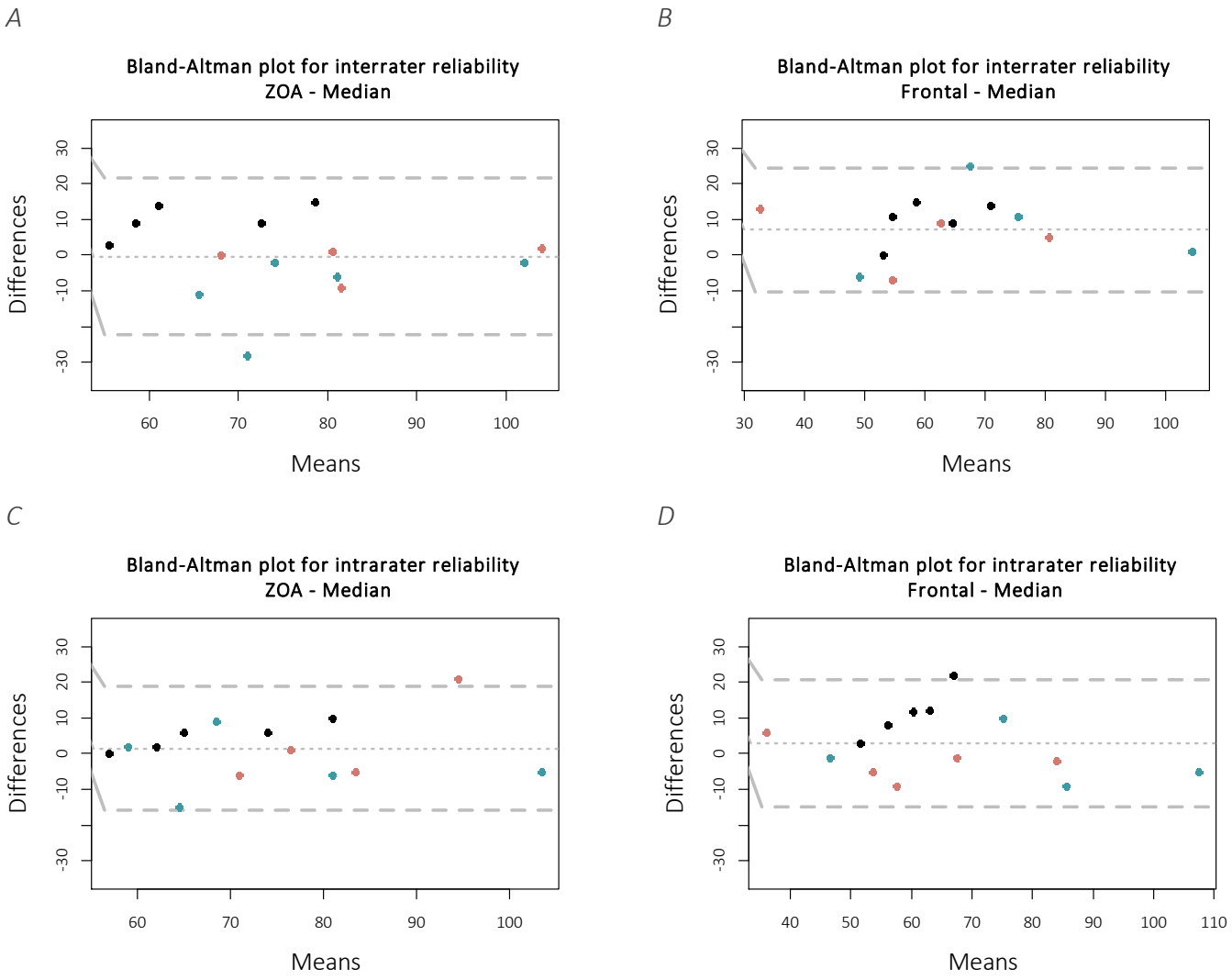

Figure 40: *Bland Altman plots of echogenicity results from observer 1 compared to observer 2 (interrater) of ZOA (A) and frontal (B) measurements and of the repeated measurements of observer 1 (intrarater) of ZOA (C) and frontal (D) measurement. All graphs show median echogenicity values, Bland-Altman plots for ED85 echogenicity can be found in Appendix 8.3.2. Color code: black = healthy, blue = PC, pink = PS. All Blant-Altman plots are made from results of measurements at inspiration.*

5.3.2 Subjects

The five healthy subjects (2 male) had a mean age of 27 and a mean BMI of 21.5. The 10 patients (5 male) who were measured had a mean age of 67 and a mean BMI of 27.1. Of these patients, 5 were mechanically ventilated on pressure control mode, while the 5 other patients were mechanically ventilated on pressure support or CPAP mode. The average number of days since intubation was 2.9 days. In two measurements it was not possible to measure at both probe locations, due to excessive oedema and wounds at the measurement location, resulting in one missing frontal and one missing ZOA measurement.

5.3.3 Intensity results

The mean grayscale histogram median value of the frontal diaphragm was 66.7 (SD 16.8) and the mean ED85 was 86.5 (SD 19.3) for the whole group of subjects with both inspiratory and expiratory frames combined, as measured and analysed by observer 1. The mean histogram median was 66.5 for inspiration and 66.9 for expiration for the frontal measurements, while mean ED85 was 86.8 and 86.7 respectively. Based on Shapiro-Wilk test, all measurements were normally distributed ($p > 0.05$), except for the second measurement of ED85 of the frontal diaphragm of observer 1 ($p = 0.028$) and the median measurement of the frontal diaphragm of observer 2 ($p = 0.029$). For this reason, conclusions are drawn from results at inspiration.

Table 6: Average results of measurements, for 3 averaged inspiration frames, 3 averaged expiration frames and average of all six frames. Averages for all six frames are also shown for subgroups (healthy, PS, PC).

	Frontal		ZOA	
	Mean median (SD)	Mean ED85 (SD)	Mean median (SD)	Mean ED85 (SD)
Inspiration	66.5 (17.8)	86.5 (19.3)	75.1 (14.8)	96.4 (19.3)
Expiration	66.9 (16.1)	86.8 (19.0)	76.0 (15.3)	97.7 (17.1)
All frames	66.7 (16.8)	86.5 (19.3)	75.5 (15.0)	97.1 (18.1)
• Healthy	66.1 (8.4)	86.8 (10.1)	70.5 (11.5)	100.5 (12.0)
• Patients PS	59.4 (16.1)	78.2 (16.7)	82.8 (16.5)	102.8 (24.2)
• Patients PC	76.5 (23.6)	97.0 (28.0)	74.8 (17.7)	89.1 (18.7)

The mean of the median of the histogram for the six chosen frames was 66.1 for healthy subjects, 67.5 for the patients without breathing effort (pressure control) and 58.6 for the ICU patients with breathing effort (pressure support) for the frontal measurements. **Table 6** also shows these results for the ZOA measurements, including ED85 values for both probe positions. Similar to the whole group, for the subgroups, the average medians for inspiration also differed no more than 3 grayscale levels between inspiration and expiration.

The mean delta (ZOA median – frontal median) between probe position is 9.7 (SD 22.6), which was not significantly different according to a paired t-test ($p = 0.145$). The mean delta of ED85 (ZOA ED85 – frontal ED85) is 11.9 (SD 27.6), which was not significantly different according to a paired t-test ($p = 0.146$). The mean delta between inspiration and expiration was -0.4 (SD 4.2) for median results of the frontal diaphragm and -0.9 (SD 2.8) for median results of the ZOA. Paired t-test showed no statistical difference between inspiration and expiration of frontal measurement ($p = 0.742$) nor for the ZOA measurements ($p = 0.234$).

The process of measuring echogenicity consists of two important steps, namely the ultrasound image acquisition and the offline analysis. The offline analysis comprises of choosing inspiration and expiration frames, and drawing the region of interest. To investigate the ICC of the analysis part standing on itself, both the observers have performed the analysis on one series of the same images. The resulting ICC was 0.97 (0.91-0.99) for the frontal measurements and 0.99 (0.96 – 0.99) for the ZOA measurements, calculated for the average of all six chosen frames.

5.4 Discussion

The main goal of this study was to investigate the reliability of echogenicity measurement and investigate the optimal settings and method for echogenicity measurements. It has been found that the ICC of interrater reliability (0.81) as well as intrarater reliability (0.88) of the frontal measurements at inspiration can be considered good. While the ICC values of the ZOA measurements (0.75 for interrater and 0.81 for intrarater) are slightly lower, these values are still considered as good agreement. Compared to the reproducibility reported in other studies, our bias for the ZOA probe

position (1.4 for interrater) is comparable to the reported bias of -1.5 (limits [-8.6; 5.7]) between analyser and -2.8 (limits [-15.8; 10.2]) between images. However the limits of agreement are wider, which could be explained by the smaller sample size. In addition, this cannot be compared directly as in this study the reproducibility of the whole process (image acquisition, selection and analysis) was assessed, in contrast to the study of Coiffard *et al.* (2021) in which the reliability for the analysis and the image acquisition was assessed separately. The frontal probe position was not investigated in this study [76].

The ICC results of only the offline analysis on the same video were excellent (0.97). Thus, it can be inferred that the variation between results is mainly caused by the acquisition of the ultrasound images. Due to low variance in healthy subject echogenicity values and the small sample size, lower and upper bounds of ICC values for only the healthy subjects, are found to be ranging from very low to quite high and with a very broad range. Caution is needed when interpreting ICC values of the healthy subjects subgroup, in which the lower bound of the results is very poor, due to the small homogeneous subgroup.

Another interesting finding is the fact that inspiration and expiration frames did not differs significantly, and the changes between inspiratory and expiratory frames were not consistent in the same direction. Despite the fact that these results are consistent with previous results [76], the fact that the actin and myosin filaments within a sarcomere of a muscle slide past each other during contraction would theoretically impact echogenicity values. The movement of fibres during contraction could increase the tissue density, causing a change in echogenicity. On the other hand, changes in fibre angle during contraction can have an influence on echogenicity. Besides that, other research showed a decrease in echogenicity as a result of contraction [79]. Nevertheless, our results also show no consistent difference between echogenicity at inspiration and expiration. A possible explanation could be that the effect of muscle contraction on echogenicity is negligible, particularly when compared to the effect of the tendon plate moving in or out of the window. Appendix 8.3.4 further elaborates on this aspect .

Although it was not within the main goal of this study, it is remarkable that the level of echogenicity results in the healthy subjects are similar to the ICU patients. This is in contrast to earlier published results [76]. Nevertheless, the results of the healthy subjects have low variability, while there is more variance within the results of the ICU patients. Especially one of the ICU patients (most left in **Figure 40**B and D) showed the lowest echogenicity of all subjects. It is questionable whether this is physiological or a technical artifact (e.g., a reverberation artefact seemed present in this image, causing the lower echogenicity value, as can be seen in Appendix 8.3.3). Perhaps it is possible to quantify factors that account for differences between measurements of the same subject such as depth at which the muscle lies or thickness of the subcutaneous fat layer. Namely, these are factors that we are able to quantify using the acquired images and are probably not exactly the same between different images due to inevitable variations in probe position or angle.

The aforementioned observation emphasizes the need for high quality images, as a minor artefact can significantly change the echogenicity values. Therefore, it is important to use enough ultrasound gel and use a standardized method for image acquisition, like proposed in **Table 3**. Apparently, small changes in probe position, tilt or maybe just timing, can already have an impact on the resulting image quality and echogenicity results.

In the analysis of this study, manual selection of the region of interest (ROI) was used to determine the area of the diaphragm for gray scale analysis. To avoid selection bias and automate this process, automatic selection of the ROI is a promising technique for echogenicity analysis. To investigate this, a semi-automatic ROI selection was developed with an image segmentation program written in MATLAB. This program segmented the diaphragm area in the ultrasound image by use of a rectangular region containing the diaphragm – which was defined based on the average image and thus delineated the diaphragm in all frames – and a polyline defined repeatedly for every 20 frames. This polyline only

included so-called “fore-ground” points, referring to the diaphragm muscle tissue. The “*grabcut*” function in Matlab then used this input to select the diaphragm area, which was optimized by eroding the region to prevent overshooting the diaphragm. However, the performance of this algorithm was insufficient, probably caused by different appearances of the diaphragm and the absence of a clear border between the diaphragm and surrounding tissue. Therefore, only the manual analysis tool was used in this study. Automatic segmentation of ultrasound is done before, but not for echogenicity analysis[85-87]. The relatively poor image quality, due to equal settings for all subjects, and the thinness of the diaphragm, cause additional challenges to the existing automatic ROI selection algorithms.

5.4.1 Future perspectives

It is crucial to standardize ultrasound measurement technique, as well as the settings on the ultrasound machine and the protocol for measuring echogenicity. Based on the current results, no firm conclusions can be made on the optimal measurement location (frontal or ZOA probe position). Despite that, the ICC results hint to a slightly better reliability for the frontal measurement position. Expanding the sample size of this reliability study could give a definite answer on the optimal measurement method and the reliability of this method. The next step is to explore the clinical implications of echogenicity measurements of the diaphragm. In future studies it should be investigated whether echogenicity measurements are superior compared to current techniques for monitoring the diaphragm, such as thickness and thickening fraction on ultrasound and more physiological techniques such as measuring Pdi. The exact meaning of echogenicity values of muscle and particularly the diaphragm could also be investigated in studies comparing echogenicity with a biopsy of the muscle, considered as the gold standard of investigating tissue properties. Comparing the results with other imaging tools such as MRI or CT would be a second best option and is less invasive. However, the feasibility of such a study is challenging, as a biopsy is quite invasive.

While there is a moderate to good reproducibility of echogenicity measurement, there is still a notable amount of variation within the echogenicity results between observers and also within observers. This is important to take into account when interpreting echogenicity values of a patient. With the current knowledge, it could be stated that the usability of diaphragm echogenicity is mainly in monitoring changes within a patient. Based on the results of this study, an echogenicity change of less than 15 to 20, based on the reported critical differences, should be considered within measurement variability.

6 General discussion

The described studies yielded several steps forward in the research field of respiratory muscle physiology, to be more specific on the coordination of the respiratory muscle with a focus on the expiratory phase of breathing. The clinical study provides a feasible measurement and analysis protocol for the comprehensive analysis of functional as well as timing coordination. The preliminary results showed relevant findings, some findings are contradictory with the hypothesized results. In the subject who failed the SBT, no expiration effort was found, while expiration effort was present in the subject with a successful SBT. Further subject inclusion should clarify this and give insight in the utility of the other defined outcome measures, such as phase angle and coherence parameters.

The additional analysis on the existing data of a clinical trial shows the feasibility of newly defined respiratory muscle effort parameters such as PTPmus,exp, PTPdi,exp, Pdi(end-insp) and the expiratory rise in Pes. The results give insight in the prevalence and level of ICU patients under pressure support ventilation. Also the results are promising for the possibility of detecting expiration effort without a gastric balloon.

Besides these breathing mechanics measurements, Chapter 5 investigated the feasibility and reliability of echogenicity measurements of the diaphragm. While these measurements are currently not accurate enough to assess diaphragm quality in critically ill, the results are promising. When sticking to an appropriate measurement protocol, ICC results are appropriate. Future research should focus on the validity of these measurements. To what extent does echogenicity measure the same as gold standard measurements (biopsy, CT or MRI) for muscle quality? Also implementation of echogenicity measurements in clinical practice is an aspect to focus on.

Considering the analysis techniques used, several aspects can be improved as described in the discussion section of the background. Future research should focus on improving Pes filtering, possibly template subtraction is an option. Regarding the functional EMG analysis, coherence analysis showed ambiguous results. Further work is required to establish a standardized method an evaluating normal values for coherence of the respiratory muscles. Regarding the echogenicity analysis, automatic ROI selection is a technical improvement that should be established and investigated in the future.

Several clinical questions remain. What causes expiration effort in which patient population? Is expiration muscle effort related to effort of inspiratory muscles during expiration? Is expiratory muscle recruitment beneficial for these patients? How often does the timing coordination of mechanically ventilated patients change over time (during an SBT)? Is tonic activity of the diaphragm present during the expiratory phase of breathing in humans? And is it harmful?

7 Bibliography

1. Walter, J.M., T.C. Corbridge, and B.D. Singer, *Invasive Mechanical Ventilation.* South Med J, 2018. **111**(12): p. 746-753.
2. Brochard, L., A. Slutsky, and A. Pesenti, *Mechanical Ventilation to Minimize Progression of Lung Injury in Acute Respiratory Failure.* Am J Respir Crit Care Med, 2017. **195**(4): p. 438-442.
3. Brower, R.G., et al., *Ventilation with lower tidal volumes as compared with traditional tidal volumes for acute lung injury and the acute respiratory distress syndrome.* N Engl J Med, 2000. **342**(18): p. 1301-8.
4. Goligher, E.C., et al., *Lung- and Diaphragm-Protective Ventilation.* American Journal of Respiratory and Critical Care Medicine, 2020. **202**(7): p. 950-961.
5. Heunks, L.M.A., J. Doorduin, and J.G. van der Hoeven, *Monitoring and preventing diaphragm injury.* Current opinion in critical care, 2015. **21**(1): p. 34-41.
6. Dres, M., et al., *Critical illness-associated diaphragm weakness.* Intensive Care Med, 2017. **43**(10): p. 1441-1452.
7. Jaber, S., et al., *Rapidly Progressive Diaphragmatic Weakness and Injury during Mechanical Ventilation in Humans.* American Journal of Respiratory and Critical Care Medicine, 2011. **183**(3): p. 364-371.
8. Goligher, E.C., et al., *Mechanical Ventilation–induced Diaphragm Atrophy Strongly Impacts Clinical Outcomes.* American Journal of Respiratory and Critical Care Medicine, 2018. **197**(2): p. 204-213.
9. Jung, B., et al., *Diaphragmatic dysfunction in patients with ICU-acquired weakness and its impact on extubation failure.* Intensive Care Med, 2016. **42**(5): p. 853-861.
10. Schepens, T., et al., *Diaphragm-protective mechanical ventilation.* Curr Opin Crit Care, 2019. **25**(1): p. 77-85.
11. Thille, A.W., et al., *Patient-ventilator asynchrony during assisted mechanical ventilation.* Intensive Care Med, 2006. **32**(10): p. 1515-22.
12. Pham, T., L.J. Brochard, and A.S. Slutsky, *Mechanical Ventilation: State of the Art.* Mayo Clin Proc, 2017. **92**(9): p. 1382-1400.
13. de Vries, H., et al., *Assessing breathing effort in mechanical ventilation: physiology and clinical implications.* Annals of Translational Medicine, 2018. **6**(19): p. 13.
14. Goligher, E.C., et al., *Clinical strategies for implementing lung and diaphragm-protective ventilation: avoiding insufficient and excessive effort.* Intensive Care Med, 2020. **46**(12): p. 2314-2326.
15. Shi, Z.H., et al., *Expiratory muscle dysfunction in critically ill patients: towards improved understanding.* Intensive Care Med, 2019. **45**(8): p. 1061-1071.
16. Doorduin, J., et al., *Respiratory Muscle Effort during Expiration in Successful and Failed Weaning from Mechanical Ventilation.* Anesthesiology, 2018. **129**(3): p. 490-501.
17. Parthasarathy, S., et al., *Sternomastoid, rib cage, and expiratory muscle activity during weaning failure.* J Appl Physiol (1985), 2007. **103**(1): p. 140-7.
18. Laghi, F., et al., *Diaphragmatic neuromechanical coupling and mechanisms of hypercapnia during inspiratory loading.* Respiratory Physiology & Neurobiology, 2014. **198**: p. 32-41.
19. Pellegrini, M., et al., *The Diaphragm Acts as a Brake during Expiration to Prevent Lung Collapse.* Am J Respir Crit Care Med, 2017. **195**(12): p. 1608-1616.
20. Shebl, E. and B. Burns, *Respiratory Failure*, in *StatPearls*. 2021, StatPearls Publishing Copyright © 2021, StatPearls Publishing LLC.: Treasure Island (FL).
21. Sinderby, C., *Neurally adjusted ventilatory assist (NAVA).* Minerva Anestesiol, 2002. **68**(5): p. 378-80.
22. Jonkman, A.H., et al., *Proportional modes of ventilation: technology to assist physiology.* Intensive care medicine, 2020. **46**(12): p. 2301-2313.
23. Prinianakis, G., E. Kondili, and D. Georgopoulos, *Effects of the flow waveform method of triggering and cycling on patient-ventilator interaction during pressure support.* Intensive Care Medicine, 2003. **29**(11): p. 1950-1959.
24. Mancebo, J., *Triggering and cycling off during pressure support ventilation: simplicity or sophistication?* Intensive Care Medicine, 2003. **29**(11): p. 1871-1872.
25. Rawal, G., S. Yadav, and R. Kumar, *Acute Respiratory Distress Syndrome: An Update and Review.* Journal of translational internal medicine, 2018. **6**(2): p. 74-77.
26. Boron, W.F. and E.L. Boulpaep, *Medical Physiology, 2e Updated Edition E-Book: with STUDENT CONSULT Online Access*. 2012: Elsevier Health Sciences.
27. De Troyer, A. and A.M. Boriek, *Mechanics of the respiratory muscles.* Compr Physiol, 2011. **1**(3): p. 1273-300.
28. Levine, S., et al., *Rapid Disuse Atrophy of Diaphragm Fibers in Mechanically Ventilated Humans.* New England Journal of Medicine, 2008. **358**(13): p. 1327-1335.
29. Vassilakopoulos, T. and B.J. Petrof, *Ventilator-induced diaphragmatic dysfunction.* Am J Respir Crit Care Med, 2004. **169**(3): p. 336-41.

30. Boles, J.M., et al., *Weaning from mechanical ventilation.* European Respiratory Journal, 2007. **29**(5): p. 1033.
31. Peñuelas, Ó., A.W. Thille, and A. Esteban, *Discontinuation of ventilatory support: new solutions to old dilemmas.* Curr Opin Crit Care, 2015. **21**(1): p. 74-81.
32. Smina, M., et al., *Cough peak flows and extubation outcomes.* Chest, 2003. **124**(1): p. 262-8.
33. Shi, Z.-H., et al., *Changes in Respiratory Muscle Thickness during Mechanical Ventilation: Focus on Expiratory Muscles.* Anesthesiology, 2021. **134**(5): p. 748-759.
34. Goligher, E.C., et al., *Diaphragmatic myotrauma: a mediator of prolonged ventilation and poor patient outcomes in acute respiratory failure.* Lancet Respir Med, 2019. **7**(1): p. 90-98.
35. Akoumianaki, E., et al., *Mechanical ventilation-induced reverse-triggered breaths: a frequently unrecognized form of neuromechanical coupling.* Chest, 2013. **143**(4): p. 927-938.
36. Wilcox, P.G. and R.L. Pardy, *Diaphragmatic weakness and paralysis.* Lung, 1989. **167**(6): p. 323-41.
37. *ATS/ERS Statement on Respiratory Muscle Testing.* American Journal of Respiratory and Critical Care Medicine, 2002. **166**(4): p. 518-624.
38. Akoumianaki, E., et al., *The application of esophageal pressure measurement in patients with respiratory failure.* Am J Respir Crit Care Med, 2014. **189**(5): p. 520-31.
39. Suarez-Sipmann, F., *New modes of assisted mechanical ventilation.* Medicina Intensiva (English Edition), 2014. **38**(4): p. 249-260.
40. Mauri, T., et al., *Esophageal and transpulmonary pressure in the clinical setting: meaning, usefulness and perspectives.* Intensive Care Med, 2016. **42**(9): p. 1360-73.
41. Jubran, A., W.B. Van de Graaff, and M.J. Tobin, *Variability of patient-ventilator interaction with pressure support ventilation in patients with chronic obstructive pulmonary disease.* Am J Respir Crit Care Med, 1995. **152**(1): p. 129-36.
42. Sassoon, C.S., et al., *Pressure-time product during continuous positive airway pressure, pressure support ventilation, and T-piece during weaning from mechanical ventilation.* Am Rev Respir Dis, 1991. **143**(3): p. 469-75.
43. Kyroussis, D., et al., *Effect of maximum ventilation on abdominal muscle relaxation rate.* Thorax, 1996. **51**(5): p. 510-5.
44. Kyroussis, D., et al., *Respiratory muscle activity in patients with COPD walking to exhaustion with and without pressure support.* Eur Respir J, 2000. **15**(4): p. 649-55.
45. Sturini, E., et al., *Respiratory variation of intra-abdominal pressure: indirect indicator of abdominal compliance?* Intensive Care Med, 2008. **34**(9): p. 1632-7.
46. Pelosi, P., M. Quintel, and M.L. Malbrain, *Effect of intra-abdominal pressure on respiratory mechanics.* Acta Clin Belg, 2007. **62 Suppl 1**: p. 78-88.
47. Hammer, J. and C.J.L. Newth, *Assessment of thoraco-abdominal asynchrony.* Paediatric Respiratory Reviews, 2009. **10**(2): p. 75-80.
48. Ito, K., et al., *Surface electromyography activity of the rectus abdominis, internal oblique, and external oblique muscles during forced expiration in healthy adults.* Journal of Electromyography and Kinesiology, 2016. **28**: p. 76-81.
49. McGill, S., D. Juker, and P. Kropf, *Appropriately placed surface EMG electrodes reflect deep muscle activity (psoas, quadratus lumborum, abdominal wall) in the lumbar spine.* Journal of Biomechanics, 1996. **29**(11): p. 1503-1507.
50. Sánchez-Zuriaga, D., et al., *Trunk muscle activation patterns and spine kinematics when using an oscillating blade: influence of different postures and blade orientations.* Arch Phys Med Rehabil, 2009. **90**(6): p. 1055-60.
51. Sharp, J.T., et al., *Comparison of diaphragm EMG centroid frequencies: esophageal versus chest surface leads.* Am Rev Respir Dis, 1993. **147**(3): p. 764-7.
52. Sinderby, C.A., et al., *Enhancement of signal quality in esophageal recordings of diaphragm EMG.* J Appl Physiol (1985), 1997. **82**(4): p. 1370-7.
53. Roesthuis, L.H., et al., *Recruitment pattern of the diaphragm and extradiaphragmatic inspiratory muscles in response to different levels of pressure support.* Annals of Intensive Care, 2020. **10**(1): p. 67.
54. Dideriksen, J.L., et al., *Coherence of the Surface EMG and Common Synaptic Input to Motor Neurons.* Front Hum Neurosci, 2018. **12**: p. 207.
55. Boonstra, T.W., *The potential of corticomuscular and intermuscular coherence for research on human motor control.* Frontiers in human neuroscience, 2013. **7**: p. 855-855.
56. Laine, C.M. and F.J. Valero-Cuevas, *Intermuscular coherence reflects functional coordination.* J Neurophysiol, 2017. **118**(3): p. 1775-1783.
57. Brown, P., et al., *Coherent cortical and muscle discharge in cortical myoclonus.* Brain, 1999. **122 (Pt 3)**: p. 461-72.
58. Kilner, J.M., et al., *Task-dependent modulation of 15-30 Hz coherence between rectified EMGs from human hand and forearm muscles.* J Physiol, 1999. **516 (Pt 2)**(Pt 2): p. 559-70.

59. Boliek, C.A., et al., *Differential Cortical Control of Chest Wall Muscles During Pressure- and Volume-Related Expiratory Tasks and the Effects of Acute Expiratory Threshold Loading.* Motor Control, 2019. **23**(1): p. 13-33.
60. Grosse, P., M.J. Cassidy, and P. Brown, *EEG-EMG, MEG-EMG and EMG-EMG frequency analysis: physiological principles and clinical applications.* Clin Neurophysiol, 2002. **113**(10): p. 1523-31.
61. Tomczak, C.R., K.R. Greidanus, and C.A. Boliek, *Modulation of chest wall intermuscular coherence: effects of lung volume excursion and transcranial direct current stimulation.* J Neurophysiol, 2013. **110**(3): p. 680-7.
62. Smith, A. and M. Denny, *High-frequency oscillations as indicators of neural control mechanisms in human respiration, mastication, and speech.* J Neurophysiol, 1990. **63**(4): p. 745-58.
63. Farina, D., F. Negro, and N. Jiang, *Identification of common synaptic inputs to motor neurons from the rectified electromyogram.* J Physiol, 2013. **591**(10): p. 2403-18.
64. Tuinman, P.R., et al., *Respiratory muscle ultrasonography: methodology, basic and advanced principles and clinical applications in ICU and ED patients—a narrative review.* Intensive Care Medicine, 2020. **46**(4): p. 594-605.
65. Zambon, M., et al., *Assessment of diaphragmatic dysfunction in the critically ill patient with ultrasound: a systematic review.* Intensive Care Med, 2017. **43**(1): p. 29-38.
66. Baydur, A., et al., *A simple method for assessing the validity of the esophageal balloon technique.* Am Rev Respir Dis, 1982. **126**(5): p. 788-91.
67. Jonkman, A.H., et al., *Estimated ECG Subtraction method for removing ECG artifacts in esophageal recordings of diaphragm EMG.* Biomedical Signal Processing and Control, 2021. **69**: p. 102861.
68. Lessard, M.R., F. Lofaso, and L. Brochard, *Expiratory muscle activity increases intrinsic positive end-expiratory pressure independently of dynamic hyperinflation in mechanically ventilated patients.* Am J Respir Crit Care Med, 1995. **151**(2 Pt 1): p. 562-9.
69. Gherini, S., R.M. Peters, and R.W. Virgilio, *Mechanical Work on the Lungs and Work of Breathing with Positive End-Expiratory Pressure and Continuous Positive Airway Pressure.* Chest, 1979. **76**(3): p. 251-256.
70. Albani, F., et al., *Flow Index: a novel, non-invasive, continuous, quantitative method to evaluate patient inspiratory effort during pressure support ventilation.* Critical Care, 2021. **25**(1): p. 196.
71. Bellani, G., et al., *Measurement of Diaphragmatic Electrical Activity by Surface Electromyography in Intubated Subjects and Its Relationship With Inspiratory Effort.* Respiratory Care, 2018. **63**(11): p. 1341-1349.
72. Ninane, V., J.C. Yernault, and A. de Troyer, *Intrinsic PEEP in patients with chronic obstructive pulmonary disease. Role of expiratory muscles.* Am Rev Respir Dis, 1993. **148**(4 Pt 1): p. 1037-42.
73. Mukhopadhyay, S.K. and S. Krishnan, *A singular spectrum analysis-based model-free electrocardiogram denoising technique.* Comput Methods Programs Biomed, 2020. **188**: p. 105304.
74. Umbrello, M., et al., *Diaphragm ultrasound as indicator of respiratory effort in critically ill patients undergoing assisted mechanical ventilation: a pilot clinical study.* Crit Care, 2015. **19**(1): p. 161.
75. Stock, M.S. and B.J. Thompson, *Echo intensity as an indicator of skeletal muscle quality: applications, methodology, and future directions.* Eur J Appl Physiol, 2021. **121**(2): p. 369-380.
76. Coiffard, B., et al., *Diaphragm echodensity in mechanically ventilated patients: a description of technique and outcomes.* Critical Care, 2021. **25**(1): p. 64.
77. Varanoske, A.N., et al., *Influence of muscle depth and thickness on ultrasound echo intensity of the vastus lateralis.* Acta Radiologica, 2020: p. 0284185120958405.
78. Young, H.-J., et al., *Measurement of intramuscular fat by muscle echo intensity.* Muscle & nerve, 2015. **52**(6): p. 963-971.
79. de Jong, L., et al., *Three-dimensional quantitative muscle ultrasound in a healthy population.* Muscle Nerve, 2021. **64**(2): p. 199-205.
80. Paris, M.T., et al., *Ultrasound image resolution influences analysis of skeletal muscle composition.* Clin Physiol Funct Imaging, 2020. **40**(4): p. 277-283.
81. Steffel, C.N., et al., *Influence of Ultrasound System and Gain on Grayscale Median Values.* Journal of Ultrasound in Medicine, 2019. **38**(2): p. 307-319.
82. Pillen, S. and N. van Alfen, *Skeletal muscle ultrasound.* Neurol Res, 2011. **33**(10): p. 1016-24.
83. Jago, J., et al., *XRES: adaptive Enhancement of Ultrasound Images.* 2002. **46**: p. 36-41.
84. Bartko, J.J., *On various intraclass correlation reliability coefficients.* Psychological Bulletin, 1976. **83**(5): p. 762-765.
85. Cunningham, R.J., P.J. Harding, and I.D. Loram, *Real-Time Ultrasound Segmentation, Analysis and Visualisation of Deep Cervical Muscle Structure.* IEEE Trans Med Imaging, 2017. **36**(2): p. 653-665.
86. Darby, J., et al., *Automated regional analysis of B-mode ultrasound images of skeletal muscle movement.* J Appl Physiol (1985), 2012. **112**(2): p. 313-27.
87. Salvi, M., et al., *Transverse Muscle Ultrasound Analysis (TRAMA): Robust and Accurate Segmentation of Muscle Cross-Sectional Area.* Ultrasound Med Biol, 2019. **45**(3): p. 672-683.

8 Appendices

8.1 Appendices chapter 3

8.1.1 Additional figures subject 1

8.1.1.1 Breathing mechanics

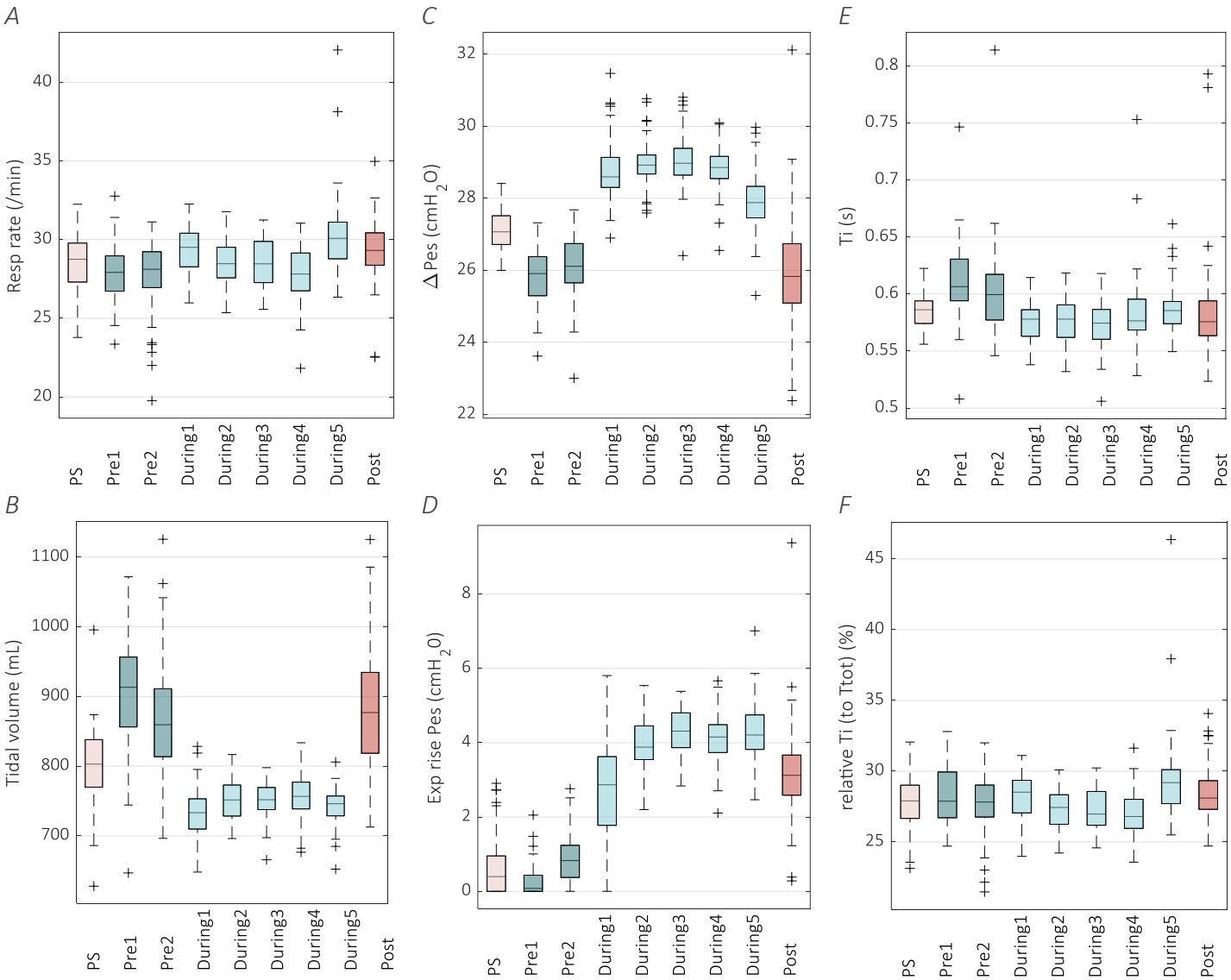

Figure 41: *Additional breathing mechanics and functional coordination results, showing* ***A)*** *respiratory rate,* ***B)*** *Tidal volume,* ***C)*** *inspiratory Pes swings,* ***D)*** *Expiratory rise of Pes above Pcw,* ***E)*** *inspiratory times and* ***F)*** *relative inspiratory time to total time of respiration cycle. Rapid shallow breathing index (RSBI = resp. rate/tidal volume [L]) increases during the SBT ranging from a median of 65.0 up to 71.6 breaths/min/L, compared to a RSBI of 58.5 immediately before the SBT. This is all below critical value 105, as a cut-off for prediction of SBT failure.*

8.1.1.2 Additional EAdi analysis

Besides the peak EAdi, the area under the EAdi curve is also investigated. This is shown in **Figure 42**. The AUC is calculated for both the servo EAdi signal and the envelope signal of the raw EAdi. The AUC values remain constant over the duration of the SBT. The AUC values of the raw EAdi are slightly

higher and show less variation compared to the AUC values of servo EAdi signal. In **Figure 43**, the EAdi results are shown in more detail. The shape of the EAdi curves (**Figure 43**A) differ a lot between the raw EAdi and the Servo EAdi signal. The Servo ventilator uses an unknown filtering algorithm, resulting in diaphragm activity curves of similar shapes, especially when looking at the decay which is an exponential fit starting at 70% of peak EAdi. **Figure 43**B shows a scatter plot of the AUC values of both the signals for every breath, color-coded by the analysis period. From this graph it can also be concluded that the Servo EAdi signal is slightly lower, as the majority of the breaths are beneath the linear line, but this does not differ between analysis intervals.

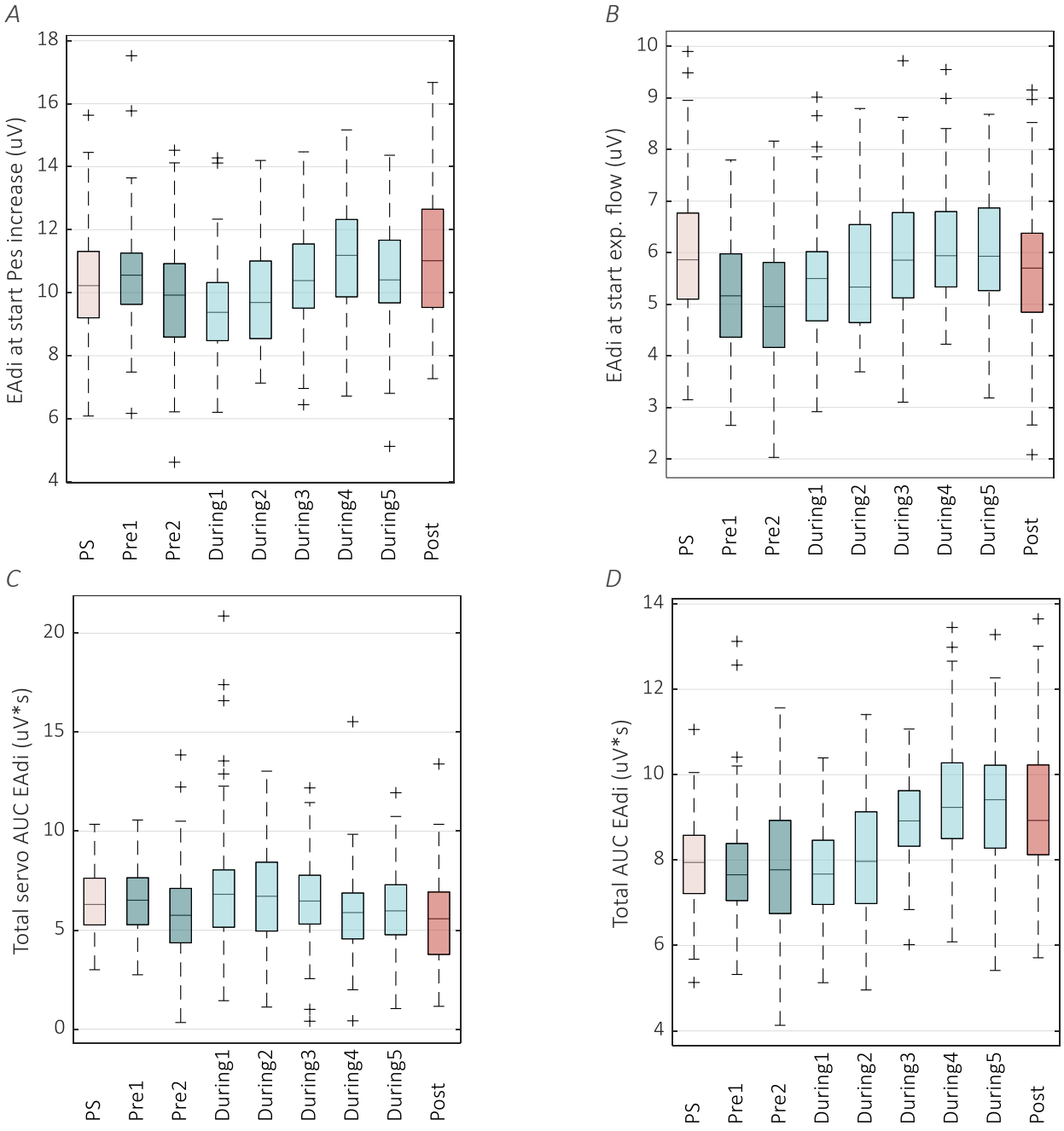

*Figure 42: Additional EAdi result, showing **A)** the EAdi level at the start of Pes increase, **B)** the level of EAdi at the start of expiratory flow **C)** the area under the curve of the servo EAdi signal and **D)** the area under the curve of the raw EAdi signal.*

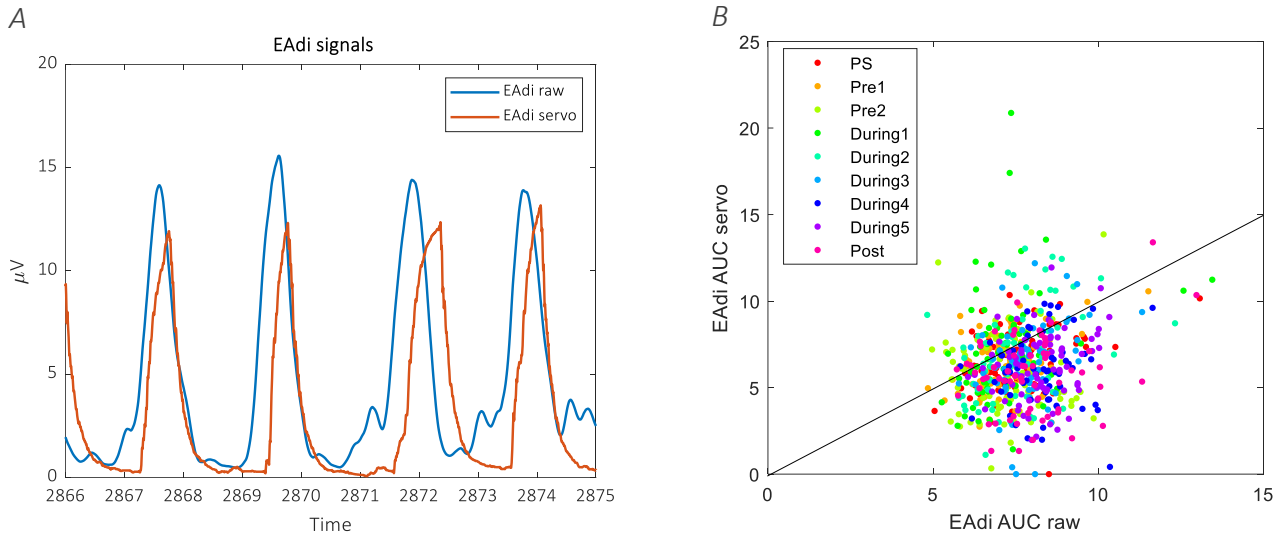

Figure 43: *Additional EAdi results showing* ***A)*** *the difference between Eadi raw and EAdi servo curves and* ***B)*** *a scatterplot of the AUC values of EAdi from raw signal and from servo tracker.*

8.1.1.3 Additional phase angle results

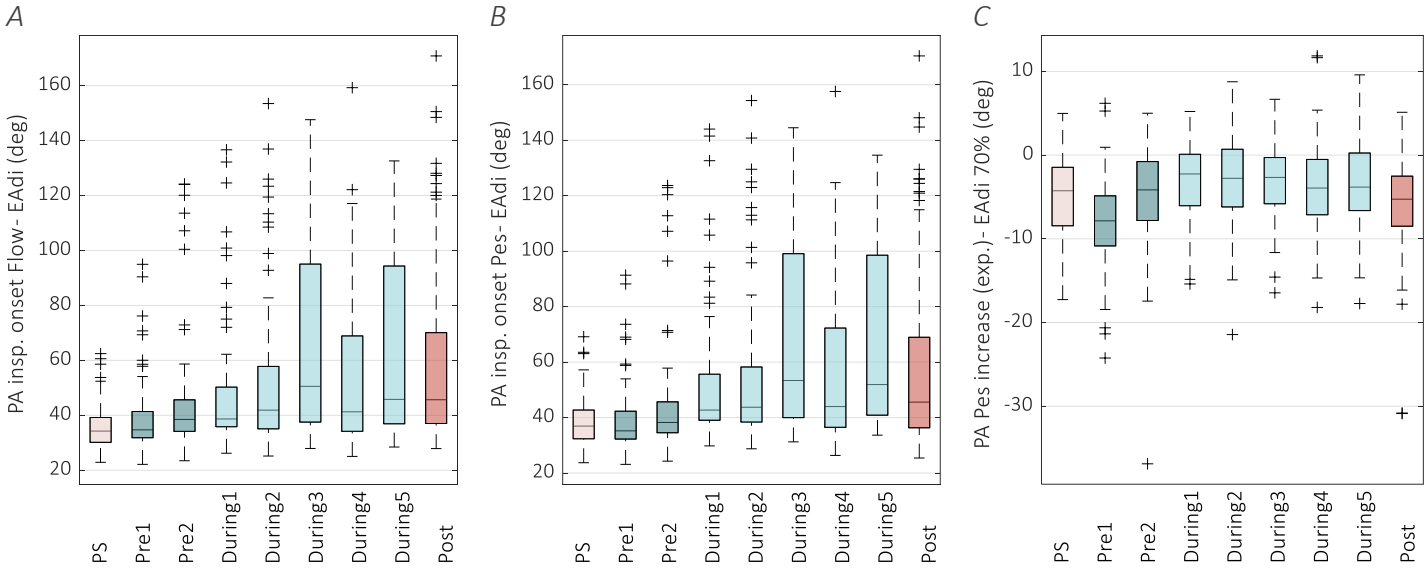

Figure 44*: Additional phase angle results showing PA between* ***A)*** *inspiratory flow and start of EAdi inspiratory activity,* ***B)*** *start of inspiratory Pes effort and start of EAdi inspiratory activity and* ***C)*** *end-inspiratory Pes increase and EAdi return to 70%.*

8.1.1.4 Example of coherence results

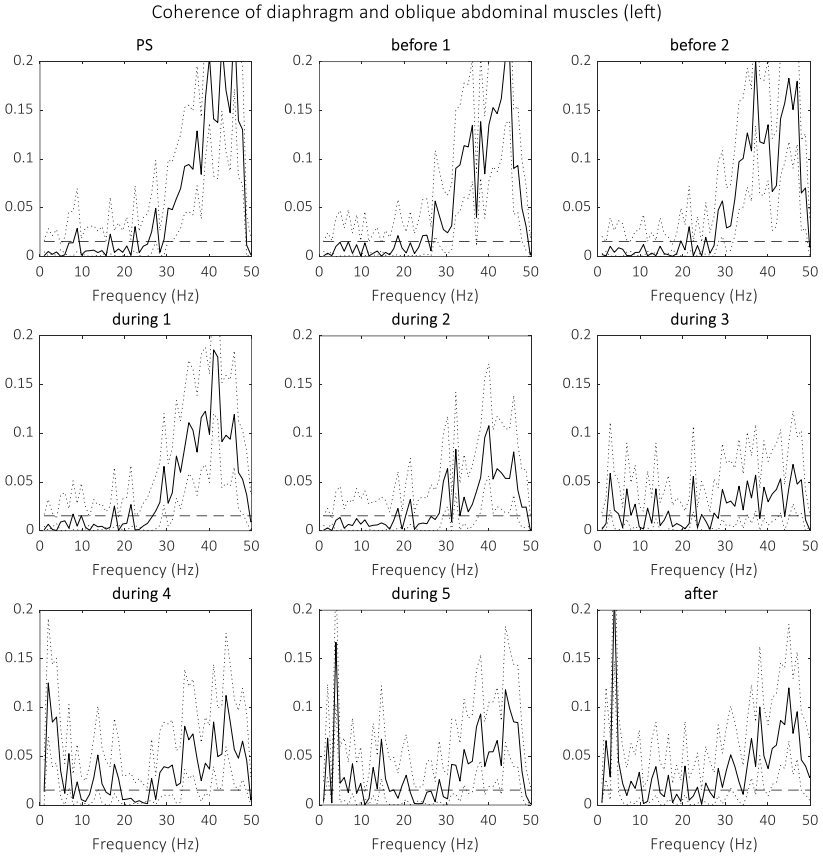

Figure 45: *Example of coherence results per analysis interval*

8.1.1.5 Coherence results

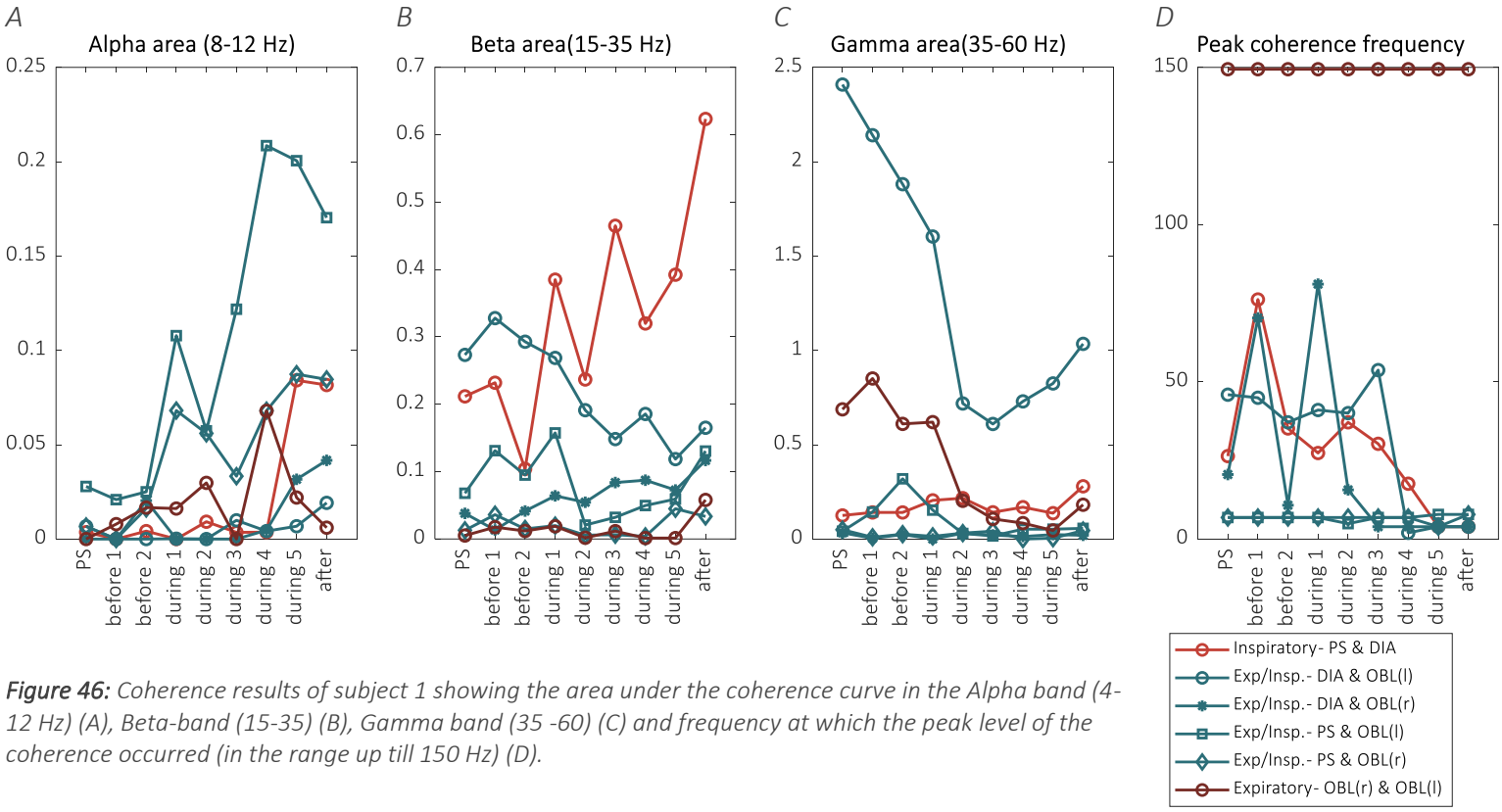

Figure 46: *Coherence results of subject 1 showing the area under the coherence curve in the Alpha band (4-12 Hz) (A), Beta-band (15-35) (B), Gamma band (35 -60) (C) and frequency at which the peak level of the coherence occurred (in the range up till 150 Hz) (D).*

8.1.2 Summary data table subject 1

Variable	Pre1	Pre2	During1	During2	During3	During4	During5
Ti (s)	0.61 (0.60 - 0.62)	0.60* (0.59 - 0.61)	0.58* (0.57 - 0.58)	0.58 (0.57 - 0.58)	0.57 (0.57 - 0.58)	0.58* (0.58 - 0.59)	0.58#% (0.58 - 0.59)
Te (s)	1.55 (1.52 - 1.58)	1.57 (1.53 - 1.6)	1.47* (1.45 - 1.50)	1.53* (1.51 - 1.55)	1.54 (1.51 - 1.56)	1.58* (1.55 - 1.61)	1.42*#% (1.39 - 1.45)
Resp rate (breaths/min)	27.9 (27.5 - 28.2)	27.9 (27.4 - 28.3)	29.4* (29.1 - 29.7)	28.5* (28.3 - 28.8)	28.5 (28.2 - 28.8)	27.9* (27.5 - 28.2)	30.1*#% (29.6 - 30.6)
Tidal volume (mL)	906 (890 - 922)	868* (8501 - 885)	732* (725 - 740)	751* (746 - 757)	753 (748 - 759)	757 (750 - 764)	742*#% (738 - 747)
ΔPes (cmH_2O)	25.8 (25.7 – 26.0)	26.1* (25.9 - 26.3)	28.7* (28.6 - 28.9)	29.0* (28.8 - 29.1)	29.0 (28.9 - 29.2)	28.9 (28.7 – 29.0)	27.9*#% (27.8 - 28.1)
ΔPmus (cmH_2O)	30.6 (30.5 - 30.8)	30.7 (30.5 - 30.9)	32.9* (32.7 - 33.1)	33.3* (33.2 - 33.4)	33.4 (33.2 - 33.5)	33.2 (33.1 - 33.4)	32.2*#% (32.0 - 32.4)
Insp. AUC EAdi (µV*s)	6.0 (5.8 - 6.2)	6.0 (5.8 - 6.2)	5.7* (5.6 - 5.9)	6.1* (5.9 - 6.3)	6.5* (6.3 - 6.7)	6.8* (6.6 - 7.0)	6.7#% (6.5 - 6.9)
Total AUC EAdi (µV*s)	7.8 (7.5 - 8.0)	7.8 (7.5 - 8.2)	7.7 (7.5 - 7.9)	8.1* (7.8 - 8.4)	8.9* (8.7 - 9.1)	9.5* (9.2 - 9.8)	9.3#% (9.0 - 9.6)
Peak EAdi (uµV)	12.7 (12.4 - 13.1)	12.7 (12.3 - 13.1)	12.6 (12.3 - 12.9)	13.2* (12.8 - 13.6)	14.1* (13.7 - 14.4)	14.6* (14.2 – 15.0)	14.2#% (13.8 - 14.6)
EAdi at start exp. flow (µV)	5.2 (5.0 - 5.5)	5.0 (4.7 - 5.3)	5.5* (5.2 - 5.7)	5.6 (5.3 - 5.8)	6.0* (5.7 - 6.2)	6.2 (5.9 - 6.4)	6.0#% (5.8 - 6.3)
EAdi at start Pes increase (µV)	10.5 (10.2 - 10.9)	9.8* (9.4 - 10.2)	9.4 (9.1 - 9.7)	9.9* (9.6 - 10.3)	10.5* (10.1 - 10.9)	11.1* (10.7 - 11.5)	10.6#% (10.2 – 11.0)
Insp. servo AUC EAdi (µV*s)	4.6 (4.3 - 4.8)	4.0* (3.7 - 4.4)	4.5* (4.2 - 4.8)	4.0* (3.8 - 4.3)	4.2 (3.9 - 4.5)	3.9 (3.6 - 4.2)	4.2 (3.9 - 4.5)
Total servo AUC EAdi (µV*s)	6.5 (6.1 – 6.8)	5.8* (5.3 – 6.2)	7.1* (6.4 – 7.7)	6.9 (6.4 – 7.5)	6.5 (6.1 – 7.0)	5.9 (5.4 – 6.4)	6.0% (5.5 – 6.4)
Peak EAdi servo (µV)	14.2 (13.5 – 14.9)	12.5* (11.6 – 13.5)	14.3* (13.4 – 15.4)	13.1* (12.4 – 13.9)	13.7 (12.8 – 14.5)	12.5 (11.6 – 13.4)	13.2 (12.3 – 14.1)
PA insp. onset Flow - EAdi (°)	38.7 (36.1 – 41.4)	44.9* (40.6 – 49.2)	47.7* (42.9 – 52.4)	51.8 (46.2 – 57.4)	65.2* (57.7 - 72.6)	55.3* (48.5 – 62.0)	61.5#% (55.1 - 68.0)
PA insp. onset Pes - EAdi (°)	39.1 (36.5 – 41.6)	44.5* (40.2 – 48.8)	51.5* (46.6 – 56.4)	54.7 (49.1 – 60.3)	68.2* (60.9 – 75.6)	57.6* (51.0 – 64.3)	65.8#% (59.4 – 72.3)

PA peak EAdi - servo EAdi (deg)	-32.7 (-34.8 - -30.7)	-39.2* (-42.3 - -36.1)	-36.3 (-39.7 - -32.8)	-44.9* (-49.7 - -40.2)	-37.5* (-40.9 - -34.1)	-35.7 (-38.7 - -32.7)	-37.1 (-39.4 - -34.9)
PA onset EAdi - servo EAdi (°)	-44.3 (-47.7 - -40.9)	-53.9* (-59.0 - -48.7)	-54.1 (-59.6 - -48.7)	-59.9 (-66.2 - -53.6)	-72.5* (-80.9 - -64.0)	-64.0 (-71.5 - -56.4)	-69.7% (-77.0 - -62.4)
PA 70% EAdi - servo EAdi (°)	-18.1 (-19.4 - -16.8)	-21.2* (-23.6 - -18.7)	-23.0 (-26.5 - -19.5)	-31.4* (-36.0 - -26.8)	-24.5* (-28.0 - -21.0)	-21.9 (-24.7 - -19.1)	-18.4*#% (-19.7 - -17.0)
PA exp. flow - EAdi peak (°)	46.5 (45.0 – 48.0)	51.3* (49.6 - 53.1)	47.9* (46.5 - 49.3)	47.9 (46.3 - 49.6)	48.3 (46.5 - 50.1)	46.7 (45.0 - 48.4)	51.9*% (50.0 - 53.9)
PA exp. flow - EAdi 70% (°)	17.0 (15.9 - 18.1)	19.0* (17.8 - 20.3)	16.8* (15.8 - 17.8)	16.6 (15.5 - 17.7)	16.8 (15.8 - 17.8)	16.3 (15.2 - 17.4)	17.9* (16.8 - 19.0)
PA exp. flow - EAdi zero (°)	-85.0 (-91.2 - -78.7)	-78.6 (-84.9 - -72.3)	-88.7* (-94.2 - -83.3)	-82.7 (-88.0 - -77.4)	-68.7* (-74.2 - -63.3)	-76.0 (-84.7 - -67.4)	-65.2#% (-75.4 - -54.9)
PA Pes increase (exp.) - EAdi peak (°)	21.5 (20.0 – 23.0)	27.4* (25.9 - 28.9)	27.9 (26.5 - 29.2)	27.9 (26.3 - 29.5)	28.7 (26.9 - 30.5)	26.5 (24.9 - 28.1)	30.8*#% (28.9 - 32.7)
PA Pes increase (exp.) - EAdi 70% (°)	-8.0 (-9.1 - -7.0)	-4.9* (-6.1 - -3.6)	-3.3* (-4.2 - -2.3)	-3.5 (-4.5 - -2.4)	-2.8 (-3.8 - -1.8)	-3.9 (-5.0 - -2.7)	-3.2# (-4.3 - -2.0)
PA Pes increase (exp.) - EAdi zero (°)	-110.0 (-116.0 - -104.0)	-102.5 (-108.9 - -96.2)	-108.8 (-114.1 - -103.4)	-102.7 (-107.9 - -97.4)	-88.4* (-93.7 - -83.0)	-96.2 (-104.9 - -87.6)	-86.3#% (-96.5 - -76.1)
WOB total (J/L)	2.26 (2.25 - 2.28)	2.24 (2.22 - 2.27)	2.28* (2.26 - 2.29)	2.29 (2.28 - 2.30)	2.29 (2.27 - 2.31)	2.29 (2.27 - 2.30)	2.24*% (2.22 - 2.25)
WOB expiratory (J/L)	0.0005 (0.0003 - 0.001)	0.009 (0.007 - 0.011)	0.044* (0.038 - 0.050)	0.073* (0.069 - 0.077)	0.079* (0.075 - 0.083)	0.073* (0.069 - 0.077)	0.074#% (0.069 - 0.079)
PTPmus insp. (cmH_2O x s / min)	324.9 (319.2 - 330.6)	316* (310.7 - 321.4)	342.8* (337.8 - 347.8)	338.5 (334.4 - 342.5)	336.5 (332.2 - 340.7)	334.7 (329.6 - 339.8)	351.1*#% (345.3 - 357)
PTPmus exp. positive (cmH_2O x s / min)	124.9 (116.4 - 133.4)	113.5* (108.2 - 118.9)	132.2* (127.3 - 137)	127.7 (124.4 - 131.1)	126.8 (122 - 131.6)	124.5 (117.8 - 131.2)	135.3*# (130.2 - 140.4)
PTPmus exp. negative (cmH_2O x s / min)	0.5 (0.3 - 0.7)	3.7* (2.9 - 4.5)	17.9* (15.4 - 20.4)	28.0* (26.3 - 29.7)	30.8* (29.0 - 32.6)	28.1* (26.4 - 29.9)	29.1#% (27.0 - 31.2)
Exp rise Pes (cmH_2O)	0.3 (0.2 - 0.3)	0.9* (0.7 - 1.0)	2.8* (2.5 - 3.0)	4.0* (3.8 - 4.1)	4.3* (4.2 - 4.4)	4.1 (4.0 - 4.3)	4.3#% (4.1 - 4.4)

Data is presented as mean with 95% confidence interval per analysis interval (pre1 and pre2 refer to period before SBT), during1 till during5 represent intervals of SBT. Differences between subsequent intervals, during 1 vs during 5 and pre2 vs during5 were evaluated at the 0.05 significant level by computing the 95% CI for the difference of the means. * significant difference from preceding interval, #significant difference from pre2, %significant difference from during1. Often a significant difference is found, however this is not a clinically relevant difference per se.

8.1.3 Additional figures subject 2

8.1.3.1 Breathing mechanics

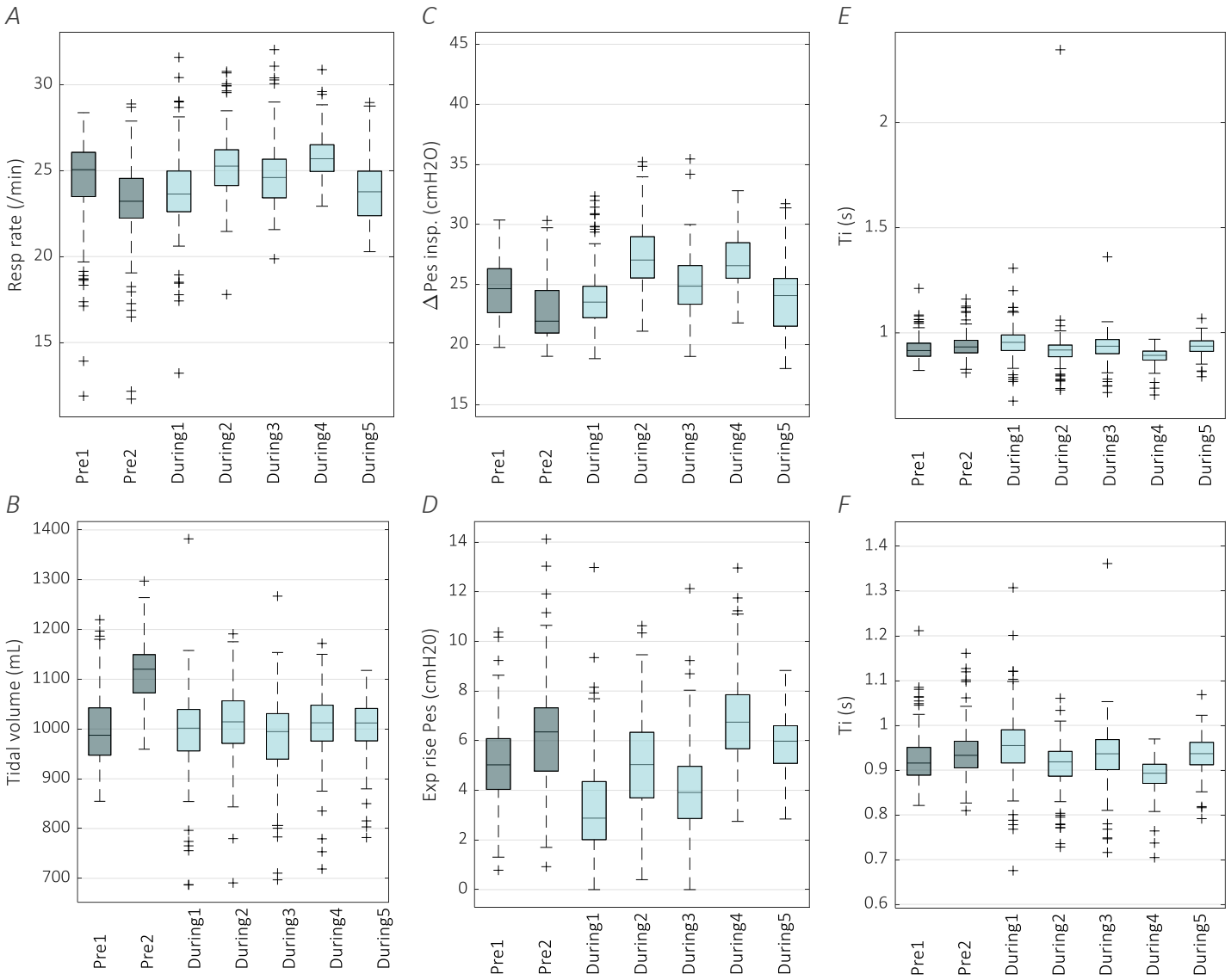

Figure 47: *Additional breathing mechanics and functional coordination results, showing* ***A)*** *respiratory rate,* ***B)*** *Tidal volume,* ***C)*** *inspiratory Pes swings,* ***D)*** *Expiratory rise of Pes above Pcw,* ***E)*** *inspiratory times and* ***F)*** *also inspiratory time (zoomed). Rapid shallow breathing index (RSBI = resp. rate/tidal volume [L]) varies during the SBT between 23.8 and 25.9 breaths/min/L, compared to a RSBI of 21 immediately before the SBT. This is all far below critical value 105, as a cut-off for prediction of SBT failure.*

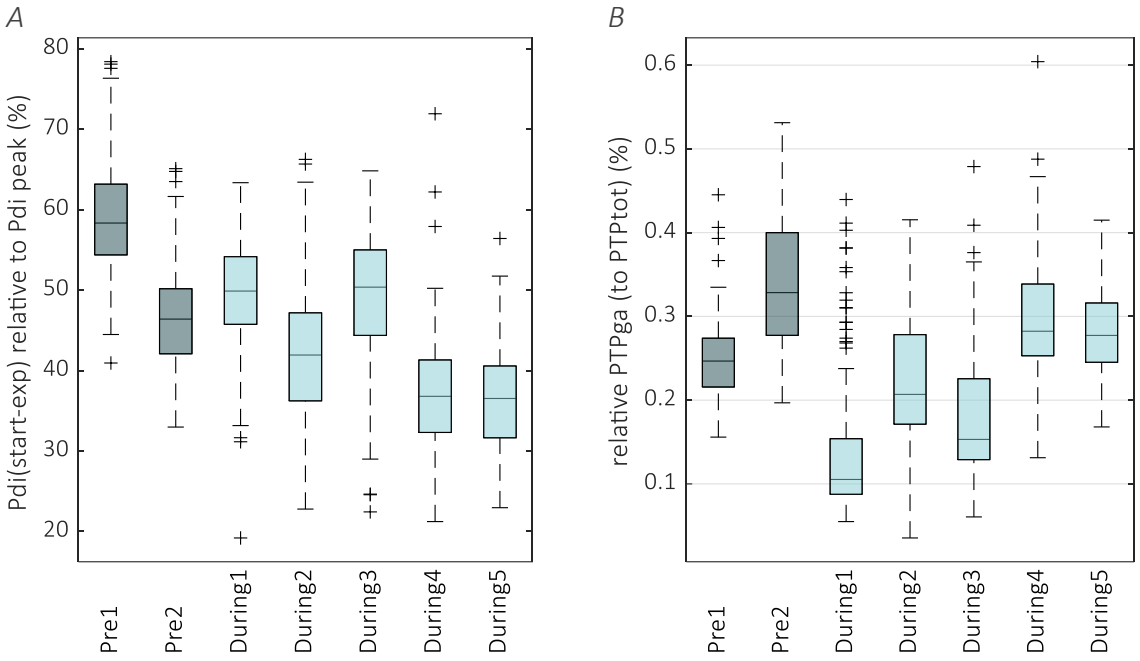

***Figure 48**: Additional functional coordination results, showing **A)** Pdi at end-inspiration relative to Pdi peak and **B)** PTPga relative to PTPtot*

8.1.3.2 Additional EMGdi results

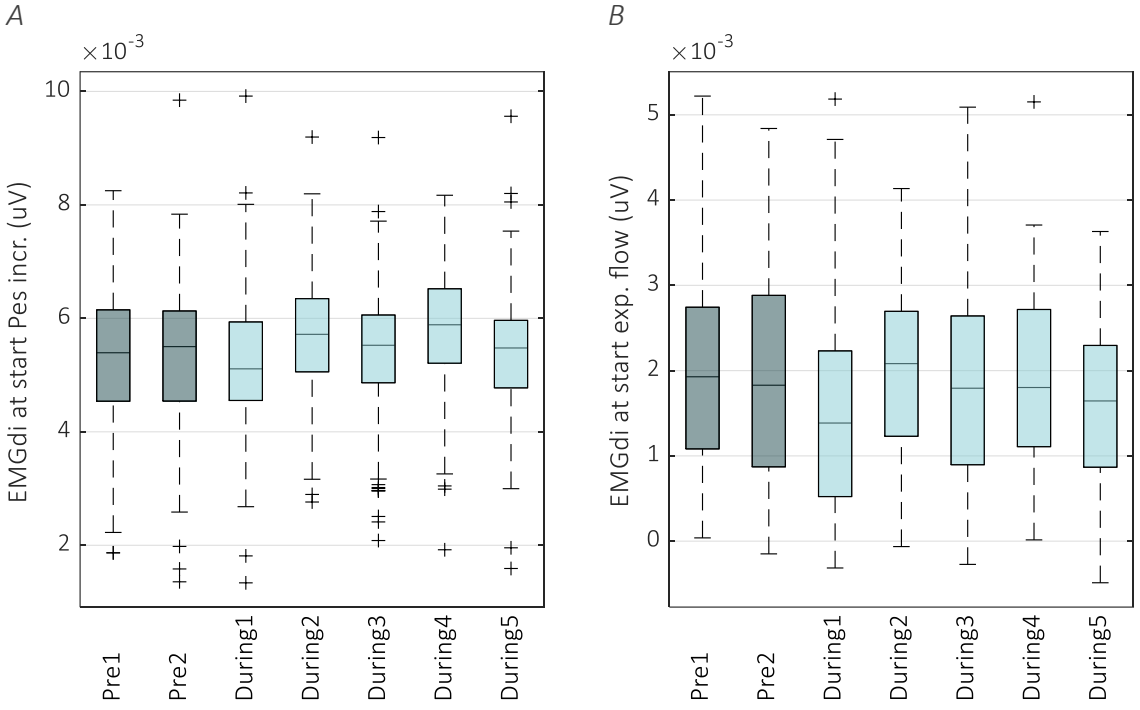

***Figure 49**: Additional EMGdi results, showing **A)** EMGdi at the start of Pes increase at end-inspiration **B)** EMGdi at the start of expiratory flow*

8.1.3.3 Additional phase angle results

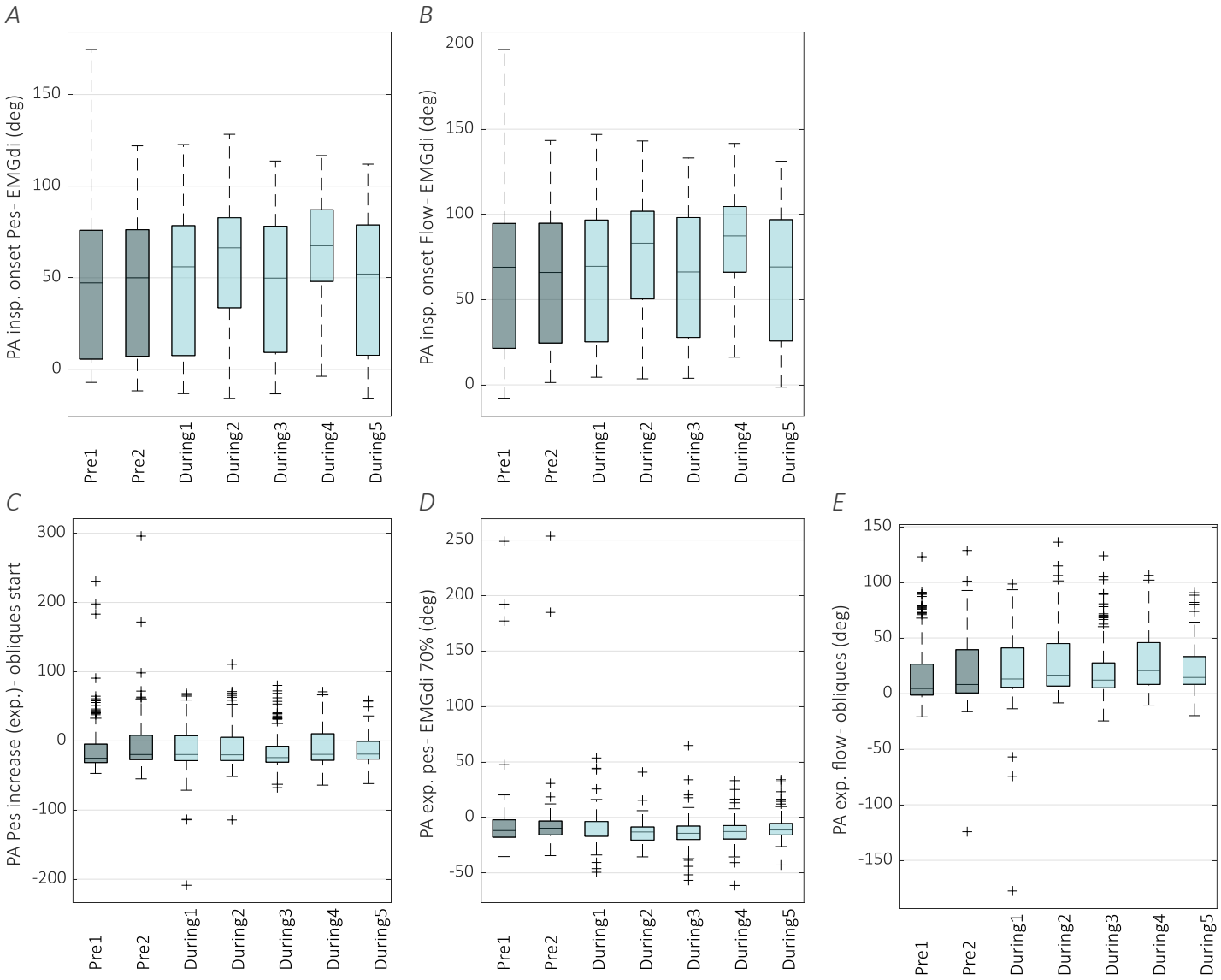

Figure 50: *Additional phase angle results, showing PA between* ***A)*** *inspiratory start of Pes decrease and start of EMGdi activity,* ***B)*** *start of inspiratory flow and start of EMGdi,* ***C)*** *start of Pes increase at end inspiration and start of obliques activation,* ***D)*** *start of Pes increase at end inspiration and EMGdi return to 70% of peak and* ***E)*** *start of expiratory flow and activation of the obliques.*

8.1.3.4 Example of coherence results

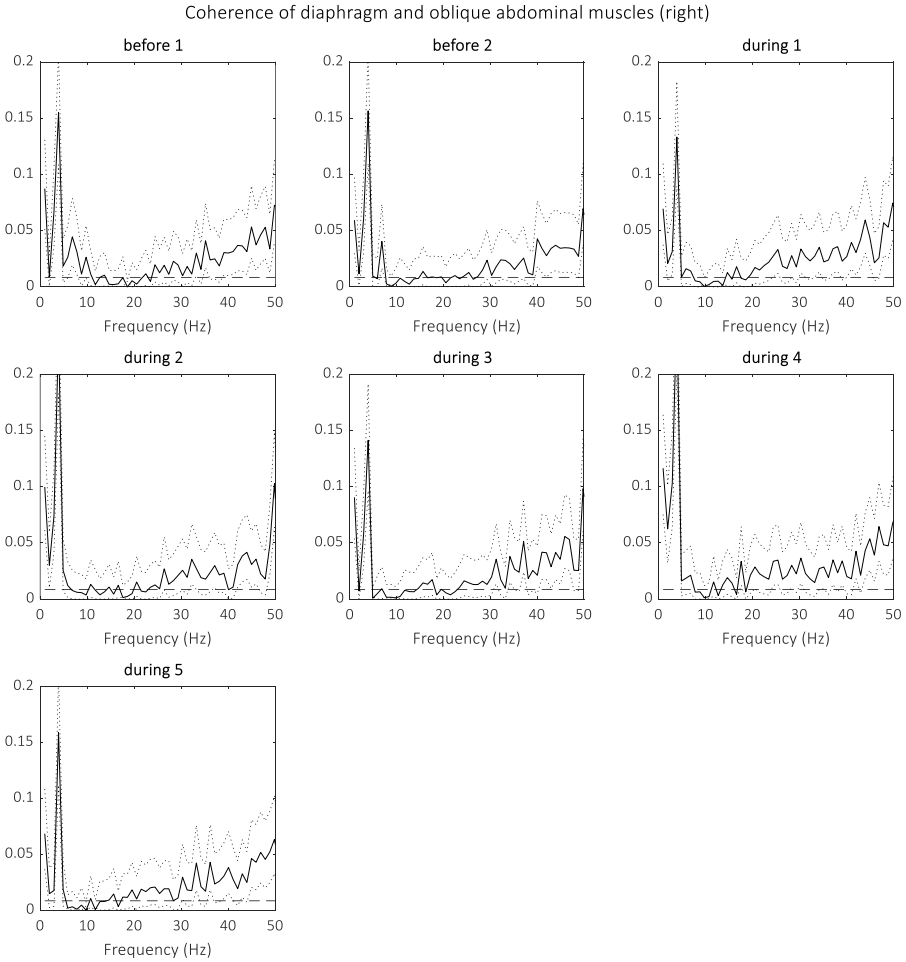

***Figure 51**: Example of coherence results per analysis interval of subject 2*

8.1.3.5 Peak coherence results

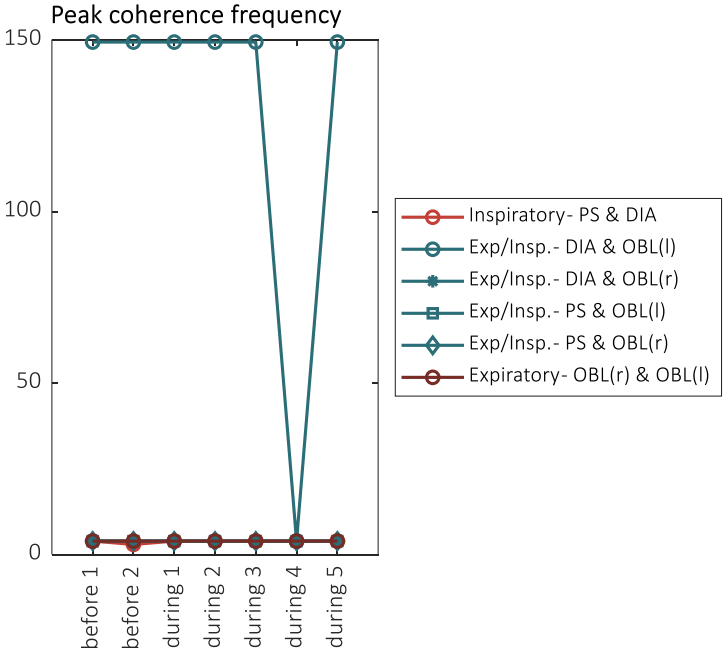

***Figure 52**: Peak coherence results of subject 2*

8.1.4 Summary data table subject 2

	Before SBT		During SBT				
Variable	**Pre1**	**Pre2**	**During1**	**During2**	**During3**	**During4**	**During5**
Ti (s)	0.92 (0.915 - 0.936)	0.94 (0.930 - 0.950)	0.96 (0.941 - 0.969)	0.92* (0.897 - 0.942)	0.93 (0.917 - 0.940)	0.89* (0.884 - 0.896)	0.94*% (0.929 - 0.944)
Te (s)	1.58 (1.515 - 1.649)	1.70* (1.626 - 1.764)	1.59* (1.551 - 1.635)	1.46* (1.438 - 1.481)	1.50* (1.481 - 1.525)	1.44* (1.417 - 1.454)	1.60*# (1.574 - 1.631)
Resp rate (/min)	24.4 (23.9 - 24.9)	23.1* (22.7 - 23.6)	23.8* (23.4 - 24.2)	25.4* (25.0 - 25.7)	24.8* (24.5 - 25.1)	25.9* (25.7 - 26.1)	23.8*# (23.5 - 24.1)
Tidal volume (mL)	1004 (990.4 - 1018)	1114* (1102 - 1125)	993* (977.6 - 1008)	1011 (998.2 - 1024)	984.8* (971.6 - 998)	1007* (995.6 - 1019)	1005# (995 - 1015)
ΔPes insp. (cmH_2O)	24.6 (24.2 – 25.0)	22.8* (22.4 - 23.3)	23.9* (23.4 - 24.3)	27.4* (27.0 - 27.9)	24.9* (24.5 - 25.3)	27.0* (26.6 - 27.3)	23.9*# (23.5 - 24.3)
ΔPga insp. (cmH_2O)	-0.9 (-1.5 - -0.4)	-4.3* (-5.0 - -3.6)	-1.1* (-1.6 - -0.6)	-4.1* (-4.6 - -3.6)	-2.2* (-2.9 - -1.6)	-3.8* (-4.7 - -2.9)	-1.0*# (-1.6 - -0.3)
ΔPmus insp. (cmH_2O)	31.0 (30.6 - 31.4)	29.9* (29.5 - 30.3)	30.0 (29.5 - 30.4)	33.5* (33.1 - 33.9)	30.9* (30.4 - 31.3)	33.0* (32.6 - 33.3)	30.0* (29.6 - 30.4)
ΔPdi insp. (cmH_2O)	21.7 (21.4 – 22.0)	19.3* (18.9 - 19.6)	22.0 (21.5 - 22.5)	23.8* (23.4 - 24.2)	22.2* (21.8 - 22.5)	22.8* (22.4 - 23.2)	20.3*#% (19.8 - 20.8)
Exp rise Pga(cmH_2O)	5.3 (5.1 - 5.5)	6.0* (5.7 - 6.3)	3.1* (2.8 - 3.3)	5.4* (5.2 - 5.7)	4.1* (3.8 - 4.3)	7.0* (6.7 - 7.2)	5.5*#% (5.4 - 5.7)
Exp rise Pes (cmH_2O)	5.2 (4.9 - 5.5)	6.2* (5.9 - 6.6)	3.3* (3.0 - 3.7)	5.0* (4.7 - 5.4)	4.1* (3.8 - 4.4)	6.9* (6.6 - 7.2)	5.9*% (5.7 - 6.1)
Pdi at start expiration (cmH_2O)	12.7 (12.4 - 13.1)	9.0* (8.7 - 9.3)	11.0* (10.6 - 11.3)	10.1* (9.7 - 10.5)	10.9* (10.5 - 11.3)	8.5* (8.2 - 8.8)	7.4*# (7.1 - 7.8)
Insp. AUC EMGdi (μV*s)	4.9 (4.65 - 5.05)	5.0 (4.77 - 5.23)	5.0* (4.75 - 5.21)	5.6* (5.38 - 5.79)	5.0* (4.80 - 5.24)	5.6* (5.48 - 5.78)	5.1* (4.87 - 5.28)
Total AUC EMGdi (μV*s)	5.1 (4.86 - 5.33)	5.3 (5.03 - 5.58)	5.1* (4.89 - 5.41)	5.8* (5.61 - 6.03)	5.2* (5.00 - 5.48)	5.9* (5.74 - 6.10)	5.3* (5.05 - 5.50)
Peak EMGdi (μV)	6.4 (6.18 - 6.54)	6.4 (6.16 - 6.57)	6.3 (6.06 - 6.47)	6.54 (6.39 - 6.69)	6.3 (6.11 - 6.49)	6.7* (6.58 - 6.89)	6.3* (6.16 - 6.51)
EMGdi at start exp. flow (μV)	2.0 (1.81 - 2.24)	1.9 (1.70 - 2.14)	1.5* (1.32 - 1.71)	2.0* (1.82 - 2.14)	1.8 (1.60 - 1.96)	1.9 (1.70 - 2.02)	1.6*# (1.39 - 1.72)
EMGdi at start Pes incr. (μV)	5.2 (4.99 - 5.45)	5.32 (5.08 - 5.56)	5.18 (4.97 - 5.40)	5.7* (5.53 - 5.86)	5.4* (5.24 - 5.63)	5.85* (5.67 - 6.02)	5.4* (5.20 - 5.61)

PA insp. onset Flow - EMGdi (°)	63.6 (56.3 - 70.9)	62.1 (55.4 - 68.8)	65.1 (58.6 - 71.7)	76.2* (70.2 - 82.1)	64.0* (57.7 - 70.3)	83.6* (78.7 - 88.5)	63.1* (56.6 - 69.6)
PA insp. onset Pes - EMGdi (°)	46.5 (39.5 - 53.6)	44.8 (38.3 - 51.3)	48.3 (41.8 - 54.8)	57.6* (51.7 - 63.6)	45.4* (39.2 - 51.6)	64.7* (59.7 - 69.6)	45.6* (39.2 - 52.1)
PA exp. flow - EMGdi peak (°)	58.5 (55.0 – 62.0)	50.4* (45.9 - 54.9)	61.7* (58.1 - 65.4)	62.2 (58.1 - 66.3)	62.7 (59.3 - 66.2)	63.2 (59.9 - 66.6)	60.5# (57.1 - 63.9)
PA exp. flow - EMGdi 70% (°)	21.2 (19.3 - 23.2)	18.6 (14.9 - 22.3)	25.5* (23.3 - 27.6)	23.3 (20.7 - 26.0)	24.2 (22.3 - 26.1)	24.5 (23.0 - 26.0)	25.0# (23.3 - 26.8)
PA exp. flow - EMGdi zero (°)	-35.0 (-38.1 - -31.9)	-35.1 (-39.6 - -30.6)	-28.1* (-30.9 - -25.2)	-31.8 (-36.3 - -27.3)	-32.0 (-35.0 - -29.1)	-34.1 (-38.0 - -30.3)	-28.6# (-31.5 - -25.7)
PA Pes increase (exp.) - EMGdi peak (°)	32.7 (26.3 - 39.2)	26.1 (20.3 - 31.9)	26.7 (23.1 - 30.4)	25.0 (21.4 - 28.7)	25.5 (21.9 - 29.1)	25.6 (21.9 - 29.3)	25.5 (22.1 - 28.9)
PA exp. pes - EMGdi 70% (°)	-4.5 (-10.9 - 1.8)	-5.7 (-11.3 - -0.10)	-9.5 (-12.1 - -6.94)	-13.8* (-15.5 - -12.2)	-13.0 (-15.2 - -10.8)	-13.1 (-15.1 - -11.2)	-10.0* (-11.9 - -8.07)
PA Pes increase (exp.) - EMGdi zero (°)	-60.7 (-68.3 - -53.2)	-59.4 (-66.4 - -52.3)	-63.1 (-66.5 - -59.6)	-68.9* (-72.9 - -64.9)	-69.2 (-72.7 - -65.8)	-71.7 (-75.8 - -67.6)	-63.6* (-66.7 - -60.5)
PA diaphragm - parasternalis (°)	19.0 (10.4 - 27.7)	16.9 (9.0 - 24.9)	28.2 (20.0 - 36.5)	11.2* (4.3 - 18.1)	27.7* (19.9 - 35.5)	2.5* (-4.6 - 9.6)	29.4*# (21.0 - 37.8)
PA diaphragm - obliques (°)	-180.3 (-189.4 - -171.2)	-171.9 (-179.8 - -164.1)	-177.1 (-185.9 - -168.3)	-186.6 (-194.1 - -179.1)	-180.1* (-187.4 - -172.7)	-191.5* (-198.8 - -184.2)	-173.8* (-181.5 - -166.1)
PA parasternalis - obliques (°)	-199.3 (-207.5 - -191.1)	-188.9 (-196.9 - -180.8)	-205.3* (-213.9 - -196.7)	-197.8 (-205.4 - -190.2)	-207.8 (-214.7 - -200.9)	-194* (-201.2 - -186.8)	-203.2# (-209.2 - -197.3)
PA exp. flow - obliques (°)	18.0 (12.6 - 23.4)	20.2 (14.5 – 26.0)	23.6 (17.4 - 29.9)	28.5 (23.5 - 33.6)	21.6* (17.1 – 26.0)	30.2* (25.41 - 34.9)	22.5* (18.6 - 26.4)
PA Pes increase (exp.) - obliques start (°)	-7.7 (-15.7 - 0.3)	-4.1 (-11.9 - 3.7)	-11.4 (-17.9 - -4.8)	-8.6 (-13.8 - -3.5)	-15.7* (-20.2 - -11.1)	-7.5* (-12.3 - -2.6)	-12.5 (-16.4 - -8.7)
PA EMGdi peak - obliques start (°)	-40.5 (-46.4 - -34.5)	-30.2* (-36.0 - -24.4)	-38.1 (-45.1 - -31.2)	-33.7 (-39.6 - -27.7)	-41.2 (-46.9 - -35.4)	-33.1* (-38.8 - -27.4)	-38.0# (-43.3 - -32.8)
PA EMGdi 70% - obliques start (°)	-3.2 (-9.0 - 2.6)	1.6 (-3.6 - 6.8)	-1.8 (-8.4 - 4.7)	5.2 (0.0 - 10.4)	-2.6* (-7.5 - 2.2)	5.7* (0.7 - 10.6)	-2.6* (-7.0 - 1.9)
PA EMGdi zero - obliques start (°)	53.0 (46.9 - 59.1)	55.3 (49.7 - 61.4)	51.7 (45.2 - 58.2)	60.3 (54.1 - 66.5)	53.6 (48.0 - 59.2)	64.3* (58.3 - 70.2)	51.0* (46.2 - 55.9)
PTPmus insp. (cmH_2O x s / min)	364.8 (355.4 - 374.2)	305.2* (294.5 - 315.8)	398.5* (384.5 - 412.6)	436.0* (424.3 - 447.7)	412.0* (401.9 - 422.1)	386.2* (376.2 - 396.2)	338.0*#% (327.6 - 348.3)
PTPmus exp. positive (cmH_2O x s / min)	120.8 (115.7 - 125.8)	80.9* (75.5 - 86.3)	124.0* (114.7 - 133.3)	107.2* (100.3 - 114.1)	120.7* (113.6 - 127.8)	80.9* (75.4 - 86.4)	70.9*#% (66.7 - 75.2)

PTPmus exp. negative (cmH_2O x s / min)	47.9 (43.2 - 52.6)	67.2* (59.6 - 74.7)	24.1* (19.9 - 28.4)	48.4* (43.3 - 53.5)	34.1* (29.8 - 38.4)	78.7* (72.8 - 84.5)	59.4*% (56.2 - 62.5)
PTPdi insp. (cmH_2O x s / min)	328.9 (320.4 - 337.4)	268.7* (261.0 - 276.4)	353.0* (343.2 - 362.9)	392.5* (384.0 - 401.1)	362.5* (354.7 - 370.4)	353.1 (345.8 - 360.3)	300.5*#% (291.0 – 310.0)
PTPdi exp. (cmH_2O x s / min)	37.5 (35.2 - 39.7)	23.0* (21.5 - 24.4)	36.5* (33.6 - 39.3)	27.5* (25.3 - 29.8)	39.6* (36.0 - 43.2)	18.0* (16.6 - 19.3)	12.9*#% (11.8 - 13.9)
PTPga exp. (cmH_2O x s / min)	109.6 (104.4 - 114.7)	142.5* (133.5 - 151.6)	59.0* (52.1 - 65.8)	116.2* (108.9 - 123.5)	83.9* (76.7 - 91.2)	153.7* (145.7 - 161.8)	117.5*#% (113.5 - 121.4)
WOB total (J/L)	2.24 (2.21 - 2.26)	2.08* (2.05 - 2.11)	2.29* (2.26 - 2.33)	2.58* (2.55 - 2.62)	2.38* (2.35 - 2.42)	2.45* (2.42 - 2.48)	2.21*#% (2.18 - 2.24)
WOB expiratory (J/L)	0.048 (0.041 - 0.056)	0.041 (0.035 - 0.047)	0.053 (0.038 - 0.069)	0.091* (0.083 - 0.099)	0.063* (0.056 - 0.069)	0.085* (0.078 - 0.091)	0.048*#% (0.043 - 0.054)

Data is presented as mean with 95% confidence interval per analysis interval (pre1 and pre2 refer to period before SBT), during1 till during5 represent intervals of SBT. Differences between subsequent intervals, during 1 vs during 5 and pre2 vs during5 were evaluated at the 0.05 significant level by computing the 95% CI for the difference of the means. * significant difference from preceding interval, #significant difference from pre2, %significant difference from during1. Often a significant difference is found, however this is not a clinically relevant difference per se.

8.2 Appendices chapter 4

8.2.1 Expiratory Pga rise

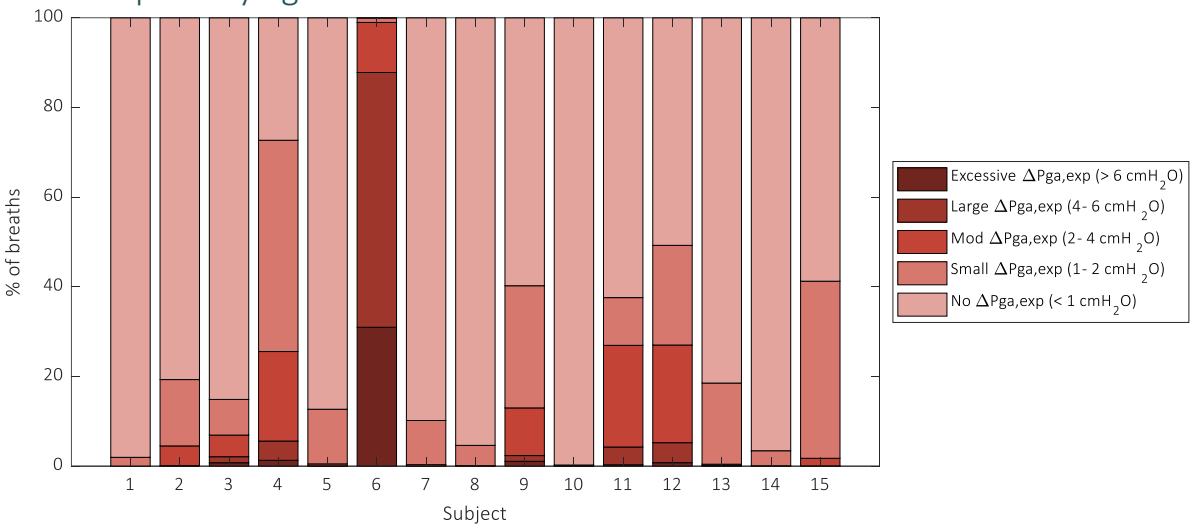

Figure 53: *Distribution of Pga rise (ΔPga,exp; absolute pressure swing) per patient. All 24 hours of analysis are taken together per patient. Legend at the right shows the colour code of the figure.*

8.2.2 Absolute PTPga,exp

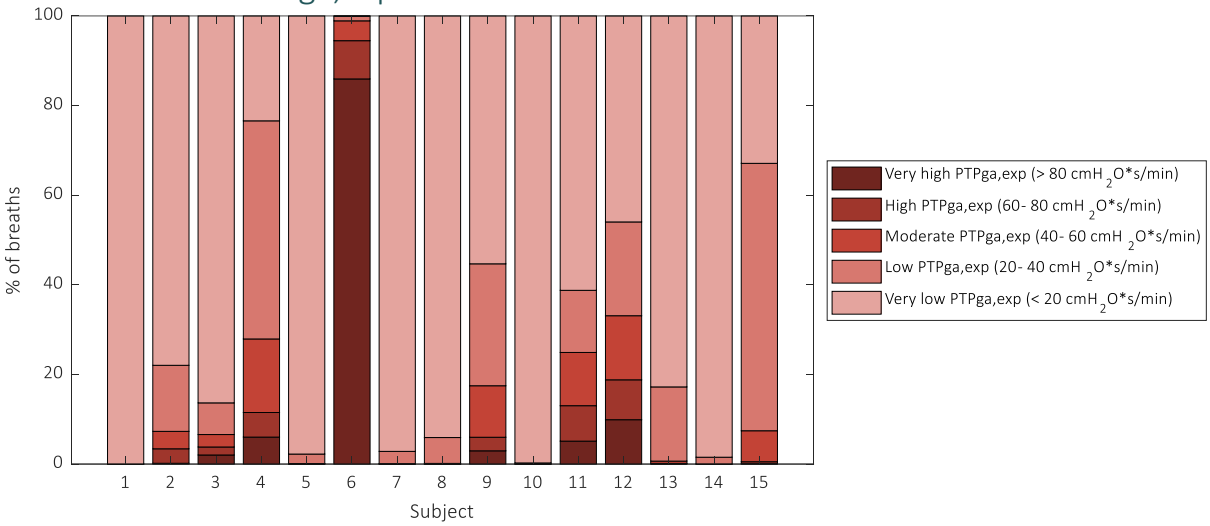

Figure 54: *Distribution of absolute pressure-time-product of gastric pressure (PTPga,exp) per patient. All 24 hours of analysis are taken together per patient. Legend at the right shows the colour code of the figure.*

8.2.3 PTPga,exp over time per subject

Subject 2 (Intervention)

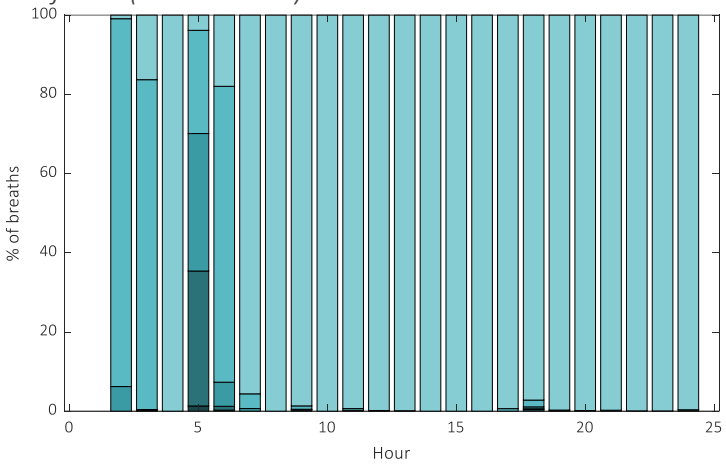

Subject 3 (Intervention))

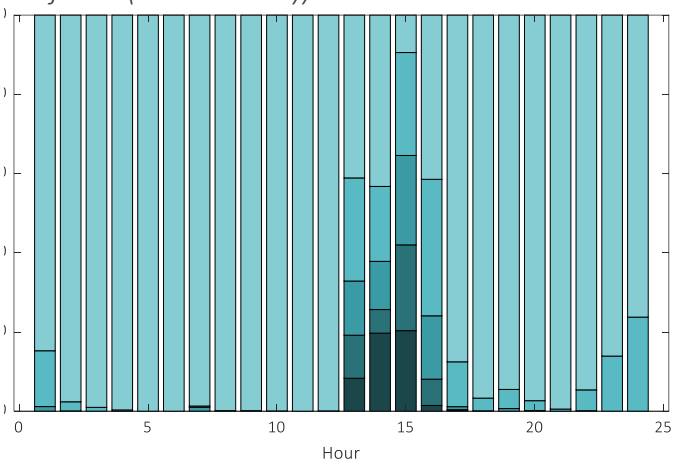

Subject 4 (Control)

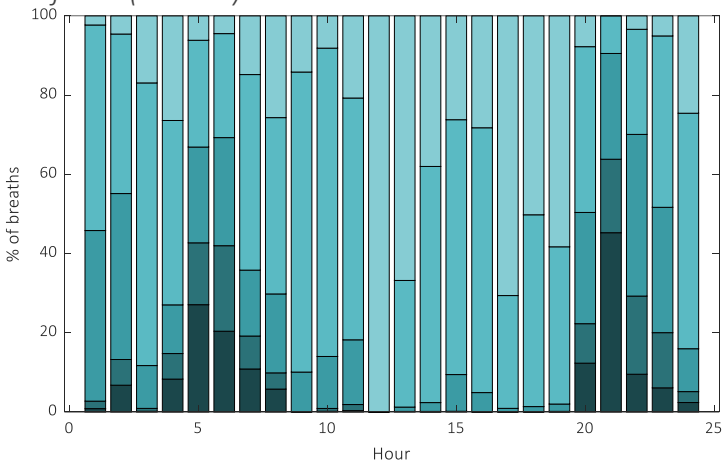

Subject 6 (Control)

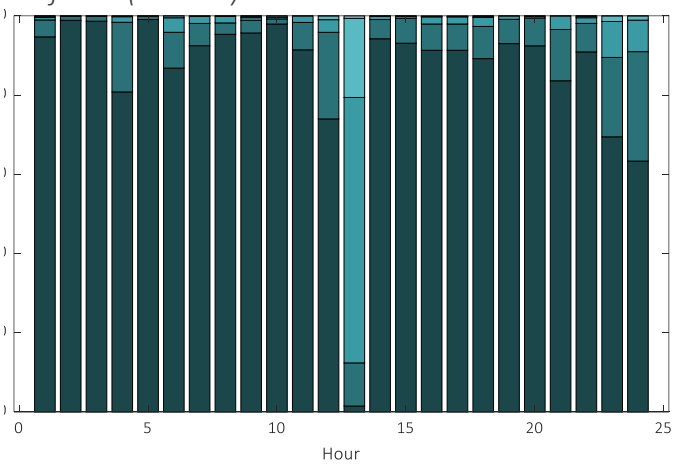

Subject 9 (Control)

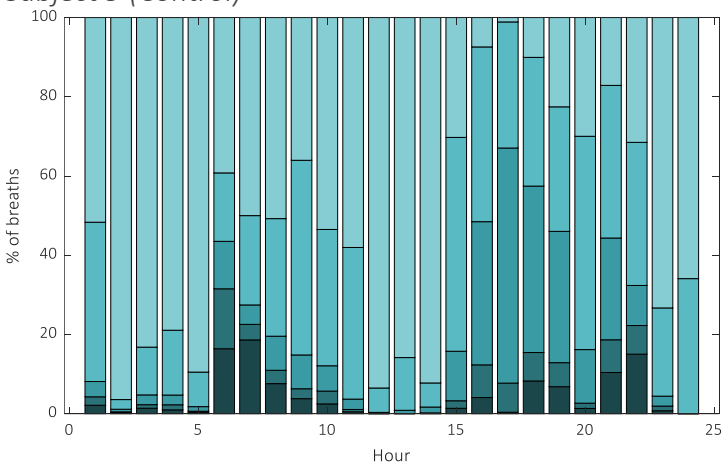

Subject 11 (Control)

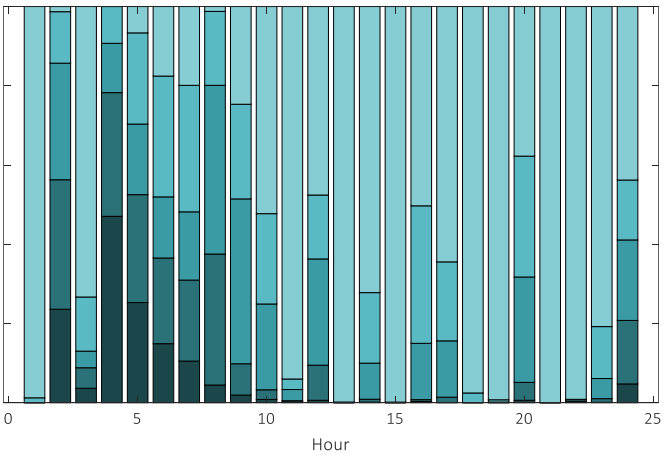

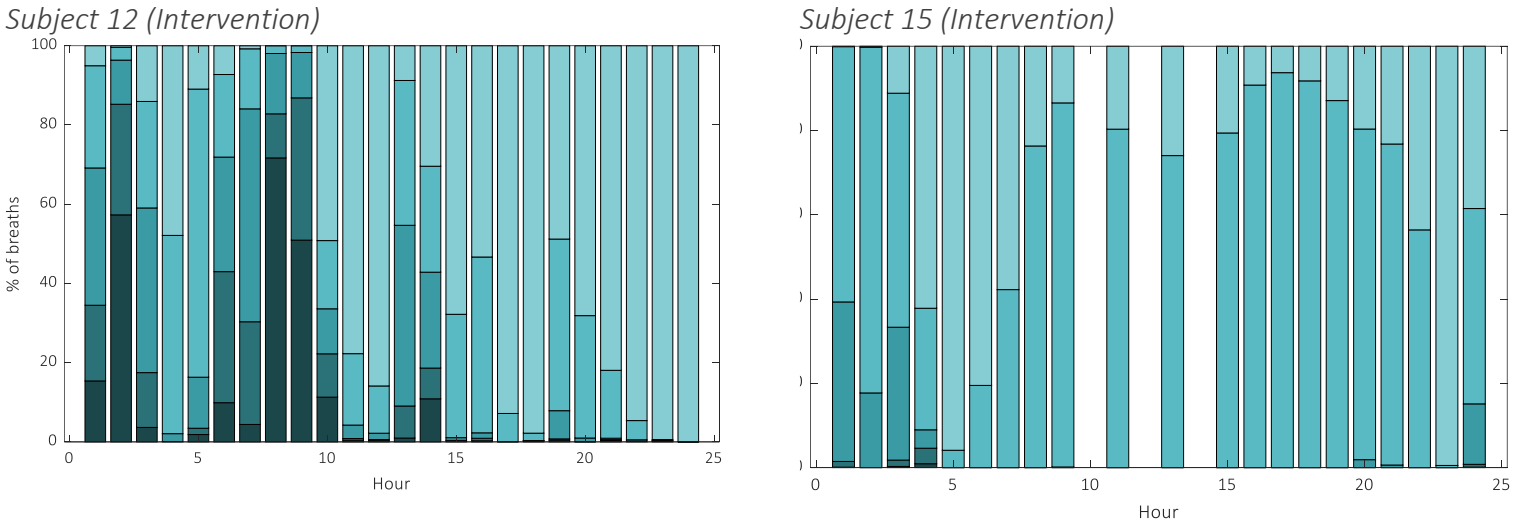

Figure 55: *PTPga,exp distribution, for eight subjects separately. Every bar represents one hour of measurements. It can be seen that in some subjects with significant expiration effort, there are also hours without expiration effort.*

8.2.4 Absolute PTPmus,exp(+)

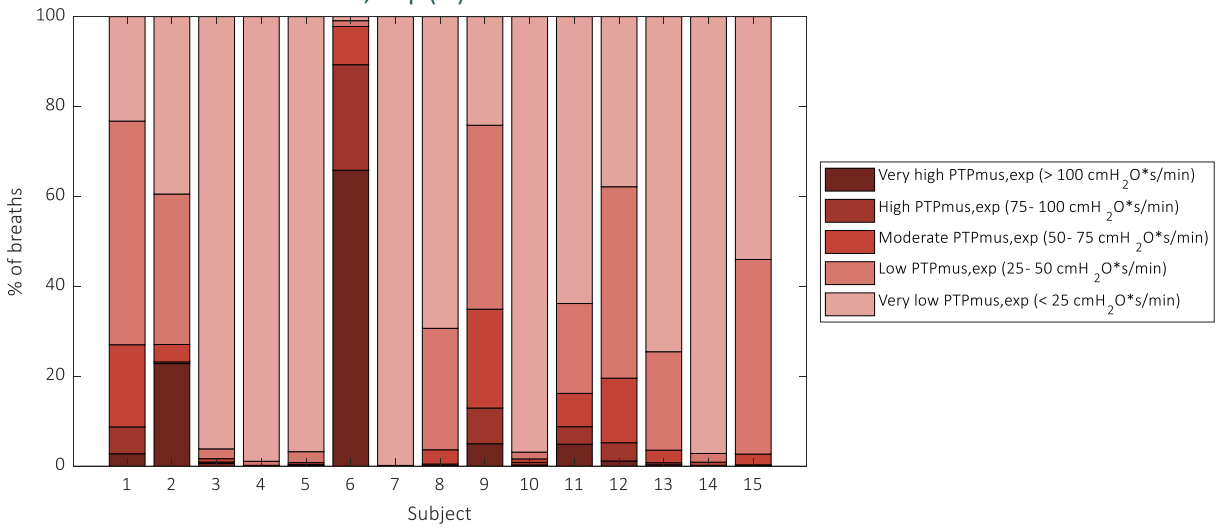

Figure 56: *Distribution of absolute positive expiratory PTPmus (PTPmus,exp(+)) per patient. All 24 hours of analysis are taken together per patient. Legend at the right shows the colour code of the figure.*

8.2.5 Relative PTPdi,exp

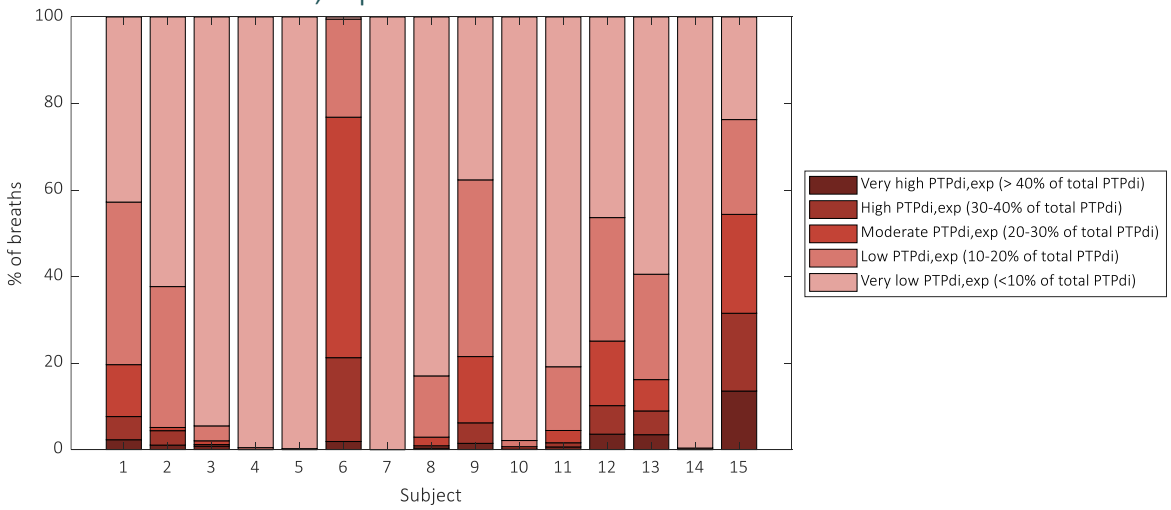

Figure 57: *Distribution of relative PTPdi,exp per patient. All 24 hours of analysis are taken together per patient. Legend at the right shows the colour code of the figure.*

8.2.6 Pmus curve examples

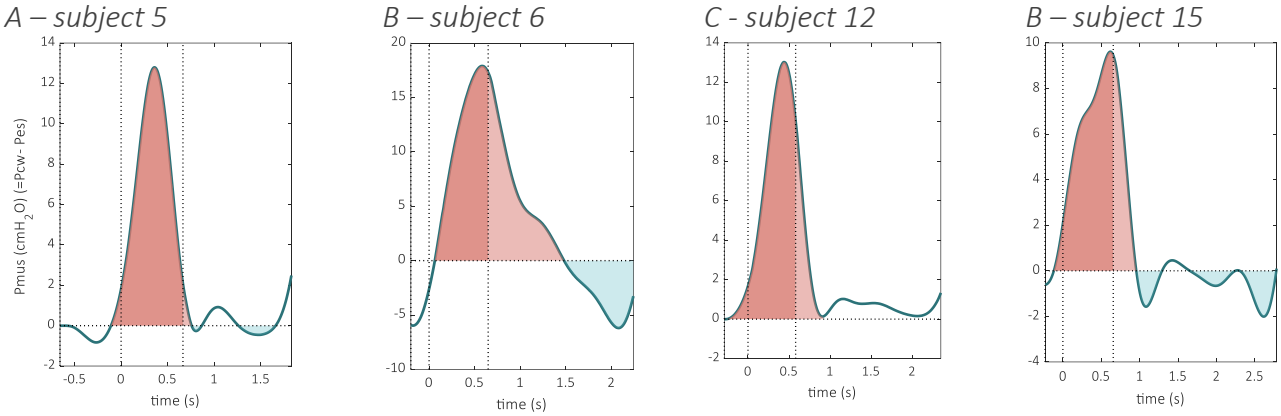

Figure 58: *Examples of Pmus curve, including PTPmus,insp (dark red area), PTPmus,exp(+) (light red area) and PTPmus,exp(-) (blue area) of 4 different subjects.*

8.2.7 Absolute PTPdi,exp

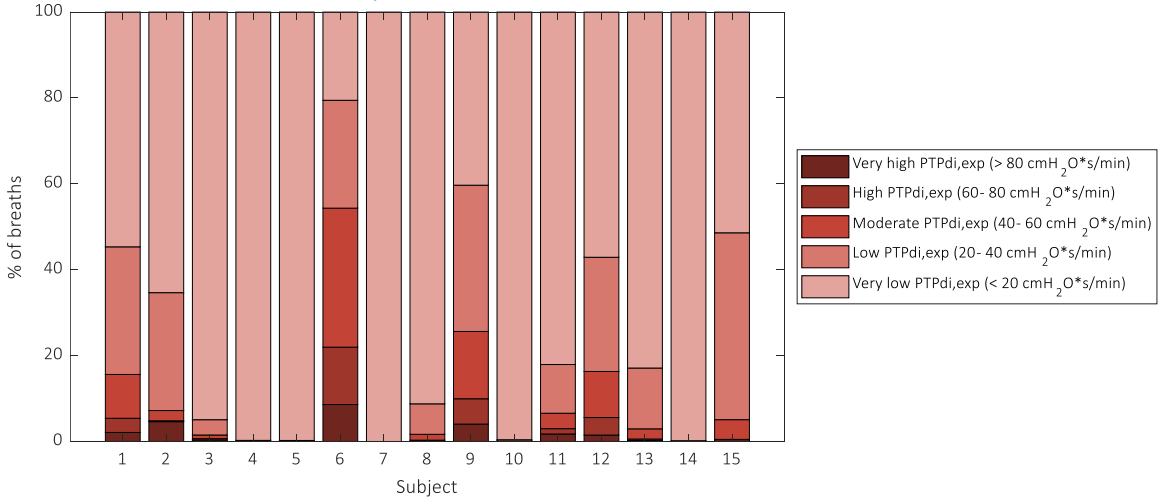

Figure 59: *Distribution of relative PTPdi,exp per patient. All 24 hours of analysis are taken together per patient. Legend at the right shows the colour code of the figure.*

8.2.8 Absolute Pdi at start expiration

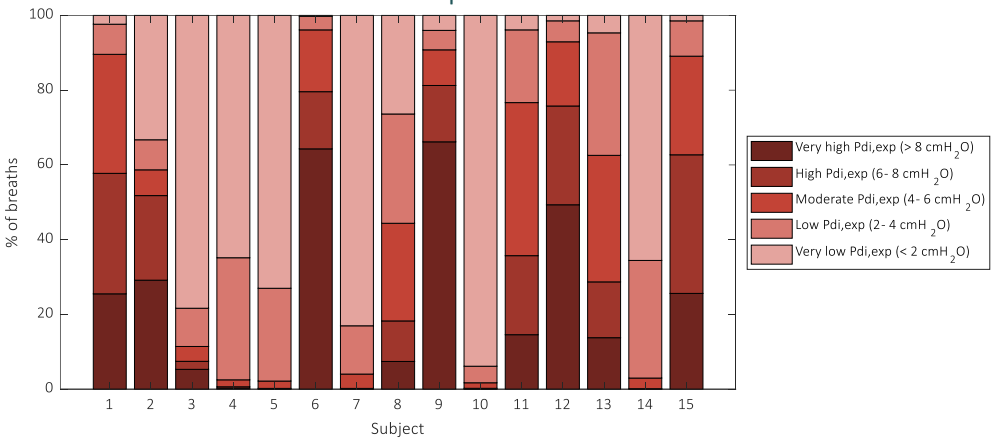

Figure 60: Distribution of absolute Pdi at the start of expiration (Pdi(start-exp)), per patient. All 24 hours of analysis are taken together per patient. Legend at the right shows the colour code of the figure.

8.2.9 Absolute PTPmus,insp

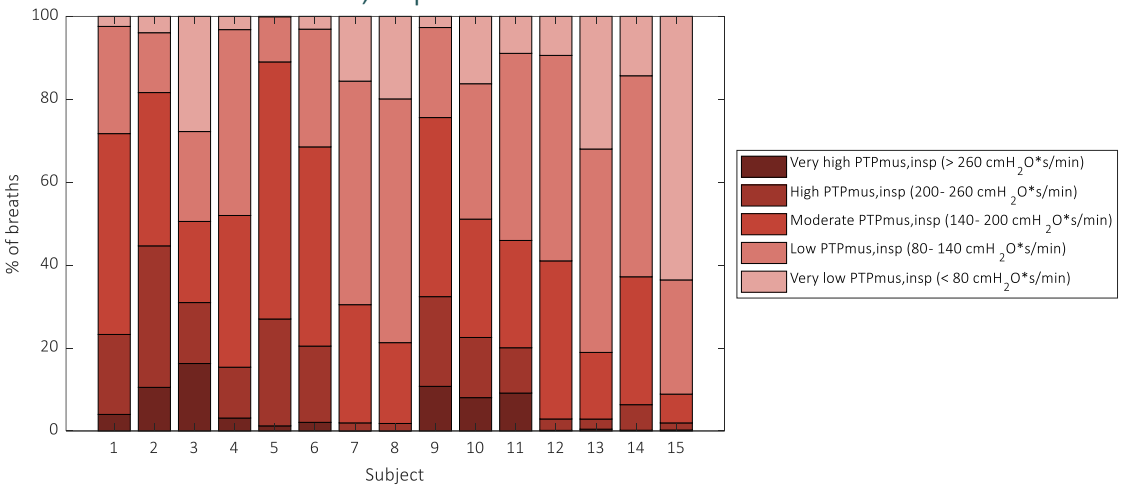

Figure 61: Distribution of absolute PTPmus,insp per patient. All 24 hours of analysis are taken together per patient. Legend at the right shows the colour code of the figure.

8.2.10 Absolute PTPdi,insp

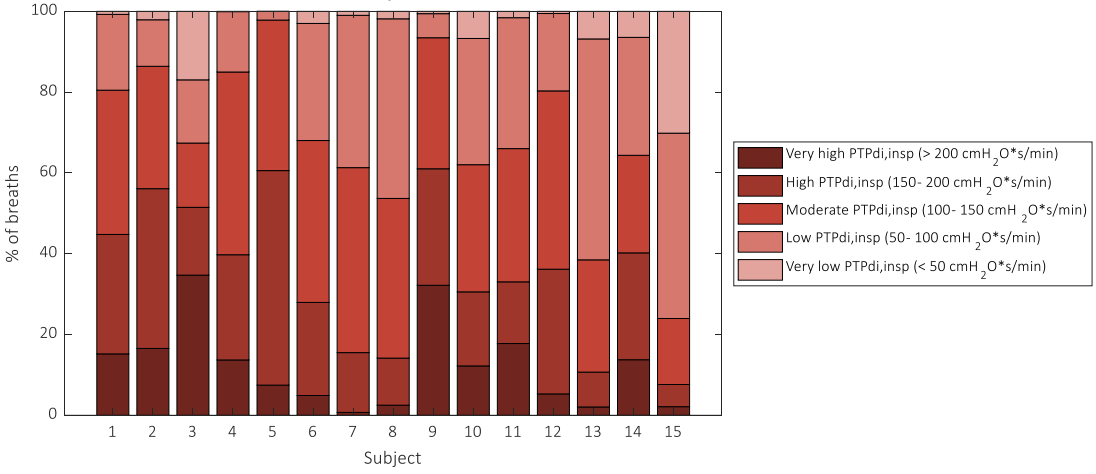

Figure 62: Distribution of absolute PTPdi,insp per patient. All 24 hours of analysis are taken together per patient. Legend at the right shows colour code of the figure.

8.2.11 R-squared of individual subjects

Subject	R^2 ΔPga,exp and PTPga,exp	R^2 ΔPes,exp and PTPmus,exp(-)	R^2 ΔPga,exp and ΔPes,exp	R^2 PTPga,exp and PTPmus,exp(-)
1	0,89	0,75	0,023	0,00
2	0,75	0,59	0,248	0,56
3	0,78	0,55	0,082	0,12
4	0,85	0,79	0,519	0,35
5	0,87	0,40	0,033	0,05
6	0,51	0,78	0,462	0,43
7	0,65	0,32	0,017	0,01
8	0,77	0,65	0,187	0,09
9	0,84	0,87	0,331	0,23
10	0,88	0,53	0,006	0,00
11	0,69	0,59	0,110	0,02
12	0,93	0,79	0,637	0,43
13	0,81	0,65	0,101	0,02
14	0,82	0,66	0,041	0,01
15	0,80	0,63	0,090	0,08
Mean	0,79	0,64	0,192	0,16

8.3 Appendices chapter 5

8.3.1 Additional XRES measurements

Table 7: *Results of XRES measurements. This table shows the delta between the median echogenicity of two repeated measurements (probe was released and positioned again). It can be seen that the absolute difference between the two measurements was smaller or the same with XRES adaptive filter turned on compared to the filter turned off.*

	XRES on measurements			XRES off measurements		
subject	#1	#2	|delta|	#1	#2	|delta|
1	44	48	4	53	58	5
2	56	53	3	55	63	8
3	45	41	4	50	46	4
4	36	33	2,5	43	37	6

8.3.2 Bland-Altman plots for ED85 results

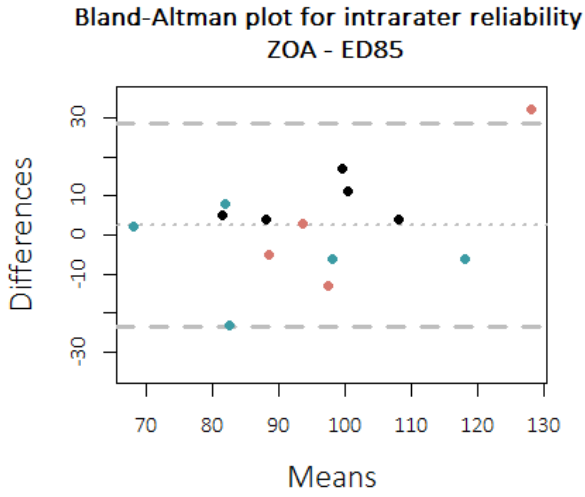

ZOA ED85 intrarater reliability: bias 2.4, limits of Agreement: [-23.6 – 28.3], critical difference 26.0.

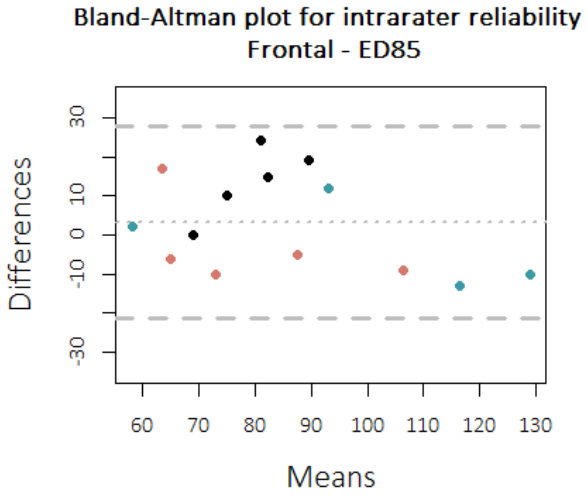

ZOA ED85 interrater reliability: bias 2.0, limits of Agreement: [-28.9 – 32.9], critical difference 30.9.

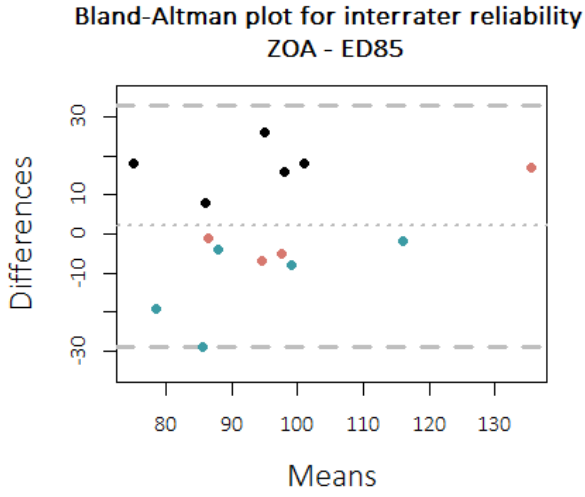

Frontal ED85 intrarater reliability: bias 3.3, limits of Agreement: [-21.4 – 27.9], critical difference 24.6.

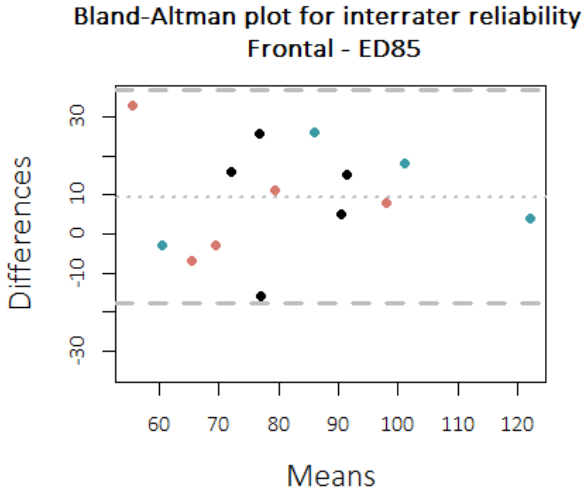

Frontal ED85 interrater reliability: bias 9.5, limits of Agreement: [-17.8 – 36.8], critical difference 27.3.

8.3.3 Artefact example

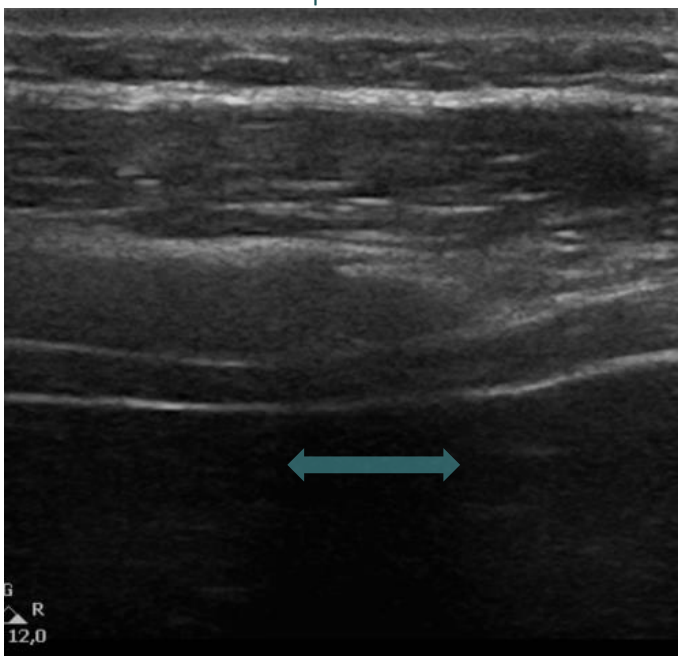

Figure 63: *Example of an artefact, indicated with the blue arrow.*

8.3.4 Tendon example

S03 inspiration frame – median 77

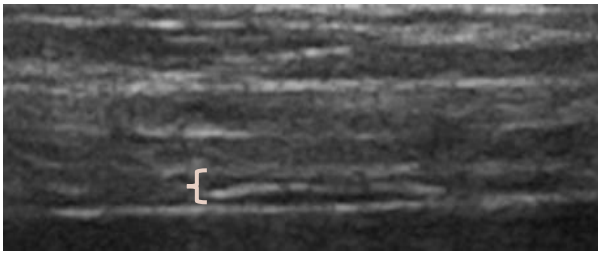

S03 expiration frame – median 88

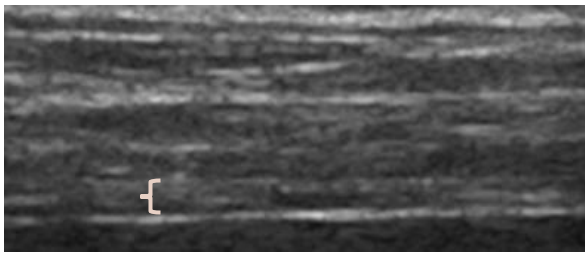

S11 inspiration frame – median 78

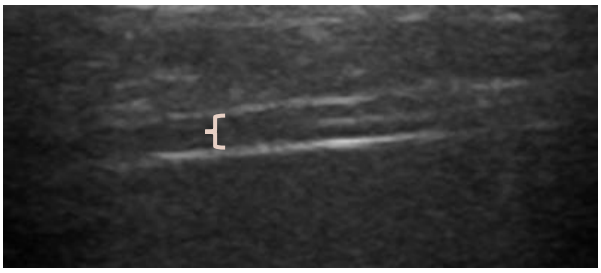

S11 expiration frame – median 71

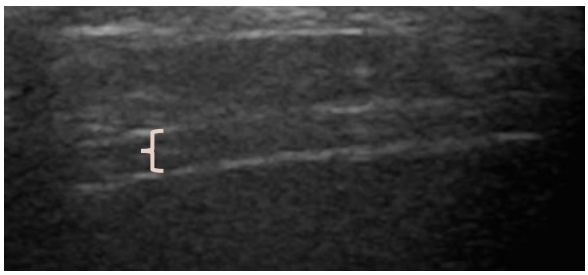

Figure 64: *Examples of the visibility of the tendon of the diaphragm. The figures show that movement of the tendon plate of the diaphragm can cause a decrease as well as an increase of echogenicity when comparing inspiration with expiration. Accolades are placed at the position of the diaphragm.*